



Supplementary Materials for

Architecture of the symmetric core of the nuclear pore

Daniel H. Lin, Tobias Stuwe, Sandra Schilbach, Emily J. Rundlet, Thibaud Perriches, George Mobbs, Yanbin Fan, Karsten Thierbach, Ferdinand M. Huber, Leslie N. Collins, Andrew M. Davenport, Young E. Jeon, André Hoelz*

*correspondence to: hoelz@caltech.edu

This PDF file includes:

Figs. S1 to S59

Tables S1 to S10

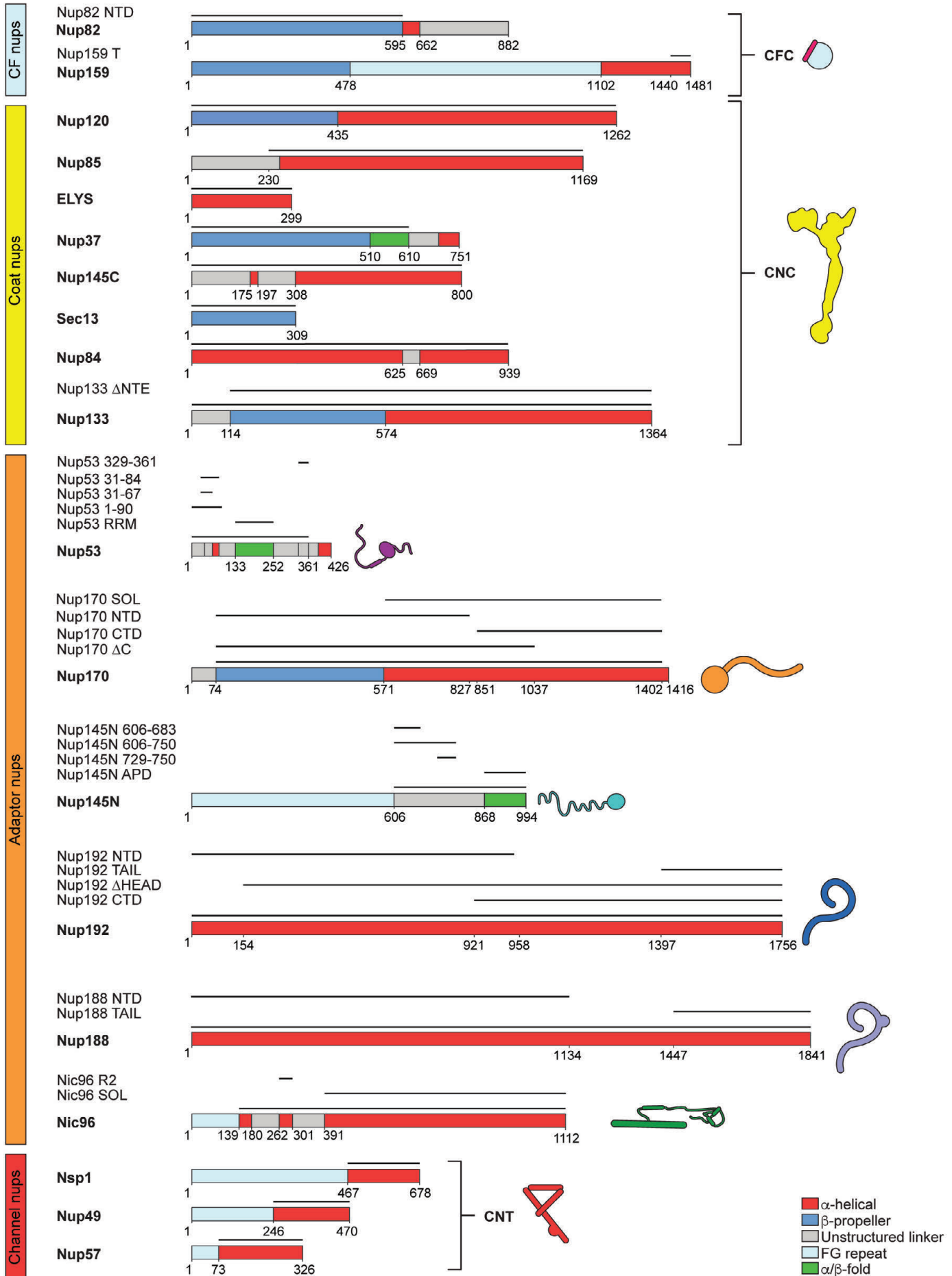


Fig.S1.

Nucleoporin fragments. Domain boundaries of all nucleoporin fragments used throughout the text are indicated by black lines.

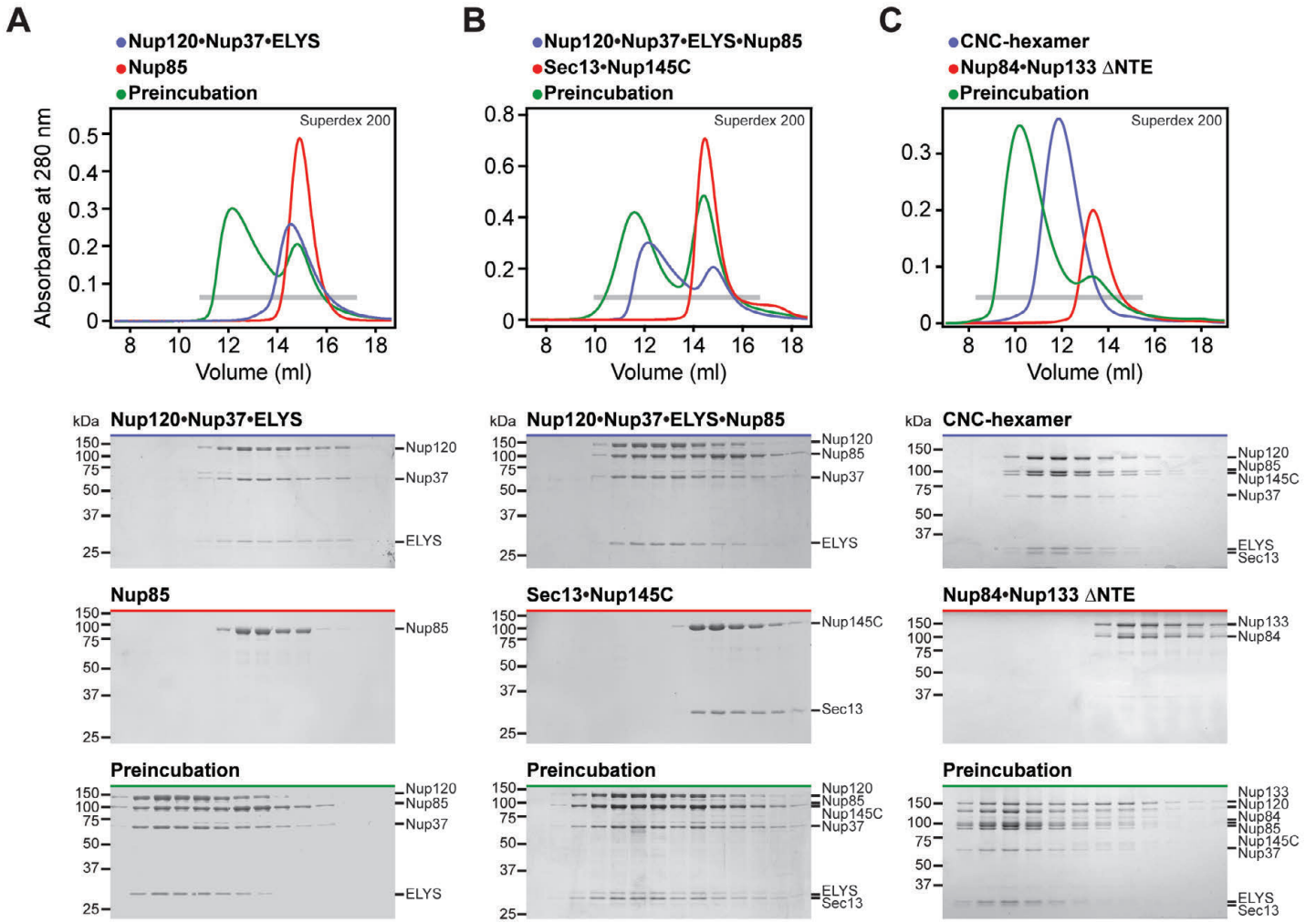


Fig. S2.

Reconstitution of the CNC. SEC and SDS-PAGE analysis for the reconstitution of **(A)** the Nup120•Nup37•ELYS•Nup85 hetero-tetramer, **(B)** the CNC-hexamer, and **(C)** the CNC-octamer. SEC profiles of nucleoporins or nucleoporin complexes are shown individually (blue and red) and after their preincubation (green). All SEC profiles were obtained using a Superdex 10/300 GL column. Gray bars indicate fractions that were resolved on SDS-PAGE gels and visualized by Coomassie staining. The CNC-octamer could only be reconstituted with a Nup133 construct lacking the NTE.

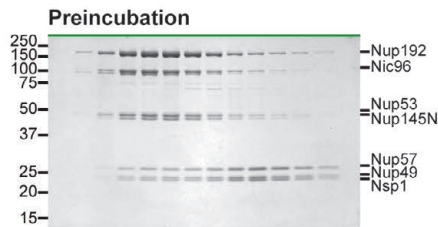
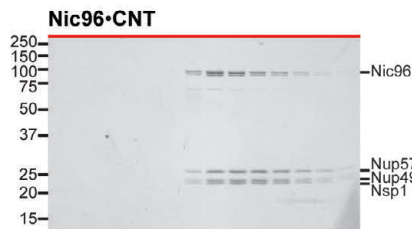
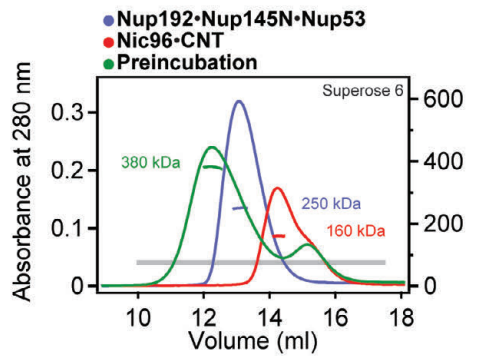
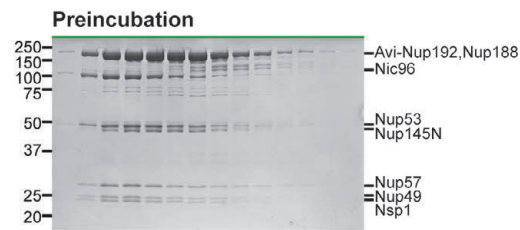
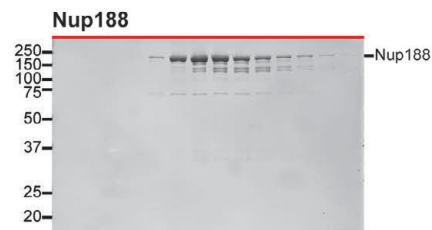
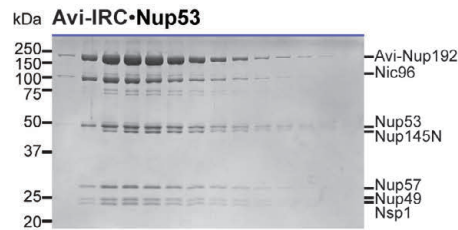
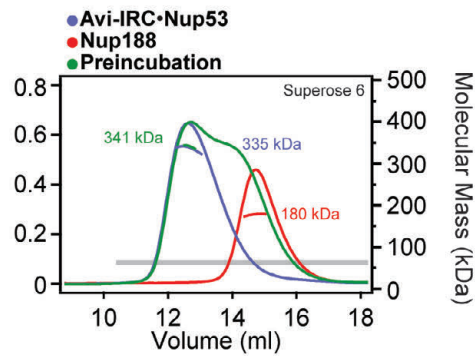
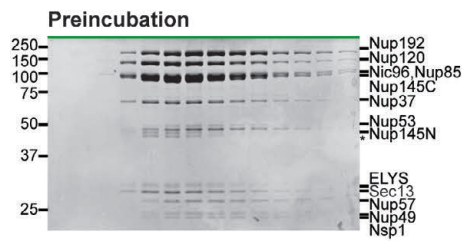
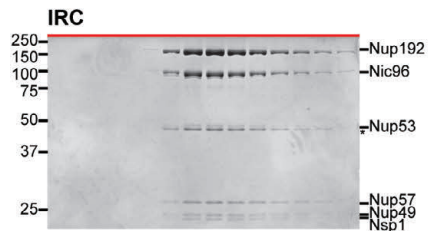
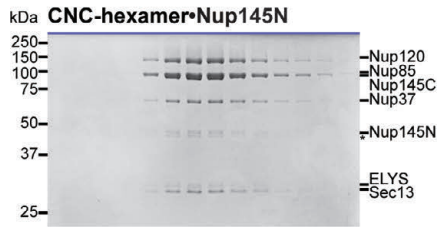
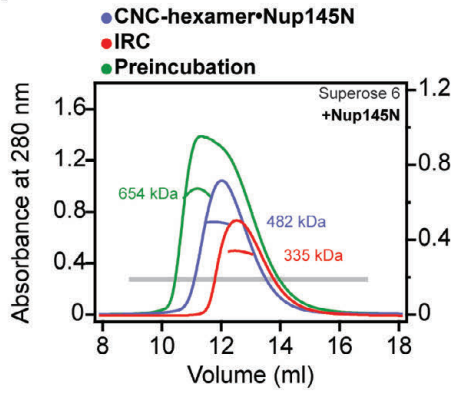
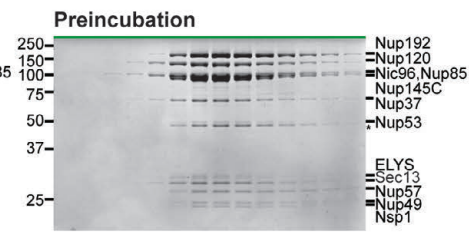
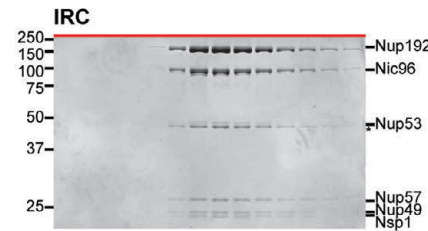
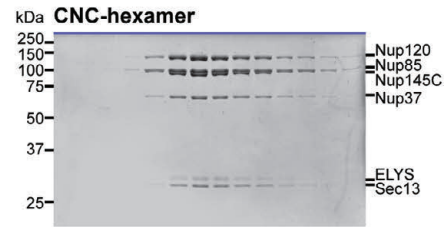
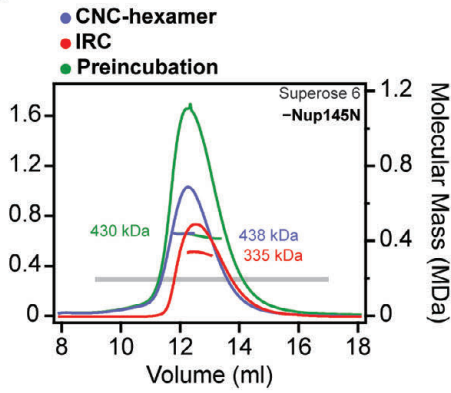
A**B**

Fig. S3.

Reconstitution of the IRC•Nup53 complex. SEC-MALS and SDS-PAGE analysis of **(A)** the reconstitution of the IRC•Nup53 hetero-heptamer and **(B)** the interaction of IRC•Nup53 with Nup188. SEC-MALS profiles of nucleoporins or nucleoporin complexes are shown individually (blue and red) and after their preincubation (green). All SEC profiles were obtained using a Superose 6 10/300 GL column. Measured molecular masses are indicated for the peak fractions. Gray bars indicate fractions that were resolved on SDS-PAGE gels and visualized by Coomassie staining or by immunoblotting with a mouse anti-AviTag antibody. As Nup188 and Nup192 cannot be distinguished by SDS-PAGE analysis, lack of Nup192 displacement from the IRC by Nup188 was confirmed by western blotting against Avi-tagged Nup192.

A**B**

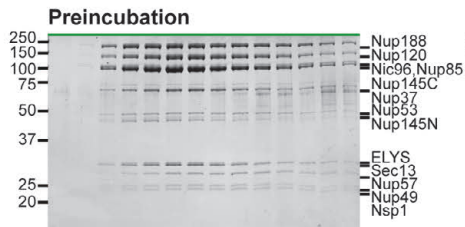
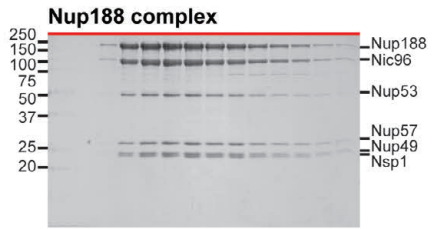
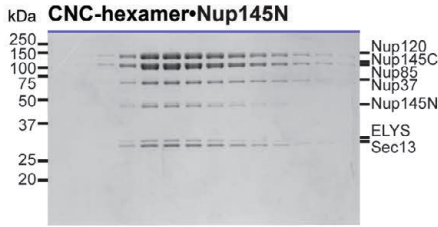
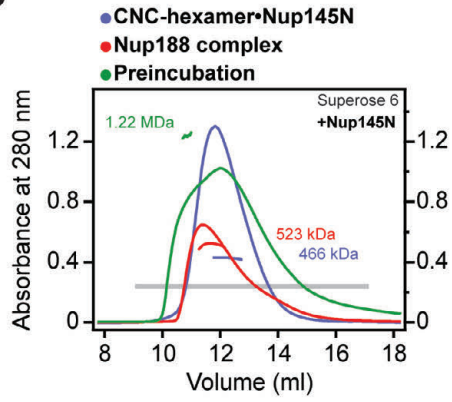
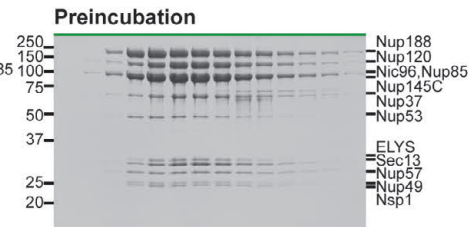
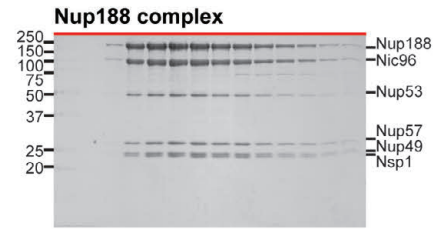
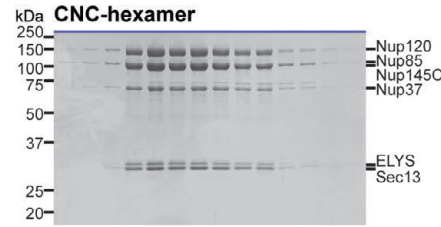
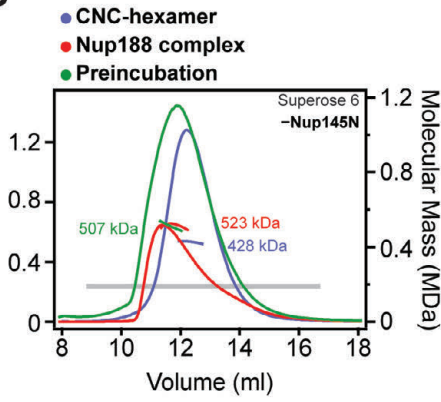
C**D**

Fig. S4.

Reconstitution of NPC core protomers. (A-D) SEC-MALS and SDS-PAGE analysis corresponding to [Fig. 1, D to G](#). SEC-MALS profiles of nucleoporin complexes are shown individually (blue and red) and after their preincubation (green). All SEC profiles were obtained using a Superose 6 10/300 GL column. Measured molecular masses are indicated for the peak fractions. Gray bars indicate fractions that were resolved on SDS-PAGE gels and visualized by Coomassie staining.

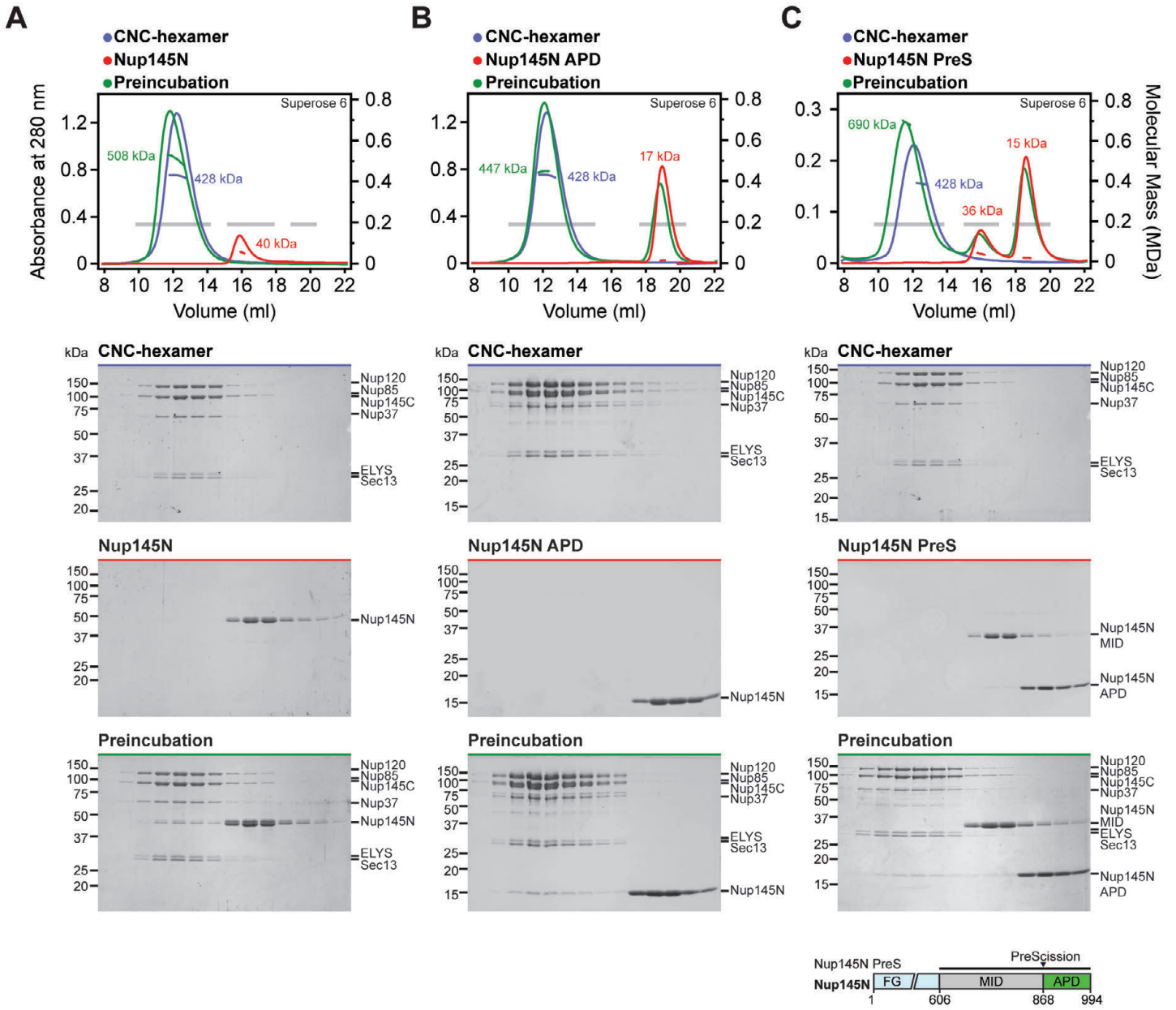


Fig. S5.

The CNC-hexamer interacts with Nup145N^{APD}. SEC-MALS and SDS-PAGE analysis of the CNC-hexamer interaction with (A) Nup145N, (B) Nup145N^{APD}, and (C) Nup145N PreS preincubated with PreScission protease. SEC-MALS profiles of nucleoporins or nucleoporin complexes are shown individually (blue and red) and after their preincubation (green). All SEC profiles were obtained using a Superose 6 10/300 GL column. Measured molecular masses are indicated for the peak fractions. Gray bars indicate fractions that were resolved on SDS-PAGE gels and visualized by Coomassie staining. As reference, the domain structure of Nup145N PreS is shown, indicating the construct boundaries and PreScission cleavage site with a black bar and a black triangle, respectively. After cleavage with PreScission protease, Nup145N^{APD} co-elutes with the CNC-hexamer, whereas Nup145N^{MID} does not incorporate into the complex.

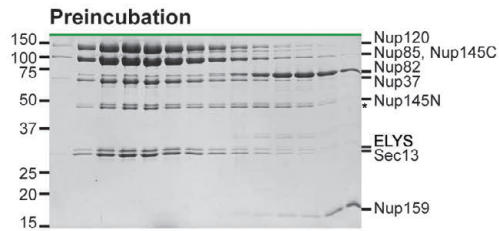
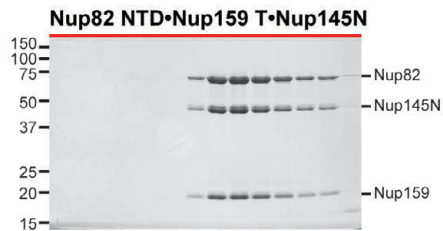
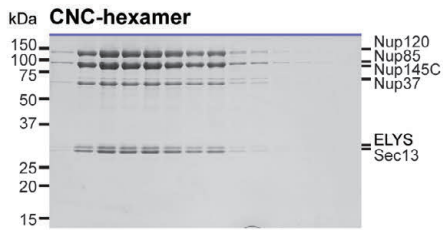
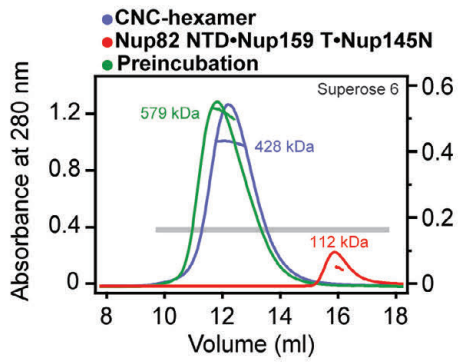
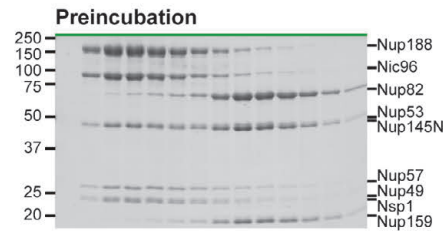
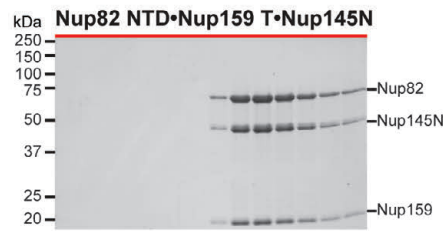
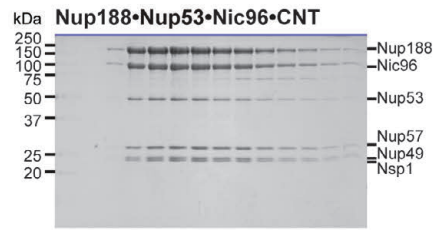
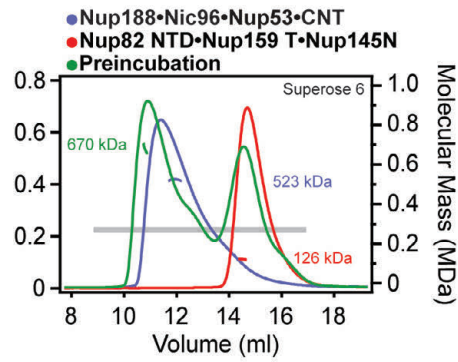
A**B**

Fig. S6.

Incorporation of Nup145N into complexes with CNC-hexamer or Nup188•Nic96•Nup53•CNT is exclusive of Nup145N binding to Nup82^{NTD}•Nup159^T. SEC-MALS and SDS-PAGE analysis of the CFC interaction with (A) the CNC-hexamer or (B) the Nup188•Nic96•Nup53•CNT complex. SEC-MALS profiles of nucleoporin complexes are shown individually (blue and red) and after their preincubation (green). SEC profiles were obtained using a Superose 6 10/300 GL column. Measured molecular masses are indicated for the peak fractions. Gray bars indicate fractions that were resolved on SDS-PAGE gels and visualized by Coomassie staining. In both preincubations, Nup145N incorporates stoichiometrically into the complexes, but the Nup82^{NTD}•Nup159^T hetero-dimer does not. However, Nup82^{NTD}•Nup159^T interacts weakly with the Nup188-containing complex.

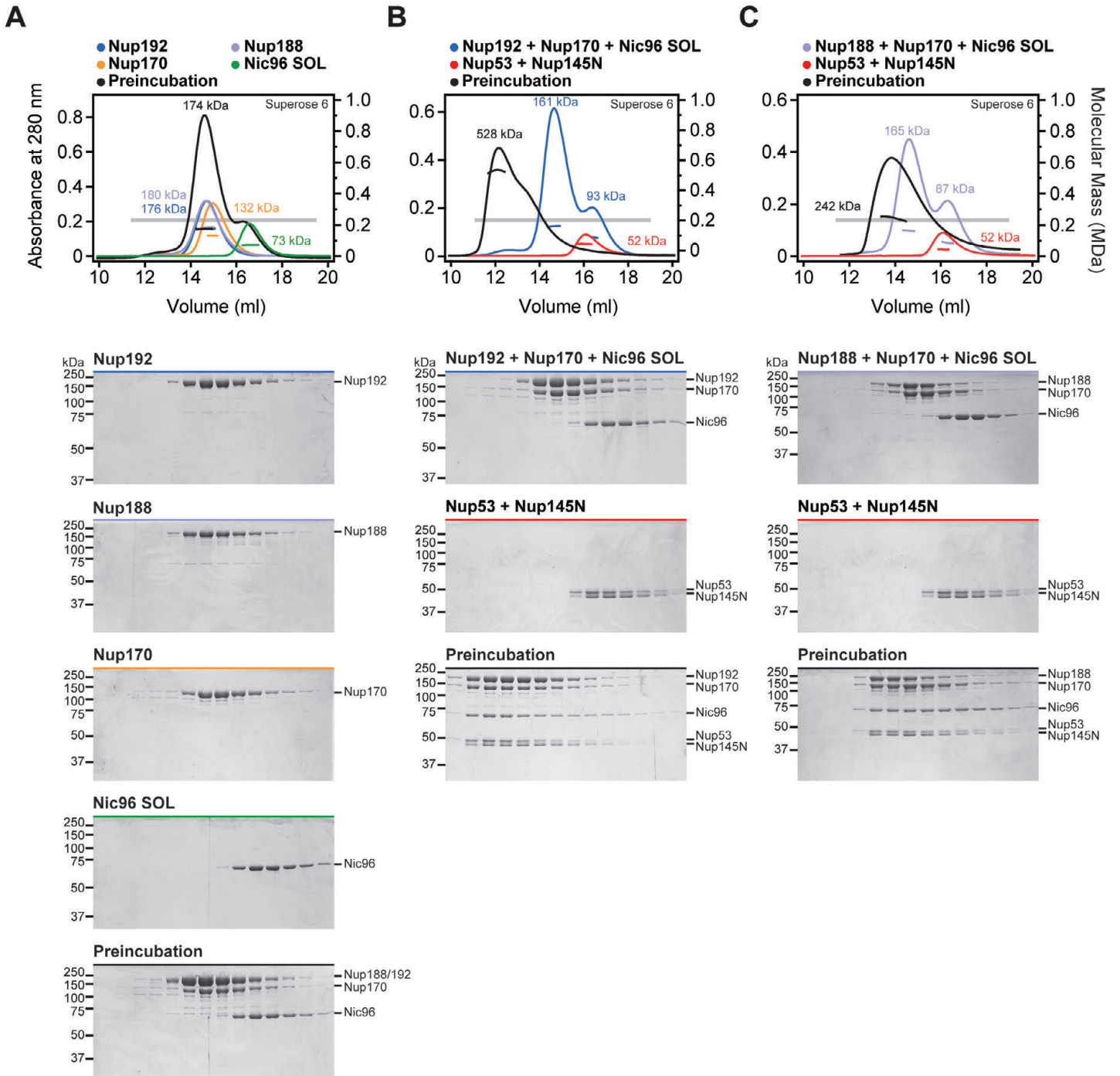


Fig. S7.

Scaffold nucleoporins are assembled by the linker nucleoporins. SEC-MALS and SDS-PAGE analysis corresponding to Fig. 2, A to C. **(A)** For interaction analysis between scaffold nucleoporins, SEC-MALS profiles of nucleoporins are shown individually (blue, purple, orange, or green) and after their preincubation (black). **(B)** To analyze the assembly of Nup192, Nup170, and Nic96^{SOL} with the linker nucleoporins Nup53 and Nup145N, SEC-MALS profiles of the scaffold mixture (blue), the linker mixture (red), or after their preincubation (black) are shown. **(C)** To analyze the assembly of Nup188, Nup170 and Nic96^{SOL} with the linker nucleoporins Nup53 and Nup145N, SEC-MALS profiles of the scaffold mixture (purple), the linker mixture (red), or after their preincubation (black) are shown. All SEC profiles were obtained using a Superose 6 10/300 GL column. Measured molecular masses are indicated for the peak fractions. Gray bars indicate fractions that were resolved on SDS-PAGE gels and visualized by Coomassie staining. Because Nup188 could not be incorporated into the IRC, Nup188 and Nup192 were not simultaneously included in preincubations.

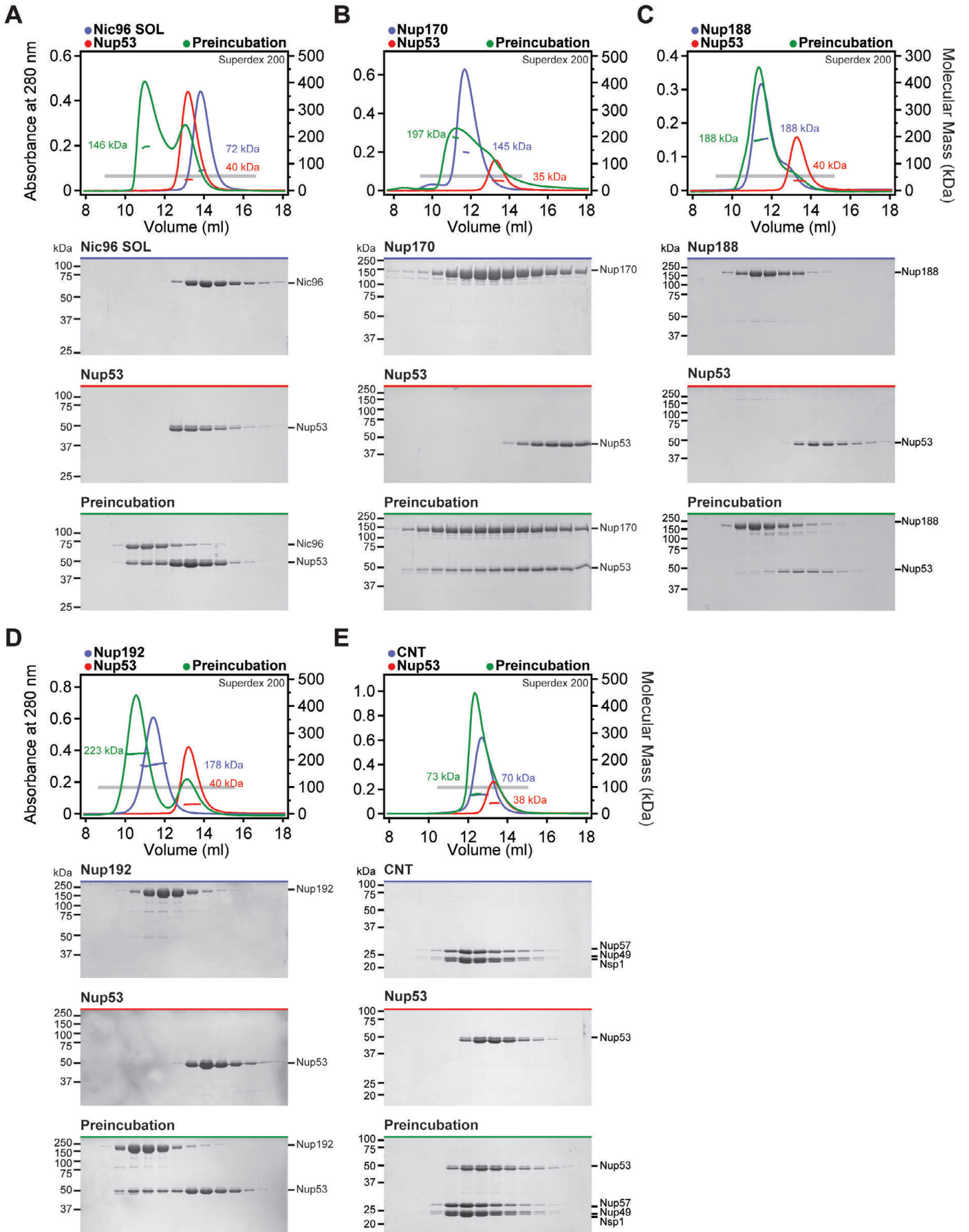


Fig. S8.

Identification of interactions between Nup53 and the scaffold nucleoporins. (A-E) SEC-MALS and SDS-PAGE analysis for Fig. 2D. SEC-MALS profiles of nucleoporins are shown individually (blue and red) and after their preincubation (green). All SEC profiles were obtained using a Superdex 200 10/300 GL column. Measured molecular masses are indicated for the peak fractions. Gray bars indicate fractions that were resolved on SDS-PAGE gels and visualized by Coomassie staining. Robust complex formation with Nup53 was observed for Nic96^{SOL}, Nup170, and Nup192. Interactions of Nup53 with Nup188 and the CNT were only barely detectable.

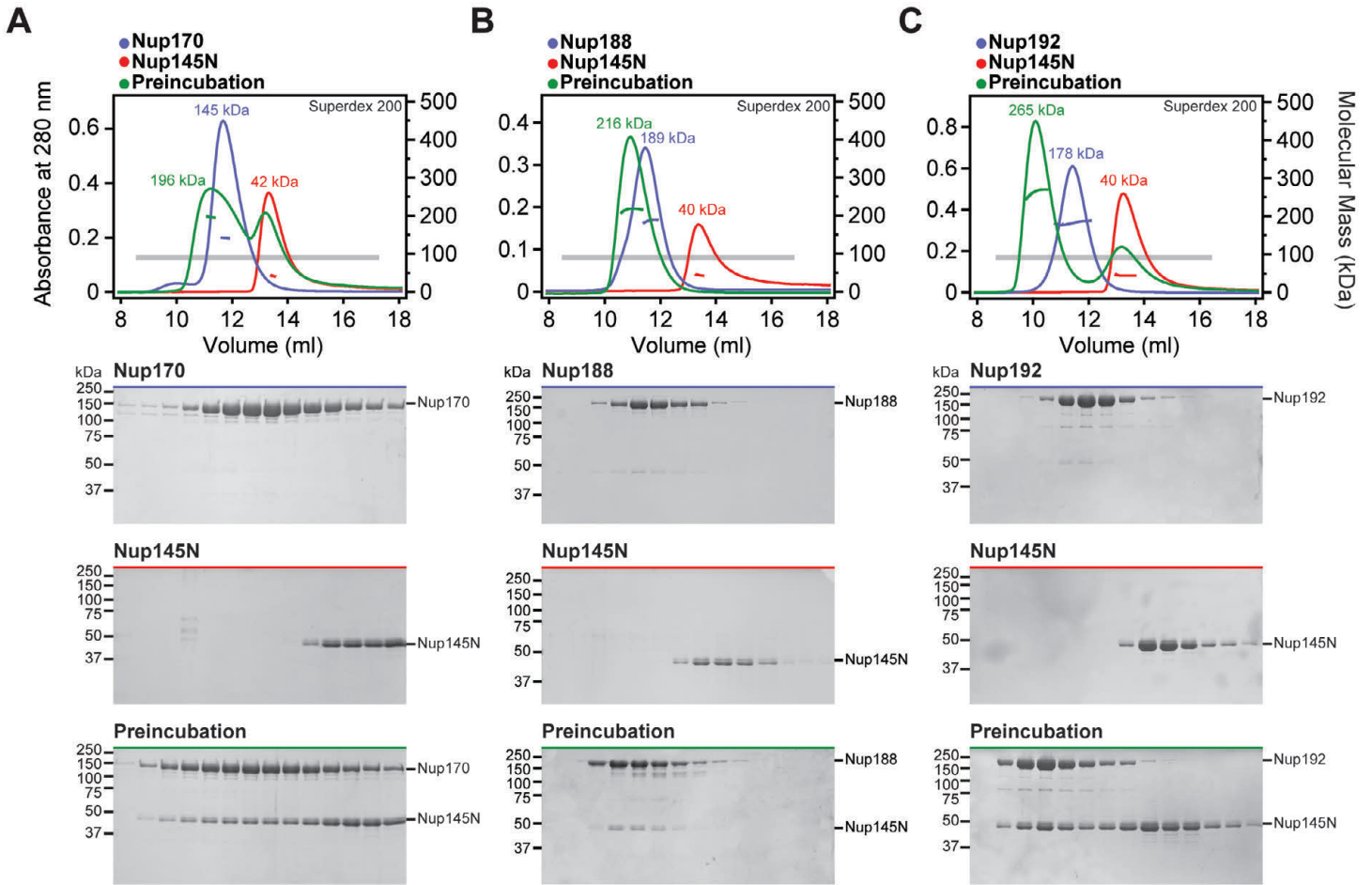


Fig. S9.

Identification of interactions between Nup145N and scaffold nucleoporins. (A-C) SEC-MALS and SDS-PAGE analysis for Fig. 2E. SEC-MALS profiles of nucleoporins are shown individually (blue and red) and after their preincubation (green). All SEC profiles were obtained using a Superdex 200 10/300 GL column. Measured molecular masses are indicated for the peak fractions. Gray bars indicate fractions that were resolved on SDS-PAGE gels and visualized by Coomassie staining. Robust complex formation with Nup145N was observed for Nup170, Nup188, and Nup192. We previously demonstrated interactions between Nup145N and Nic96 and the CNT (15).

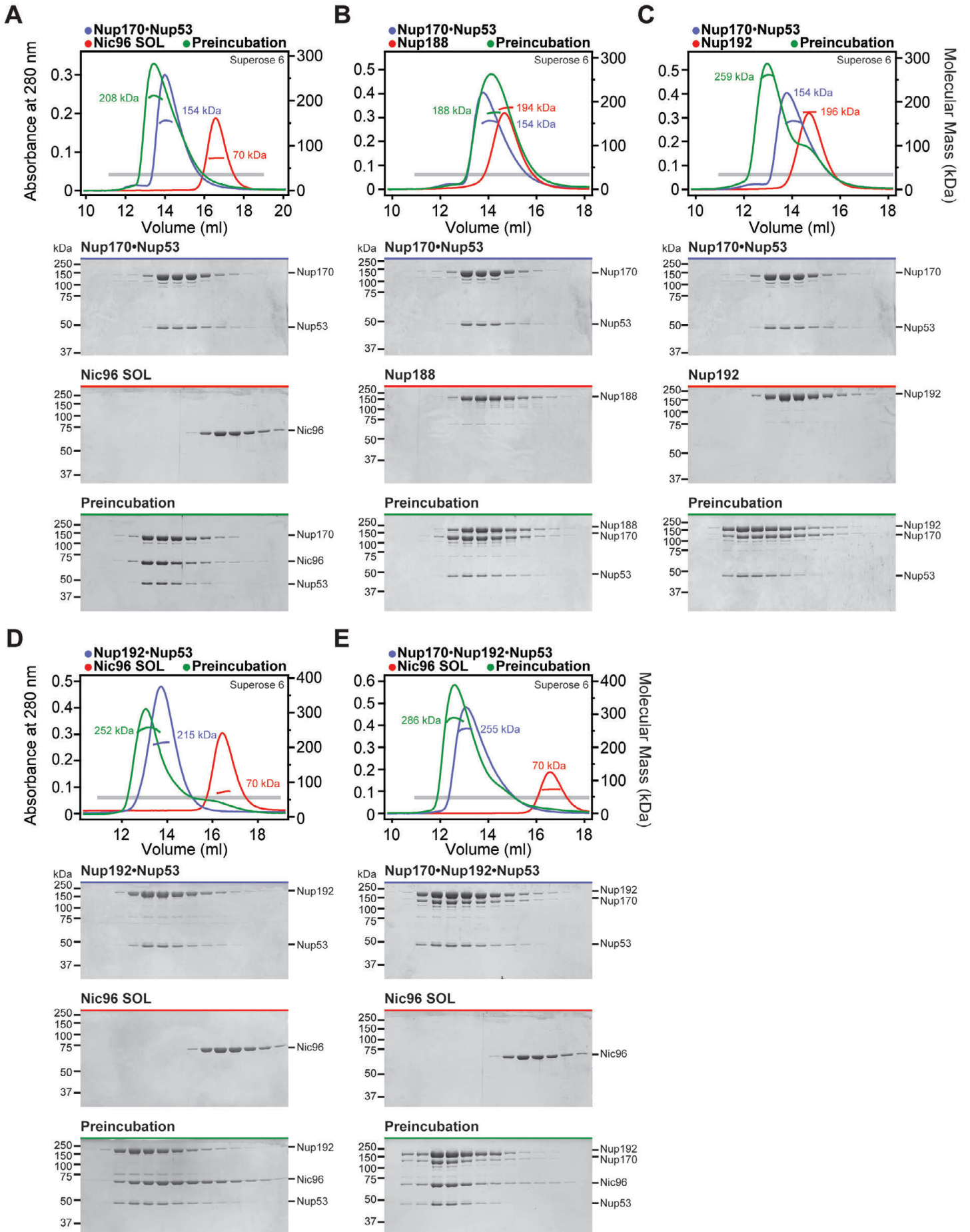
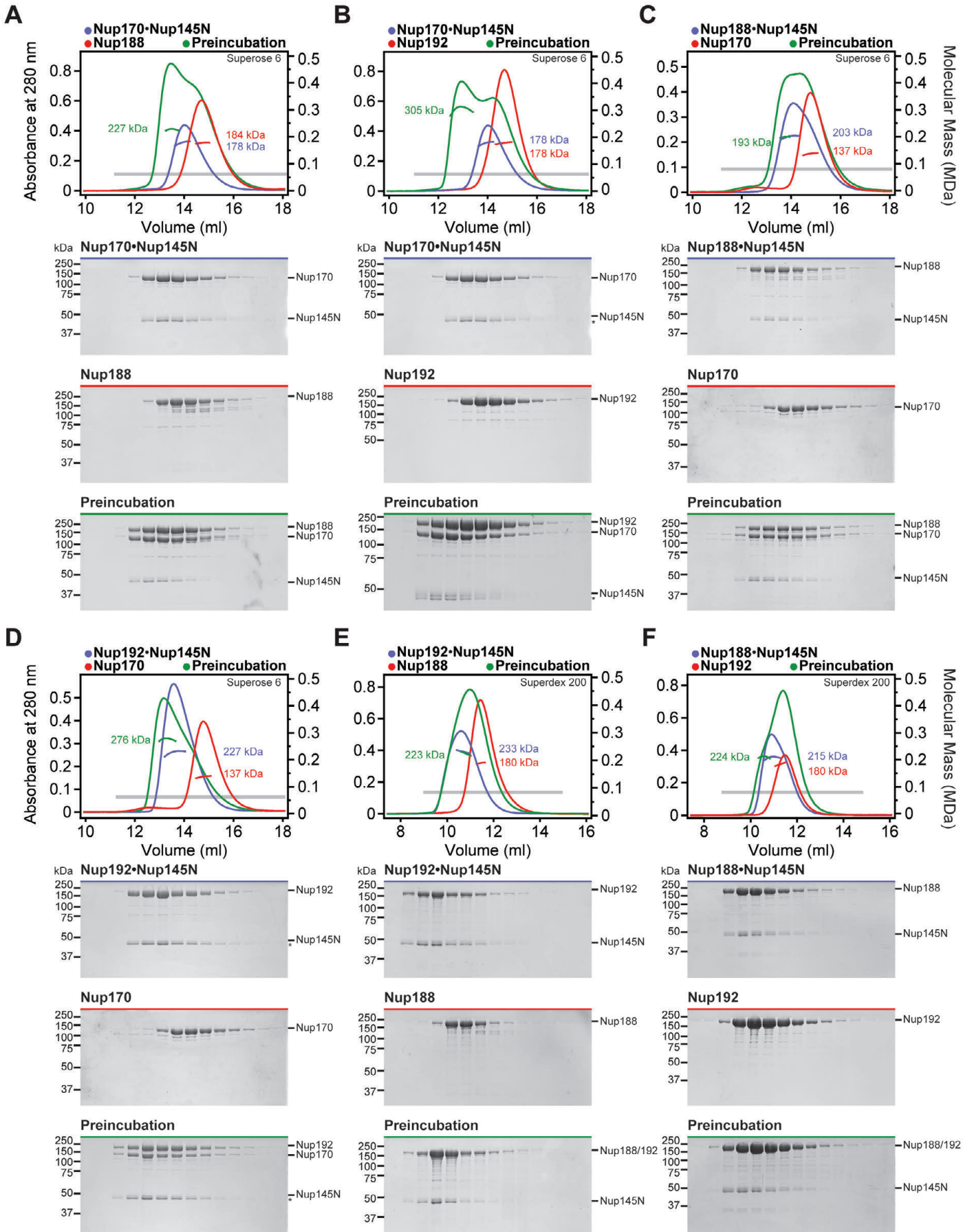


Fig. S10.

Identification of hetero-trimeric complexes assembled by Nup53. (A-E) SEC-MALS and SDS-PAGE analysis corresponding to Fig. 2D. Purified hetero-dimeric Nup53 complexes were tested for their ability to form hetero-trimers with an additional scaffold nucleoporin. SEC-MALS profiles of nucleoporins or nucleoporin complexes are shown individually (blue and red) and after their preincubation (green). All SEC profiles were obtained using a Superose 6 10/300 GL column. Measured molecular masses are indicated for the peak fractions. Gray bars indicate fractions that were resolved on SDS-PAGE gels and visualized by Coomassie staining. Nup53 is able to bind simultaneously to Nup170, Nic96^{SOL}, and Nup192. The interaction of the Nup170•Nup53 hetero-dimer with Nup188 was only barely detectable.



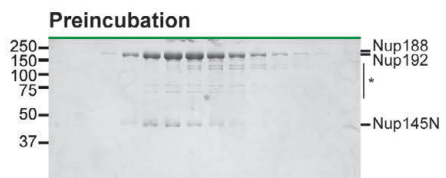
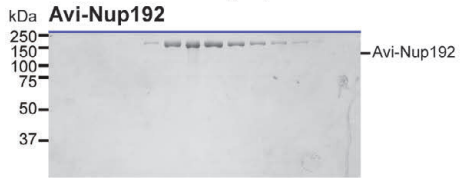
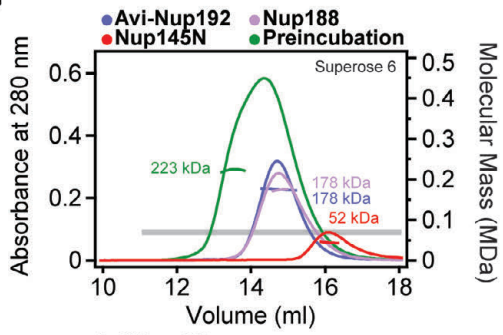
G

Fig. S11.

Identification of hetero-trimeric complexes assembled by Nup145N. (A-G) SEC-MALS and SDS-PAGE analysis corresponding to Fig. 2E. Purified hetero-dimeric Nup145N complexes were tested for their ability to form hetero-trimers with an additional scaffold nucleoporin. SEC-MALS profiles of nucleoporins or nucleoporin complexes are shown individually (blue, red, and purple) and after their preincubation (green). SEC profiles were obtained using either a Superose 6 10/300 GL column or a Superdex 200 10/300 GL column as indicated. Measured molecular masses are indicated for the peak fractions. Gray bars indicate fractions that were resolved on SDS-PAGE gels and visualized by Coomassie staining or by western blot analysis with a mouse anti-AviTag antibody. Hetero-trimeric complex formation was determined on the basis of a shift in elution volume, an increase in measured molecular mass, and the presence of all three proteins in the higher molecular mass fractions. For preincubations with Nup188 or Nup188•Nup145N, only minor shifts in elution volume and no increases in the measured molecular masses were observed, indicating the formation of a mixture of species rather than stable hetero-trimeric complexes as seen between Nup170, Nup192, and Nup145N. As Nup188 and Nup192 cannot be distinguished by SDS-PAGE, western blot analysis was employed to confirm that Nup188 and Nup192 bind to Nup145N in a mutually exclusive fashion.

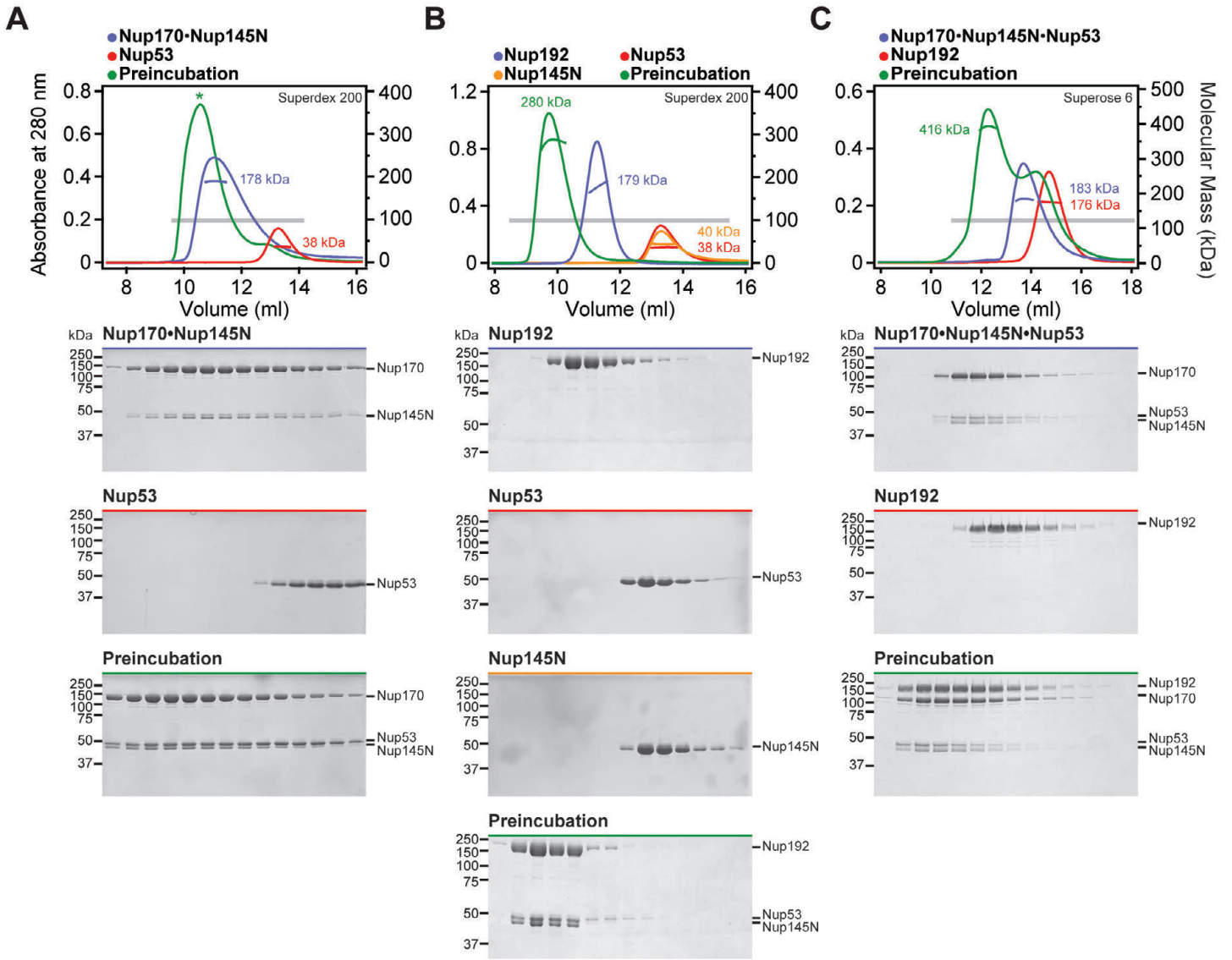


Fig. S12.

Binding sites for linker nucleoporins on Nup170 and Nup192 are distinct and compatible. (A-C) SEC-MALS profiles of nucleoporins or nucleoporin complexes are shown individually (blue, red, or yellow) and after their preincubation (green). SEC profiles were obtained using a Superdex 200 10/300 GL column for panels (A, B) and a Superose 6 10/300 GL column for panel (C). Measured molecular masses are indicated for the peak fractions. Gray bars indicate fractions that were resolved on SDS-PAGE gels and visualized by Coomassie staining. We were unable to obtain an accurate molecular mass measurement for the preincubation of Nup53 with Nup170•Nup145N, as indicated by an asterisk above the chromatogram.

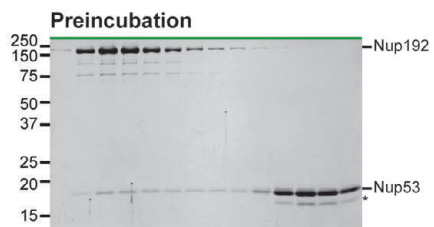
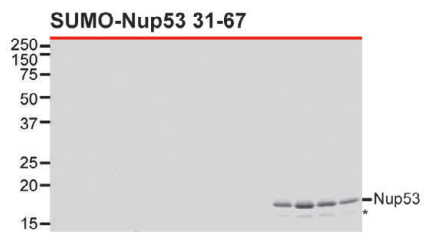
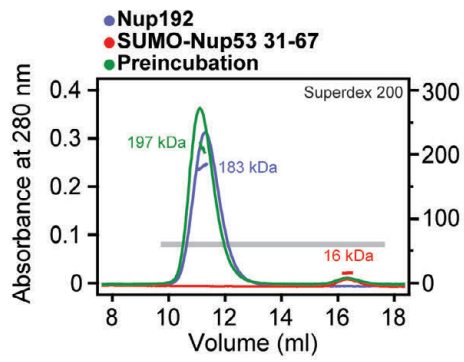


Fig. S13.

Nup192 recognizes Nup53³¹⁻⁶⁷. SEC-MALS and SDS-PAGE analysis corresponding to [Fig. 2F](#). SEC-MALS profiles of nucleoporins are shown individually (blue and red) and after their preincubation (green). All SEC profiles were obtained using a Superdex 200 10/300 GL column. Measured molecular masses are indicated for the peak fractions. Gray bars indicate fractions that were resolved on SDS-PAGE gels and visualized by Coomassie staining.

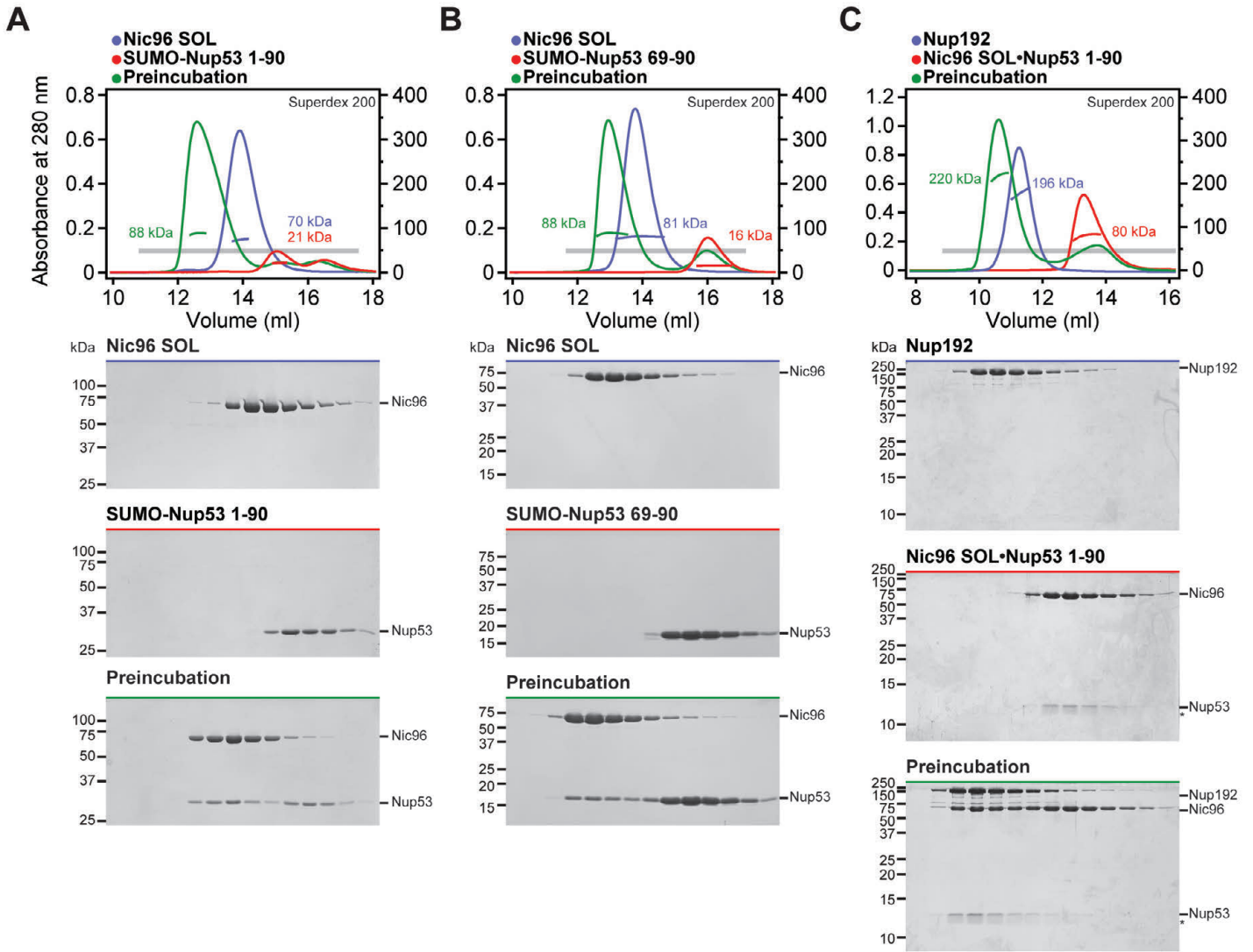


Fig. S14.

Nic96^{SOL} recognizes Nup53⁶⁹⁻⁹⁰ and Nup53¹⁻⁹⁰ binds simultaneously to Nup192 and Nic96^{SOL}. (A-C) SEC-MALS and SDS-PAGE analysis corresponding to Fig. 2F. SEC-MALS profiles of nucleoporins or nucleoporin complexes are shown individually (blue and red) and after their preincubation (green). All SEC profiles were obtained using a Superdex 200 10/300 GL column. Measured molecular masses are indicated for the peak fractions. Gray bars indicate fractions that were resolved on SDS-PAGE gels and visualized by Coomassie staining. The Nup53 binding sites for Nic96^{SOL} and Nup192 map to directly adjacent sequence fragments and are not mutually exclusive.

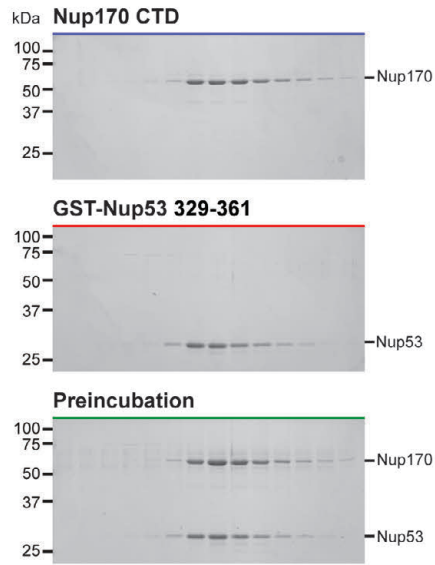
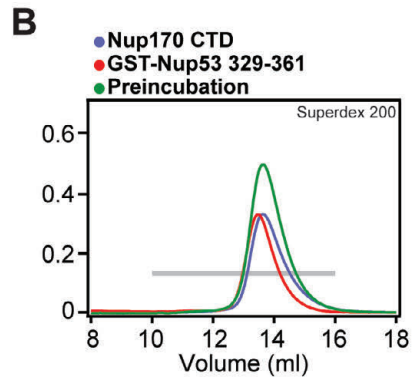
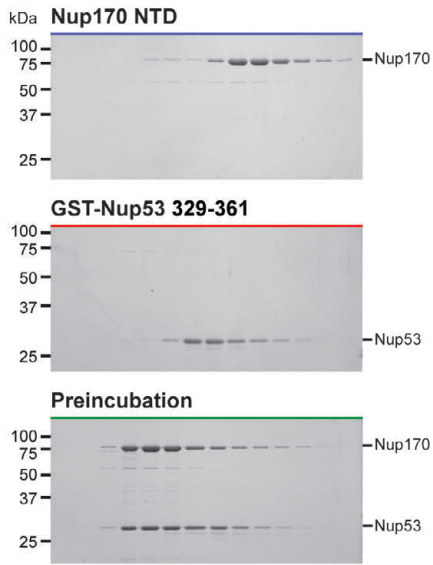
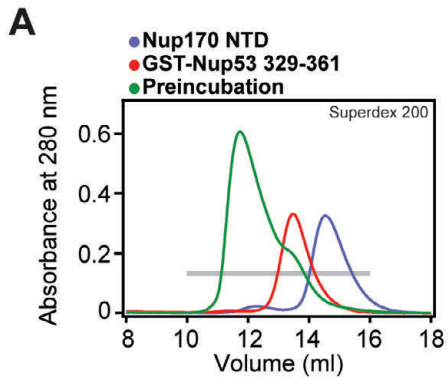


Fig. S15.

Nup170^{NTD} recognizes Nup53³²⁹⁻³⁶¹. (A, B) SEC and SDS-PAGE analysis corresponding to [Fig. 2F](#). SEC profiles of nucleoporins are shown individually (blue and red) and after their preincubation (green). All SEC profiles were obtained using a Superdex 200 10/300 GL column. Gray bars indicate fractions that were resolved on SDS-PAGE gels and visualized by Coomassie staining.

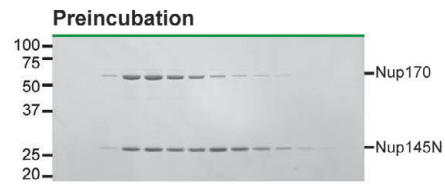
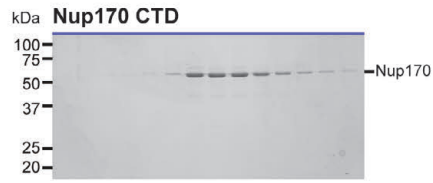
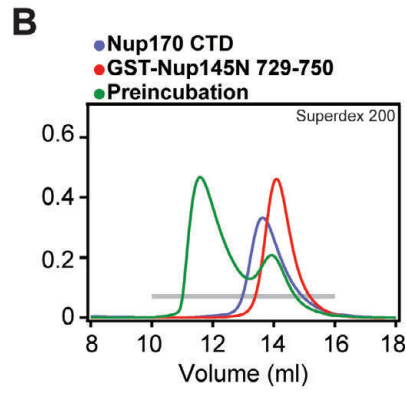
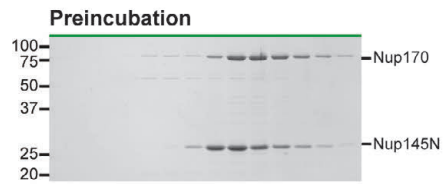
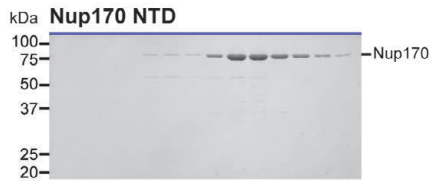
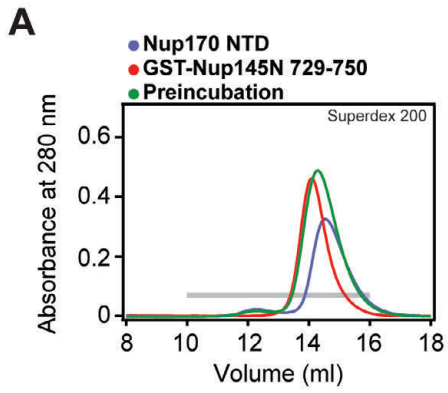
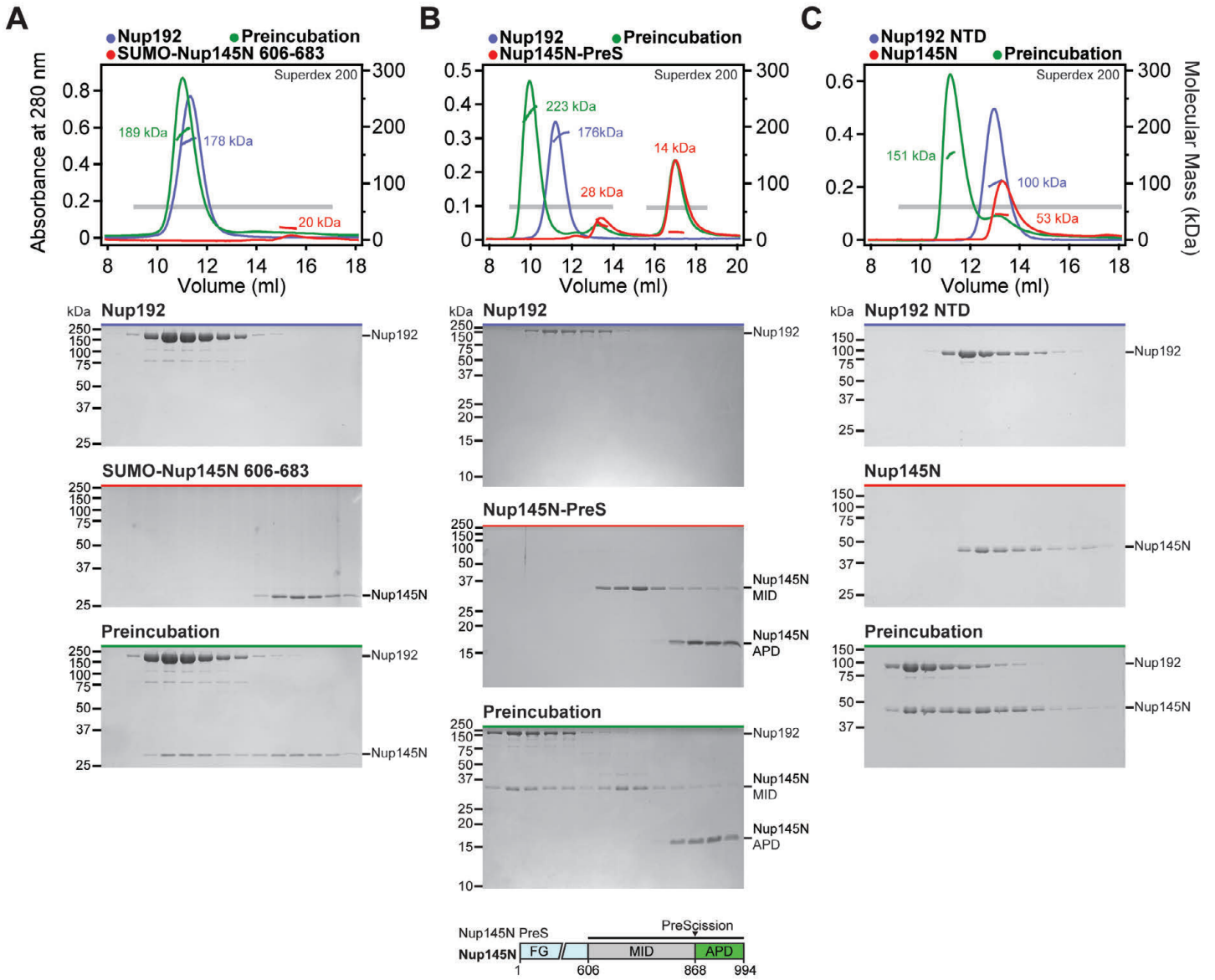


Fig. S16.

Nup170^{CTD} recognizes Nup145N⁷²⁹⁻⁷⁵⁰. (A, B) SEC and SDS-PAGE analysis corresponding to [Fig. 2F](#). SEC profiles of nucleoporins are shown individually (blue and red) and after their preincubation (green). All SEC profiles were obtained using a Superdex 200 10/300 GL column. Gray bars indicate fractions that were resolved on SDS-PAGE gels and visualized by Coomassie staining.



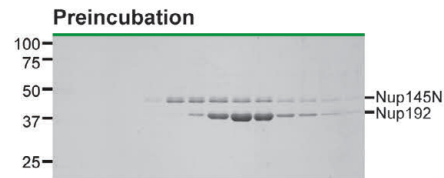
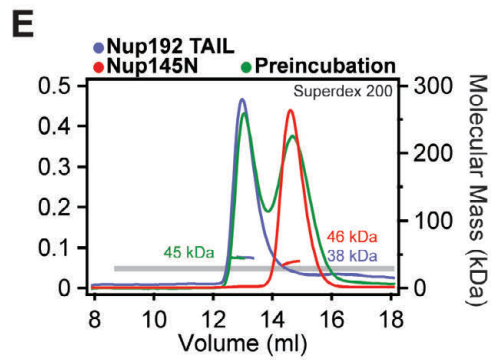
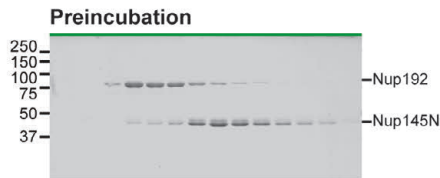
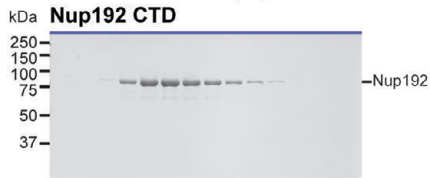
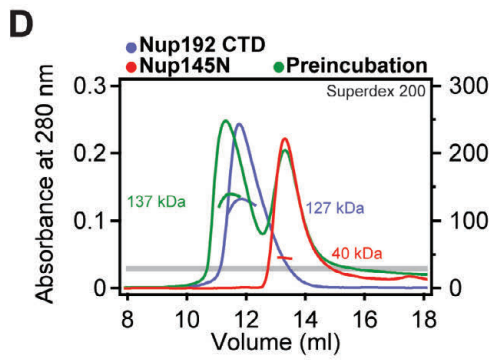
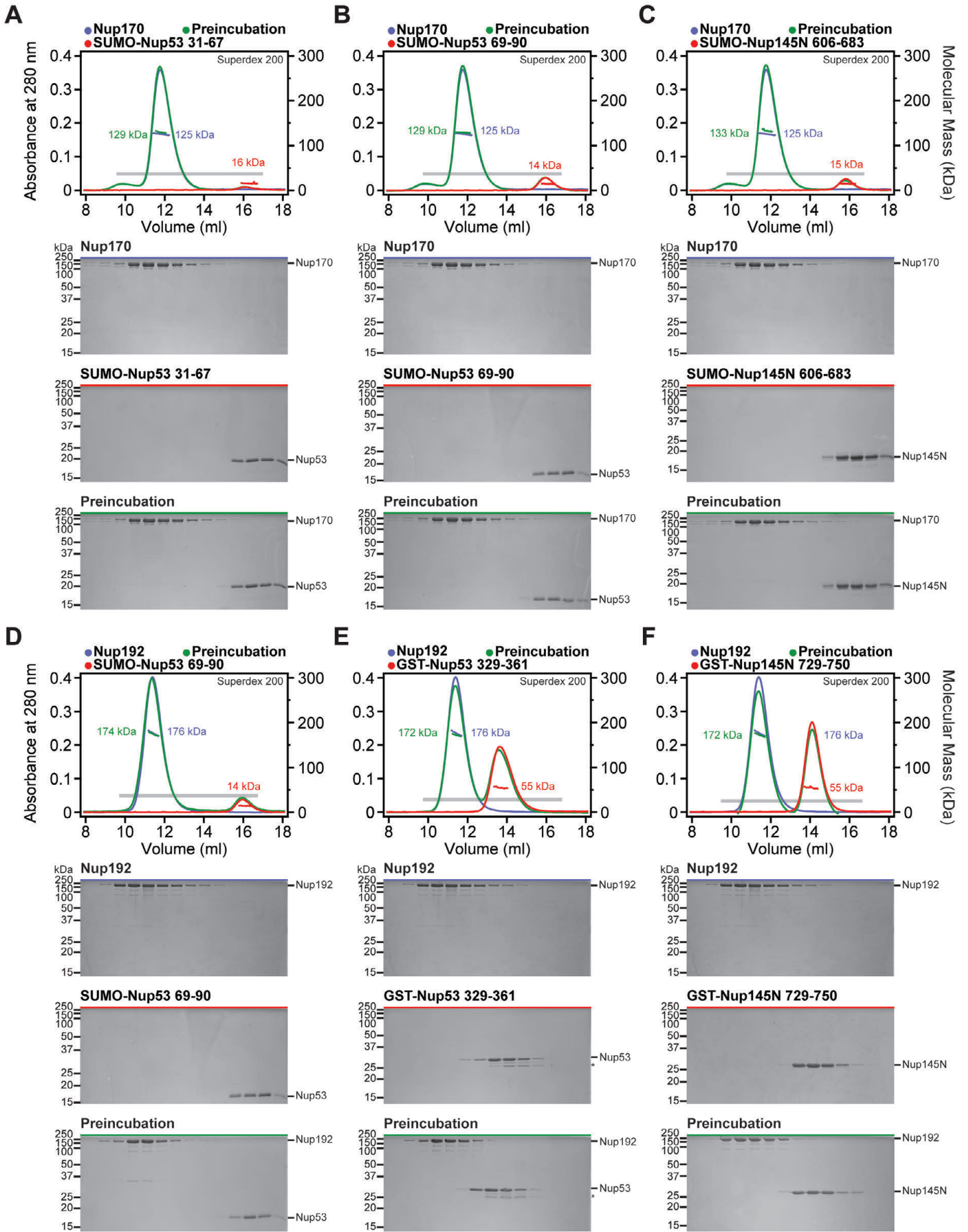


Fig. S17.

Nup192 recognizes Nup145N⁶⁰⁶⁻⁶⁸³ primarily with its NTD. (A-E) SEC-MALS and SDS-PAGE analysis corresponding to Fig. 2F. SEC-MALS profiles of nucleoporins are shown individually (blue and red) and after their preincubation (green). All SEC profiles were obtained using a Superdex 200 10/300 GL column. Measured molecular masses are indicated for the peak fractions. Gray bars indicate fractions that were resolved on SDS-PAGE gels and visualized by Coomassie staining. Nup192 binds to a minimal sequence on Nup145N between residues 606-683. After cleavage of Nup145N^{PreS} with PreScission protease, Nup145N^{MID} co-elutes with Nup192, whereas Nup145N^{APD} does not interact with Nup192. As a reference, the domain structure of Nup145N^{PreS} is shown, indicating the construct boundaries and PreScission cleavage site with a black bar and a black triangle, respectively. Nup145N forms a stoichiometric complex with Nup192^{NTD}, but Nup145N binding to Nup192^{CTD} and Nup192^{TAIL} were barely detectable and undetectable, respectively.



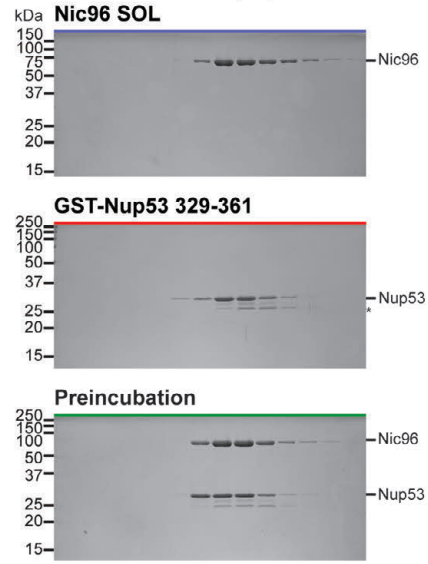
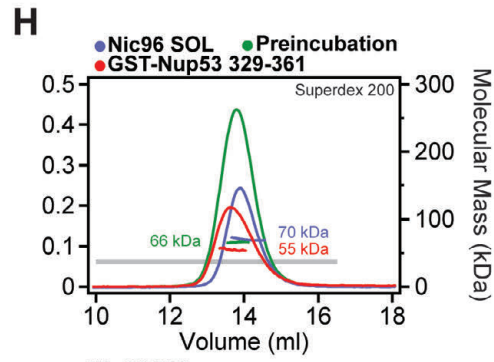
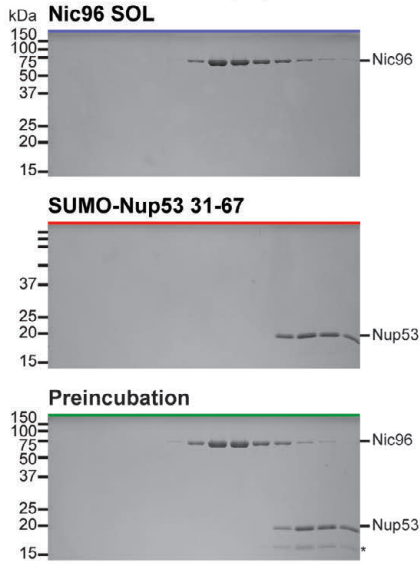
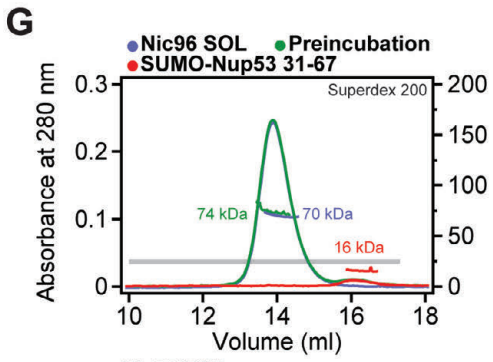
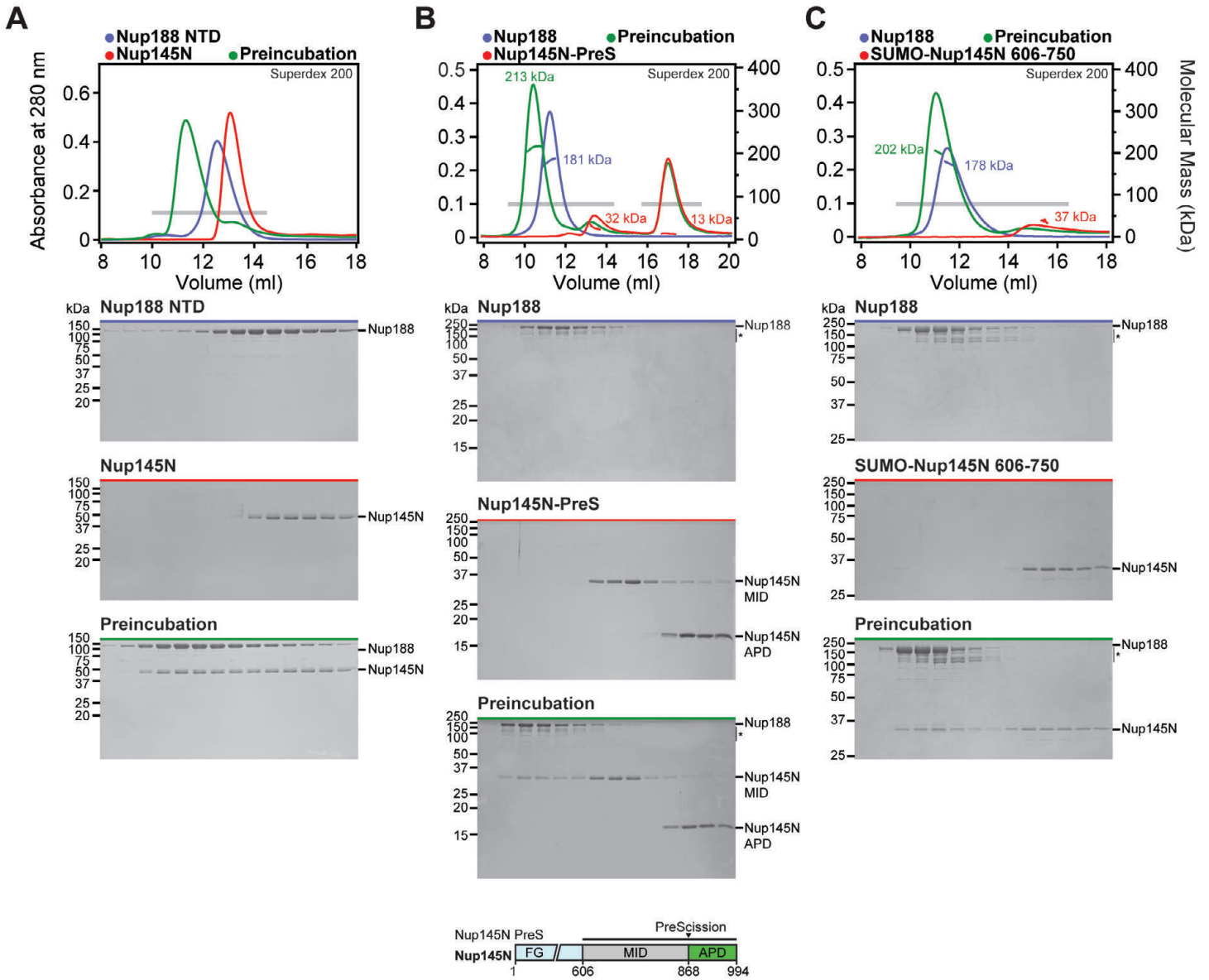


Fig. S18.

Mapped minimal linker nucleoporin fragments are specific for the identified binding partners. (A-H) SEC-MALS profiles of nucleoporins are shown individually (blue and red) and after their preincubation (green). All SEC profiles were obtained using a Superdex 200 10/300 GL column. Measured molecular masses are indicated for the peak fractions. Gray bars indicate fractions that were resolved on SDS-PAGE gels and visualized by Coomassie staining. The minimal sequence fragments of the linker nucleoporins Nup53 and Nup145N did not interact with other scaffold nucleoporins, demonstrating their specificity for a single scaffold nucleoporin.



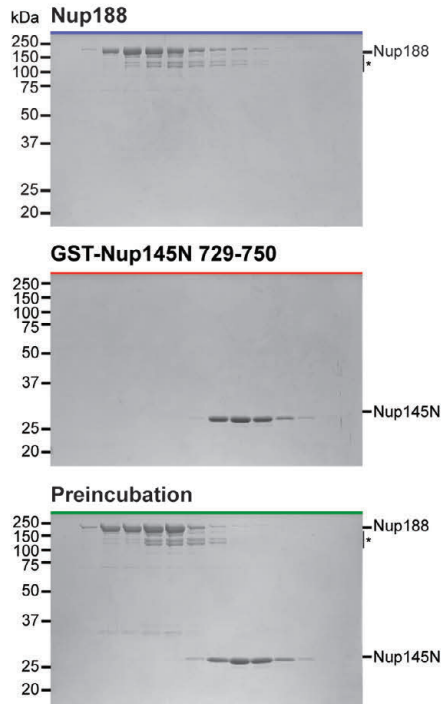
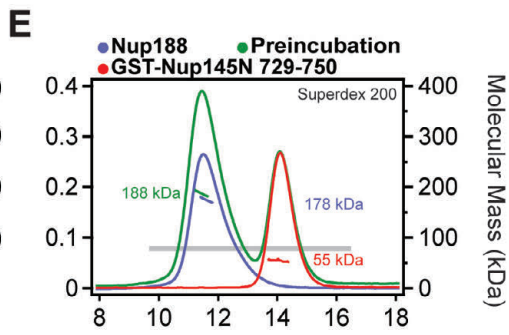
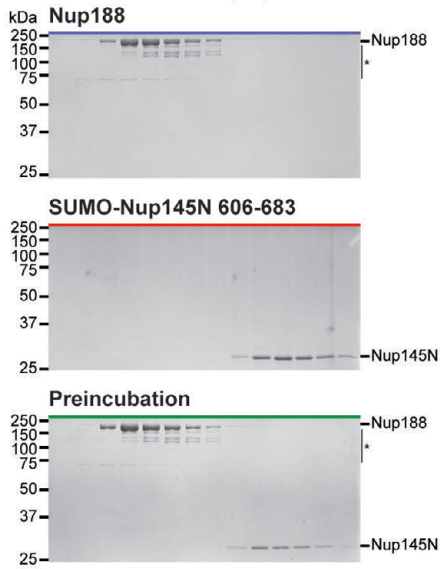
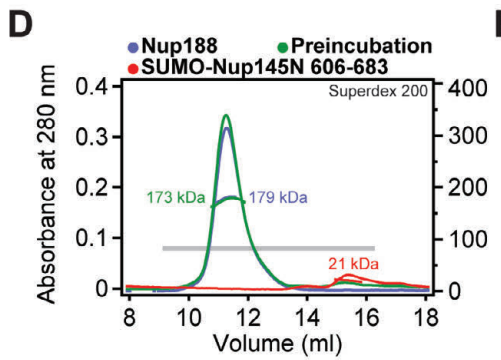
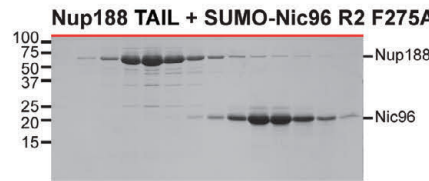
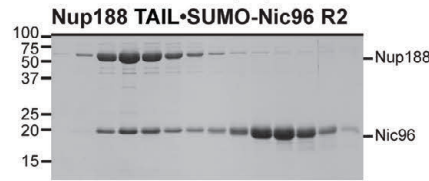
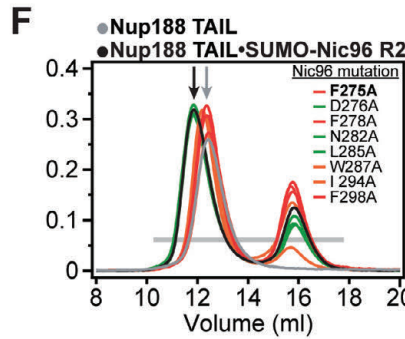
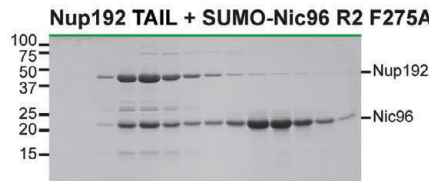
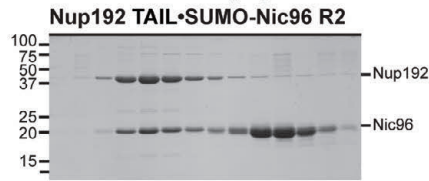
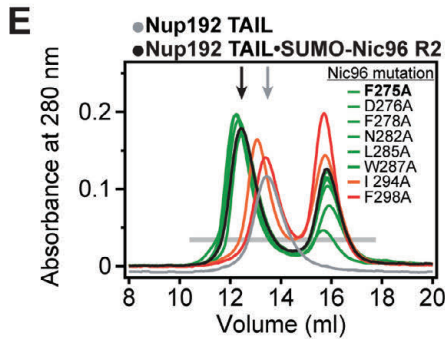
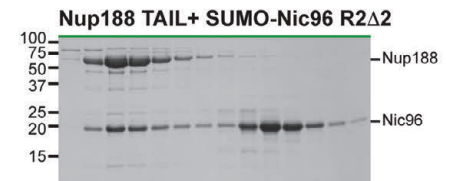
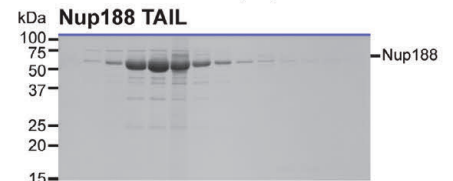
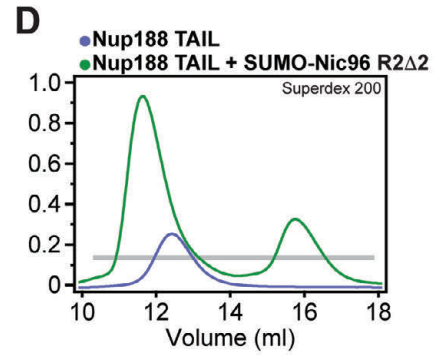
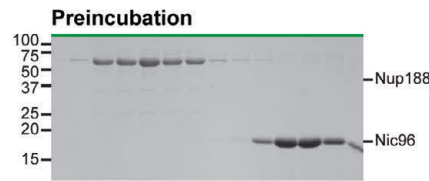
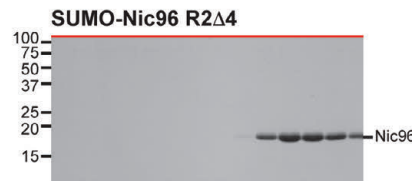
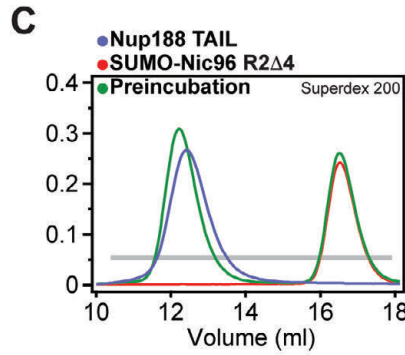
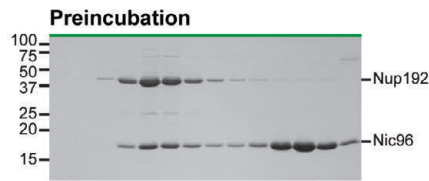
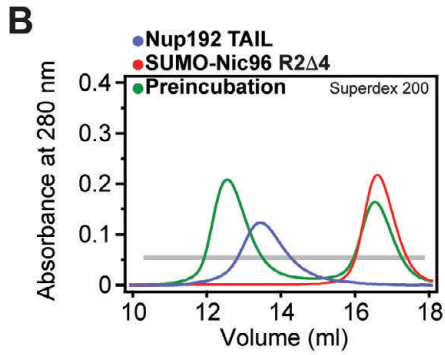
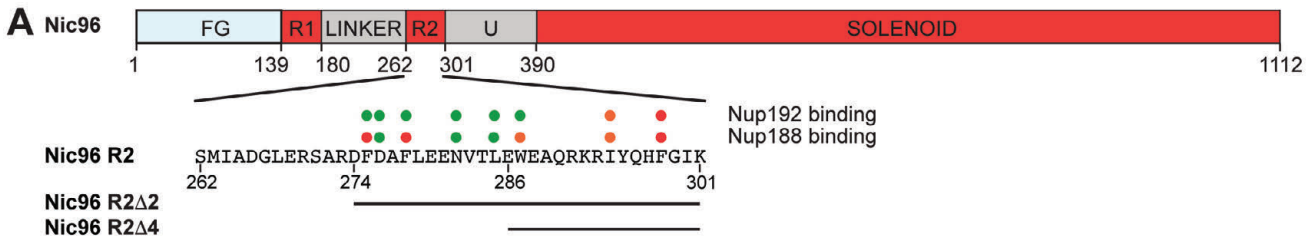


Fig. S19.

Nup188 recognizes Nup145N⁶⁰⁶⁻⁷⁵⁰ primarily via its NTD. (A-E) SEC-MALS and SDS-PAGE analysis corresponding to Fig. 2F. SEC-MALS profiles of nucleoporins are shown individually (blue and red) and after their preincubation (green). All SEC profiles were obtained using a Superdex 200 10/300 GL column. Measured molecular masses are indicated for the peak fractions. Gray bars indicate fractions that were resolved on SDS-PAGE gels and visualized by Coomassie staining. Nup188^{NTD} is responsible for binding Nup145N. After Nup145N^{PreS} cleavage with PreScission protease, Nup145N^{MID} co-elutes with Nup188, whereas Nup145N^{APD} does not interact with Nup188. As reference, the domain structure of Nup145N^{PreS} is shown, indicating the construct boundaries and PreScission cleavage site with a black bar and a black triangle, respectively. Nup188 binds to a minimal sequence on Nup145N between residues 606-750, but does not interact with the minimal Nup145N binding sequences for Nup192 or Nup170.



G

Nic96 mutation	Nup192 binding	Nic96 mutation	Nup188 binding
F275A	+++	F275A	-
D276A	+++	D276A	+++
F278A	+++	F278A	-
N282A	+++	N282A	+++
L285A	+++	L285A	+++
W287A	+++	W287A	+
I294A	+	I294A	+
F298A	-	F298A	-

Fig. S20.

Nup192^{TAIL} and Nup188^{TAIL} bind to partially overlapping sites in Nic96^{R2}. (A) Domain boundaries of Nic96 with the protein sequence corresponding to the R2 region shown below. Black lines indicate construct boundaries for Nic96^{R2}, Nic96^{R2Δ2}, and Nic96^{R2Δ4}. The effects of Nic96^{R2} alanine mutations on Nup192^{TAIL} and Nup188^{TAIL} binding are indicated by colored dots; no effect (green), reduced binding (orange), and complete disruption (red). (B-D) SEC and SDS-PAGE analysis corresponding to Fig. 2F. SEC profiles of nucleoporins are shown individually (blue and red) and after their preincubation (green). Nic96^{R2Δ2} is insoluble when expressed alone and therefore was expressed and purified in the presence of Nup188^{TAIL}. (E, F) Mutational analysis of the Nic96^{R2} interaction with Nup192^{TAIL} and Nup188^{TAIL}. SEC profiles of Nup192^{TAIL} or Nup188^{TAIL} are shown individually (gray) and after preincubation with wild type Nic96^{R2} (black) and are annotated with arrows of the same color. SEC profiles of mutant proteins preincubated with Nic96^{R2} are colored according to measured effect as in panel (A). All SEC profiles were obtained using a Superdex 200 10/300 GL column. Gray bars indicate fractions that were resolved on SDS-PAGE gels and visualized by Coomassie staining. (G) Table summarizing the measured effects of Nic96^{R2} mutation on Nup192^{TAIL} and Nup188^{TAIL} binding colored according to panel (A): no effect (+++), moderate effect (+), abolished binding (-). The Nic96^{R2} F275A mutant abolished binding to Nup188^{TAIL} but not to Nup192^{TAIL}.

Fig. S21.

Multispecies sequence alignment of Nup170. Sequences from twelve diverse species were aligned and colored by sequence similarity according to the BLOSUM62 matrix from white (less than 55 % similarity), to yellow (55 % similarity), to red (100 % identity). Numbering below alignment is relative to the *C. thermophilum* sequence. Secondary structure observed in the Nup170 structures is shown above the alignment: α -helices (red bars), β -sheets (blue bars), and unstructured regions (black lines). Mutations that affect Nup53 or Nup145N binding identified by a mutational analysis (Fig. 3; figs. S22; fig. S23) are indicated by circles above the alignment and colored according to the measured effect; weak effect (yellow), moderate effect (orange), abolished binding (red). Dashed lines indicate loops that were deleted in crystallization constructs. Disordered regions are indicated by gray dots.

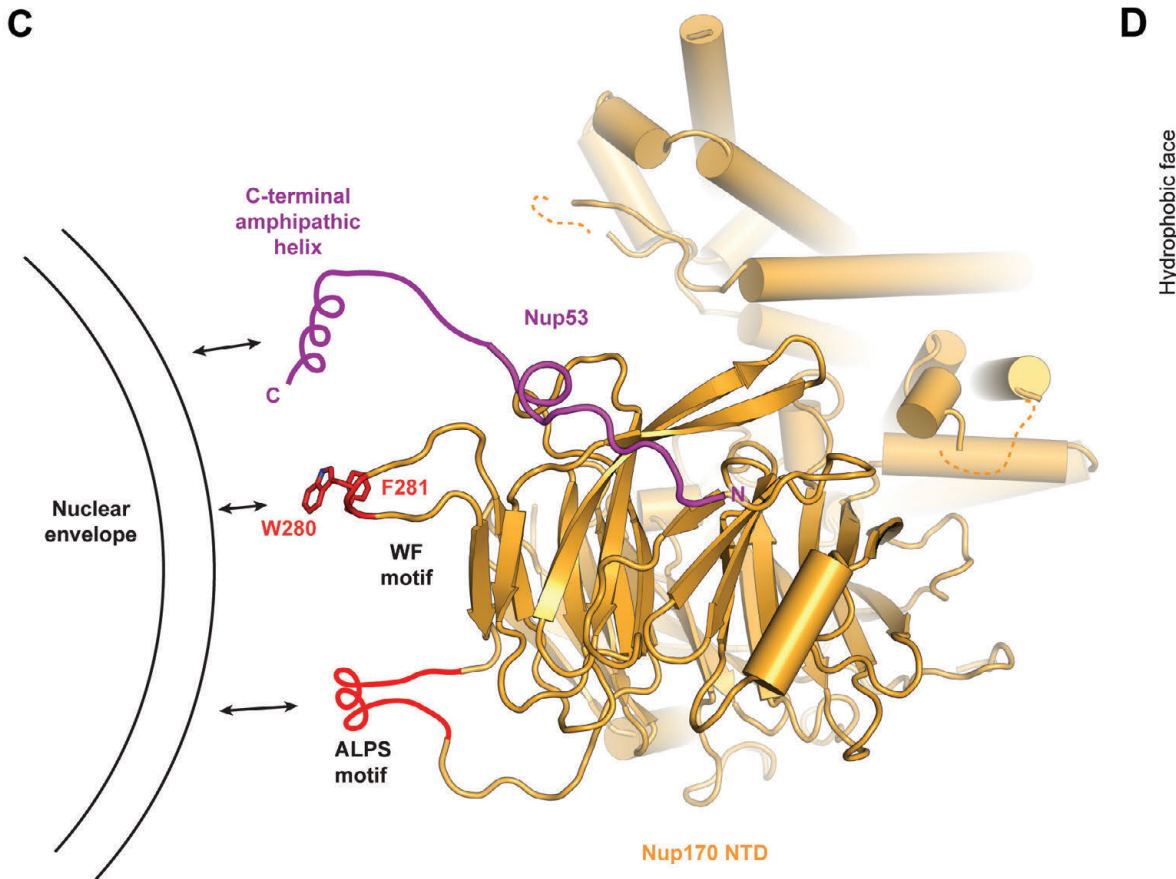
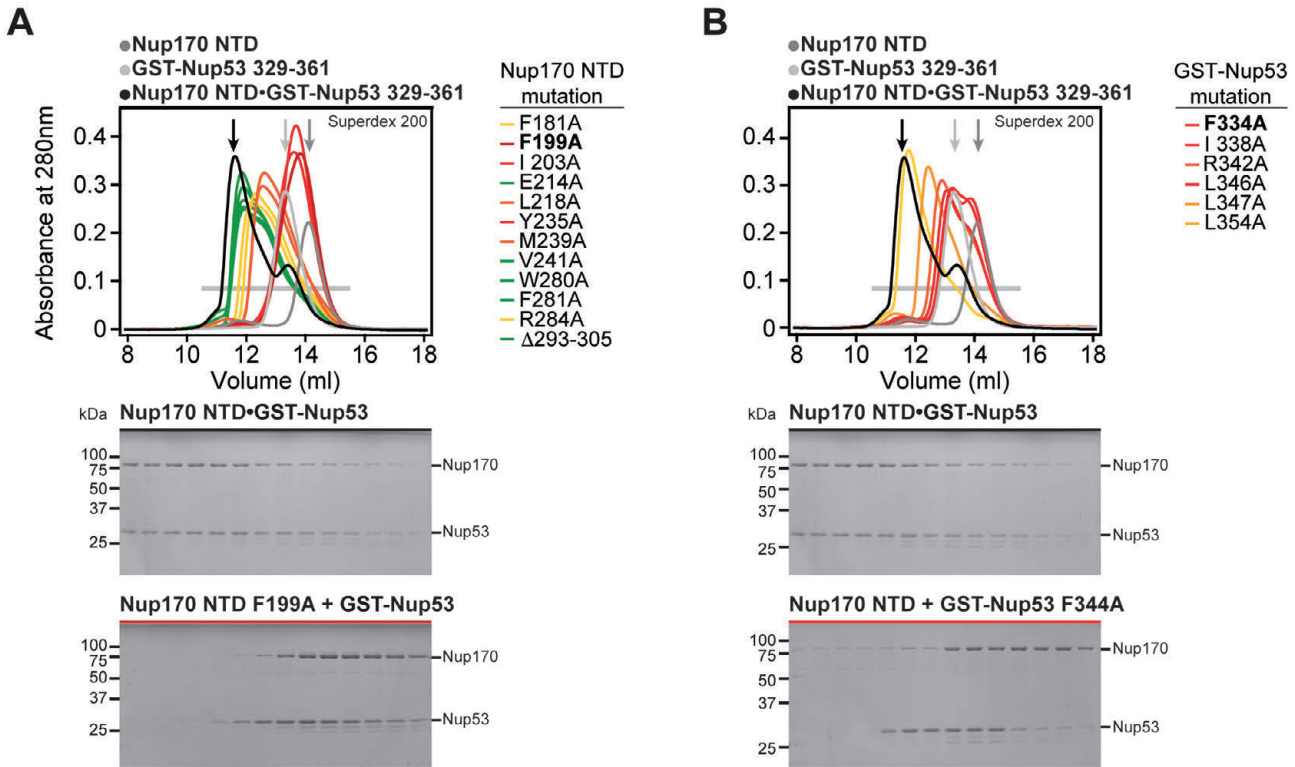
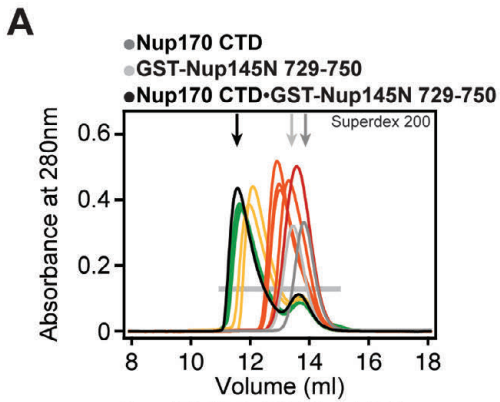


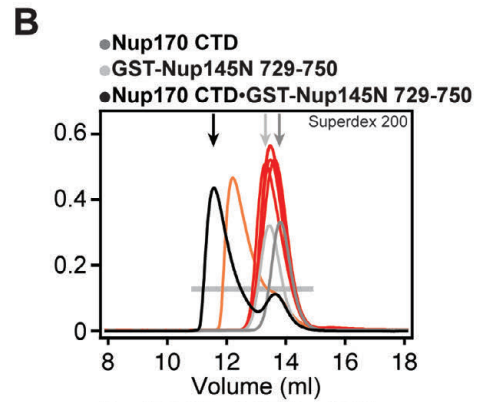
Fig. S22.

Mutational analysis of Nup170^{NTD}•Nup53 and proposed interactions with the nuclear envelope. SEC interaction experiments performed with mutants of (A) Nup170^{NTD} and (B) GST-Nup53³²⁹⁻³⁶¹. SEC profiles of wild type Nup170^{NTD} (dark gray) and GST-Nup53³²⁹⁻³⁶¹ (light gray) are shown individually and after preincubation (black) and are annotated with arrows of the same color. Mutant SEC profiles are colored according to the measured effect: no effect (green), weak effect (yellow), moderate effect (orange), and abolished binding (red). All SEC profiles were obtained using a Superdex 200 10/300 GL column. (C) Nup170^{NTD} is shown in cartoon representation and possible membrane interaction motifs are highlighted. The Nup170 β -propeller domain contains two sequence motifs, WF and ALPS, which are located on the same face directly adjacent to a C-terminal amphipathic helix of Nup53 that has previously been shown to anchor Nup53 to the nuclear envelope (18, 19). (D) Helical wheel diagrams of the Nup170 ALPS motif in *C. thermophilum*, *S. cerevisiae*, and *H. sapiens* are shown with hydrophobic and polar residues colored in yellow and purple, respectively. The universally conserved proline residue on the polar face of the helix, a feature reminiscent of antimicrobial membrane-destabilizing peptides, is colored in red (34).



Nup170 CTD mutation

- V1062A
- V1066A
- E1116A
- L1111A
- I1131A
- I1147A
- F1154A
- Y1157A
- Y1164A
- F1171A



GST-Nup145N mutation

- I735A
- L733A
- V734A
- D742A
- L743A
- F744A

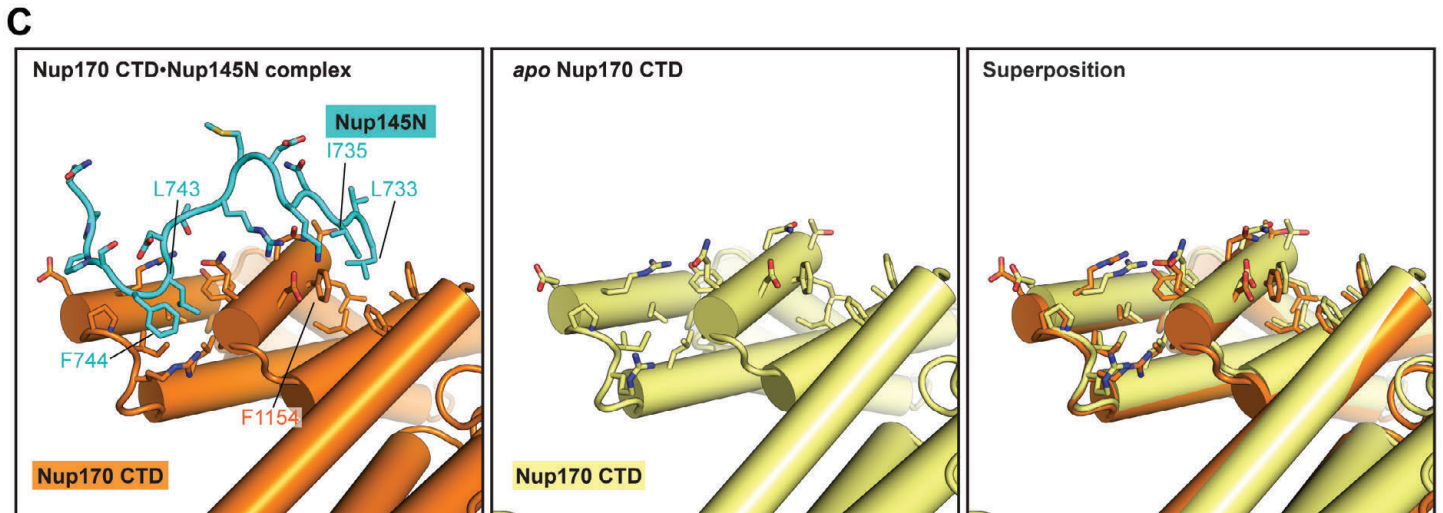
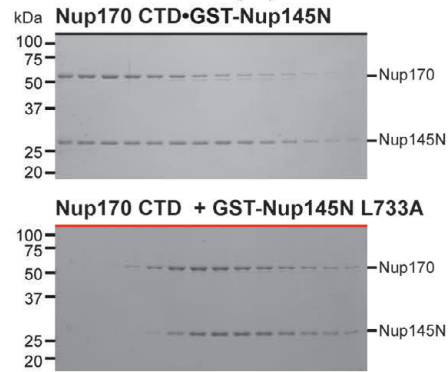
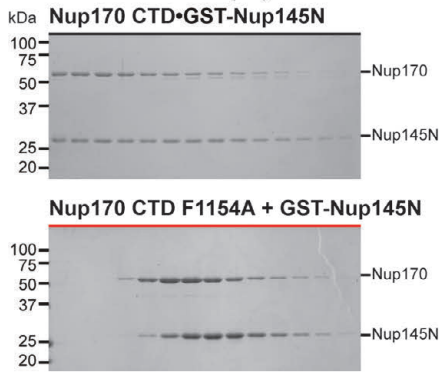


Fig. S23.

Mutational and structural analyses of the Nup170^{CTD}-Nup145N interaction. SEC interaction experiments performed with mutants of **(A)** Nup170^{CTD} and **(B)** GST-Nup145N⁷²⁹⁻⁷⁵⁰. SEC profiles of wild type Nup170^{CTD} (dark gray) and GST-Nup145N⁷²⁹⁻⁷⁵⁰ (light gray) are shown individually and after preincubation (black) and are annotated with arrows of the same color. Mutant SEC profiles colored according to measured effect: no effect (green), weak effect (yellow), moderate effect (orange), and abolished binding (red). All SEC profiles were obtained using a Superdex 200 10/300 GL column. **(C)** Comparison of the Nup145N binding pocket in Nup170 in the bound and *apo* states reveals minimal conformational changes upon binding.

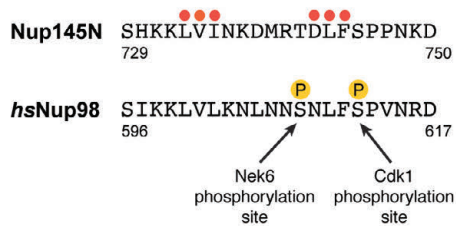
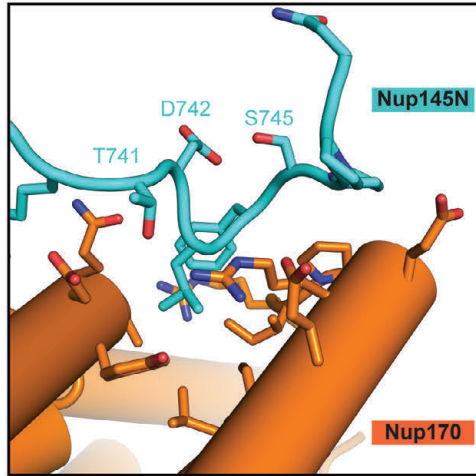
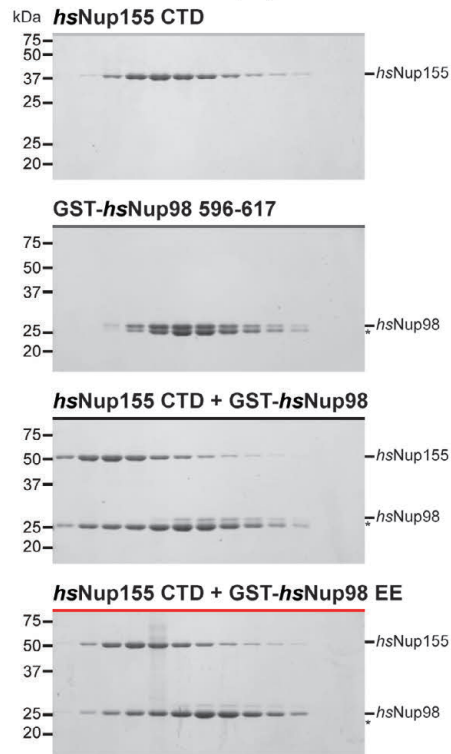
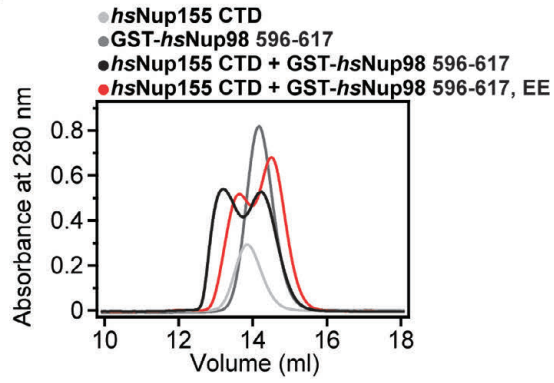
A**B****C**

Fig. S24.

The Nup170^{CTD}-Nup145N interaction is conserved in humans and partially disrupted by phosphomimetic mutations. (A) Sequence alignment of Nup145N⁷²⁹⁻⁷⁵⁰ and *hsNup98*⁵⁹⁶⁻⁶¹⁷. Nup145N⁷²⁹⁻⁷⁵⁰ mutants are indicated by circles and colored as in Fig. 3J. *hsNup98* residues S608 and S612 that are phosphorylated during mitosis are indicated (35). (B) Close-up view of the Nup170^{CTD}-Nup145N interaction indicating the positioning of T741 and S745 in Nup145N, which correspond to the mitotically phosphorylated *hsNup98* residues S608 and S612. (C) SEC interaction analysis of the *hsNup155*^{CTD}-*hsNup98*⁵⁹⁶⁻⁶¹⁷ interaction. SEC profiles of *hsNup155*^{CTD} (light gray) and *hsNup98*⁵⁹⁶⁻⁶¹⁷ (dark grey), the preincubation of the wild type proteins (black), and the preincubation of *hsNup155*^{CTD} with the phosphomimetic *hsNup98*⁵⁹⁶⁻⁶¹⁷ S608E/S612E double mutant (red) are shown. All SEC profiles were obtained using a Superdex 200 10/300 GL column. Gray bars indicate fractions that were resolved on SDS-PAGE gels and visualized by Coomassie staining.

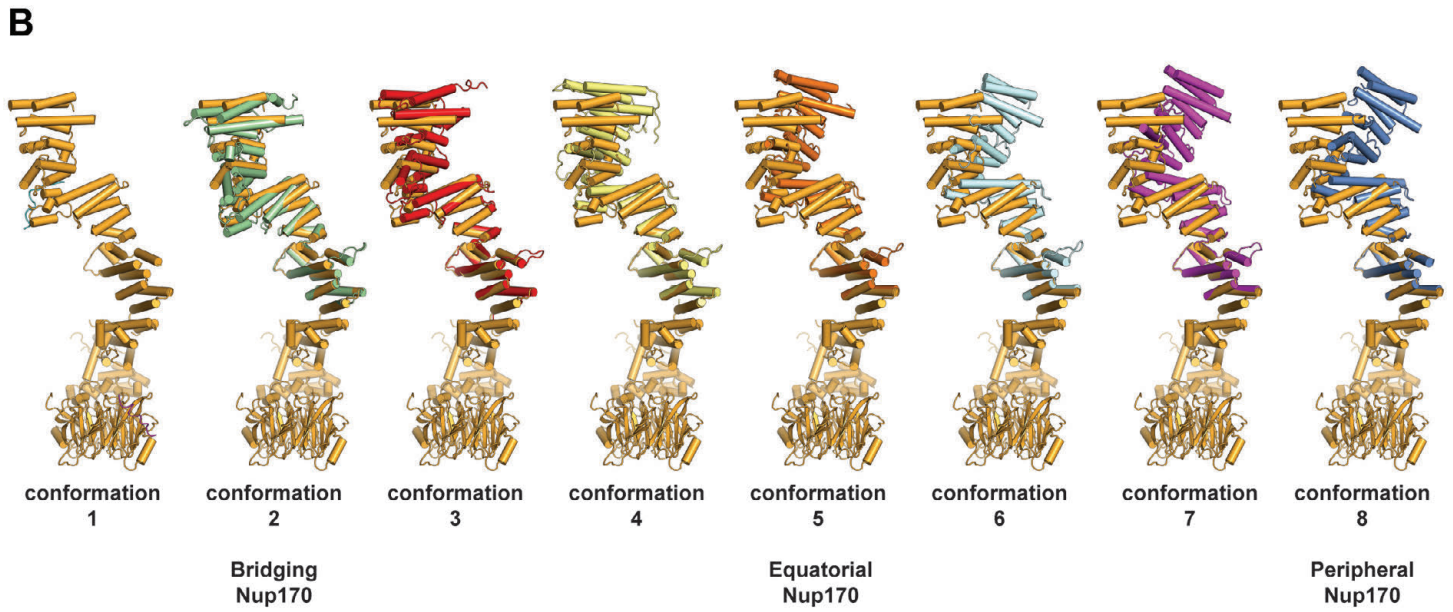
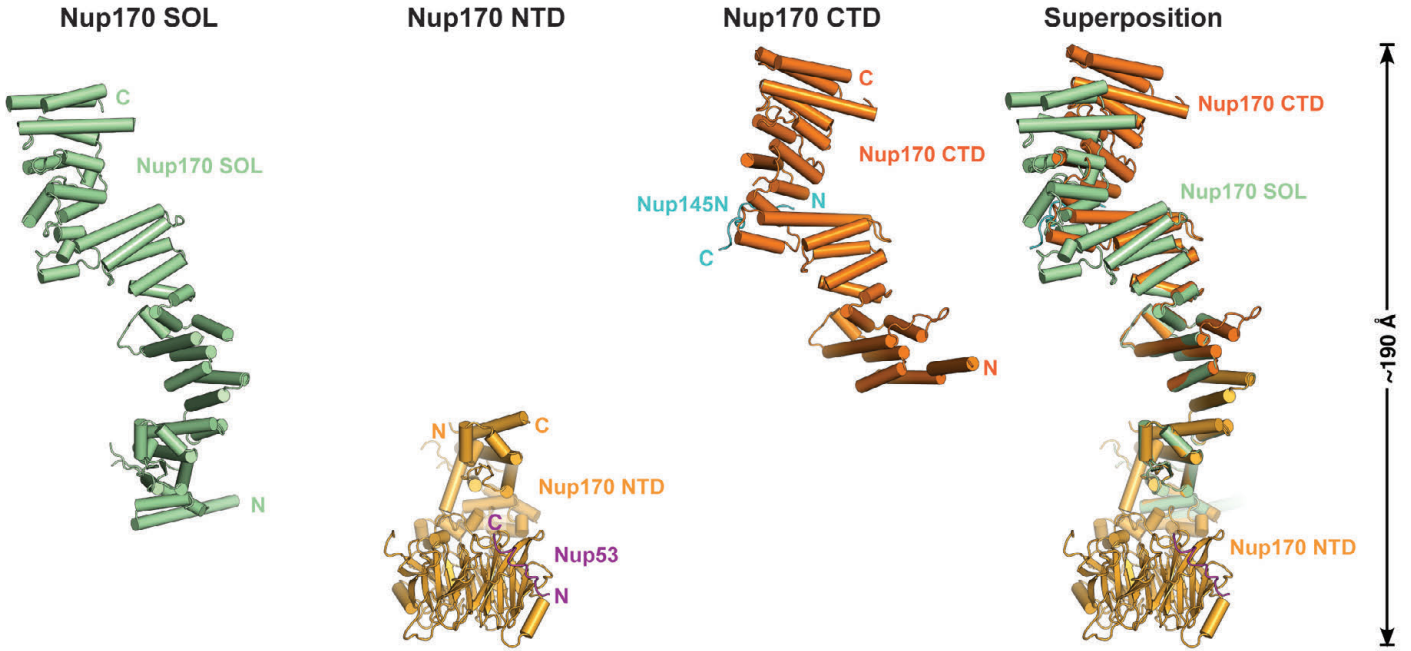
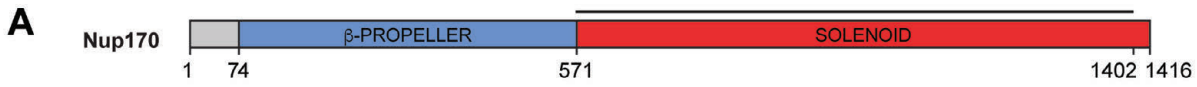


Fig. S25.

Superposition-generated structures of full-length Nup170. (A) The construct boundaries of Nup170^{SOL} are indicated by a black line above the domain structure. The crystal structures of Nup170^{SOL} (green), Nup170^{NTD} (light orange), and Nup170^{CTD} (dark orange), and their superposition are shown in cartoon representation. See also [Movie 1](#). (B) Complete conformational range of Nup170 generated by superposing different conformations of Nup170^{CTD} with the structure of Nup170^{SOL}. Conformations were obtained from the Nup170^{SOL} structure (conformation 1), different molecules in the asymmetric unit of the *apo* Nup170^{CTD} structures (conformations 2, 3, and 4), and different molecules in the asymmetric unit of the Nup170^{CTD}•Nup145N complex structure (conformations 5, 6, 7, and 8). The conformations that were docked into cryoET reconstruction of the NPC are indicated below. See also [Movie 2](#).

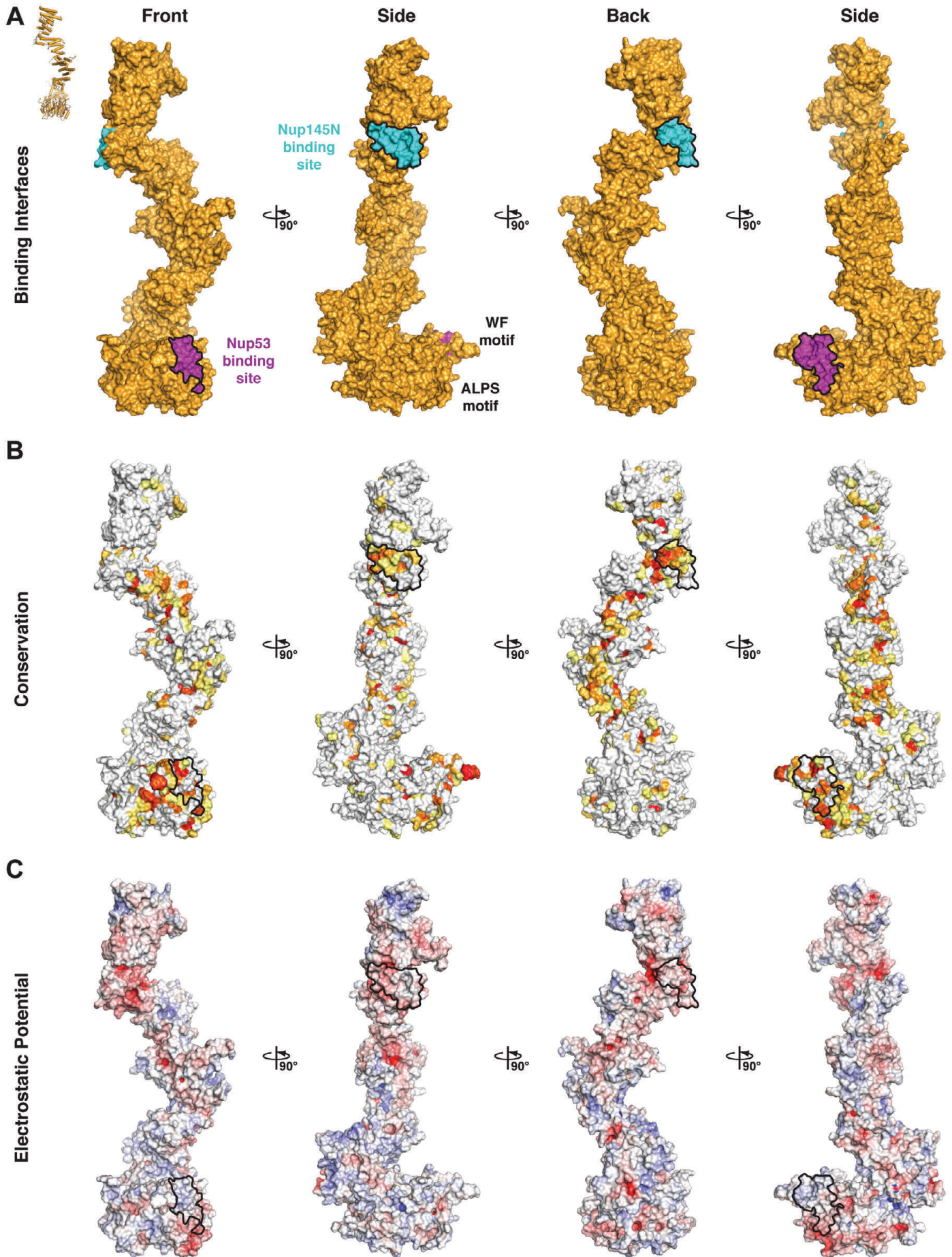


Fig. S26.

Surface properties of Nup170. Surface representations of Nup170 is shown in four different orientations related by 90° rotations. Nup53 and Nup145N binding interfaces are outlined in black. **(A)** Surface representation with the Nup53 and Nup145N binding sites colored in purple and cyan, respectively. **(B)** Surface representation colored according to sequence identity based on the alignment in [fig. S21](#). **(C)** Surface representation colored according to electrostatic potential from $-10 k_B T/e$ (red) to $+10 k_B T/e$ (blue).

Nic96

$\alpha 26$

<i>C.thermophilum</i>	V	V	S	I	V	S	R	A	L	S	E	A	I	S	L	E	I	G	E	D	P	M	R	L	I	P	V	K	P	R	.	.	V	T	N	A	E	G	Q	V	E	E	A	A	P	G	S	S	L	S	L
<i>A.nidulans</i>	V	I	D	I	I	N	R	T	L	S	D	S	V	A	T	P	L	G	S	P	T	L	R	L	Q	P	L	W	P	R	T	N	L	S	Q	E	S	G	Q	E	T	P	I	E	P	G	T	S	L	S	L
<i>N.crassa</i>	V	I	A	I	V	S	R	A	L	S	E	A	V	S	L	E	I	G	E	D	P	L	R	L	V	P	I	K	P	R	A	D	G	D	V	A	N	A	Q	Q	G	T	S	L	S	L	
<i>P.pastoris</i>	V	I	S	L	I	N	K	L	L	G	D	L	L	A	S	T	D	L	E	T	A	I	D	T	P	A	E	R			
<i>A.gossypii</i>	V	I	S	I	V	N	K	L	L	S	E	M	L	S	N	T	D	L	A	Q	P	L	M	R	Q	D	D	N	S	E	T					
<i>S.cerevisiae</i>	V	I	T	L	V	N	S	L	L	S	D	T	L	S	A	S	D	L	D	Q	P	L	V	G	P	D	D	N	S	E	T				
<i>S.pombe</i>	V	I	G	V	A	I	K	N	L	S	Q	S	I	V	S	R	G	L	W	S	I	D	S	K	E	S	K	N	M	H	I	S	S	N	V				
<i>C.elegans</i>	A	A	I	L	L	S	S	E	I	S	E	T	L	R	T			
<i>D.melanogaster</i>	A	L	R	L	V	N	S	L	L	A	Q	V	V	H	Q	P	T	Q	N	G	S	V	R	N	R				
<i>D.erio</i>	V	L	E	L	M	N	K	L	L	S	P	V	I	A	Q	V	S	E	P	Q	S	N	K	E	R					
<i>X.laevis</i>	V	L	E	L	T	N	K	L	L	S	P	V	V	S	Q	I	S	A	P	Q	S	N	R	E	R					
<i>H.sapiens</i>	V	L	E	L	M	N	K	L	L	S	P	V	V	P	Q	I	S	A	P	Q	S	N	K	E	R					
900	910										920										930										940										948										

$\alpha 27$ $\alpha 28$

<i>C.thermophilum</i>	A	A	I	D	D	P	V	E	L	A	K	A	M	M	G	M	Y	E	R	D	H	M	F	W	Q	K	I	R	E	P	N	R	V	A	C	S	V	L	L	Q	M	A	D	I	K	S	L	V	E	Q	G	
<i>A.nidulans</i>	T	V	V	E	D	P	V	V	L	A	K	N	M	I	G	L	Y	N	Q	N	A	L	Y	Y	Q	R	I	R	R	S	N	R	D	A	C	G	V	L	L	R	M	M	E	A	K	A	E	V	E	A	G	
<i>N.crassa</i>	A	A	I	D	D	P	V	E	L	A	H	T	M	M	S	M	Y	E	R	D	A	M	F	L	N	H	V	R	D	Q	N	R	I	A	C	N	I	L	L	K	M	S	E	I	K	E	M	I	Q	R	N	
<i>P.pastoris</i>	A	A	E	G	S	I	A	L	A	E	R	L	M	K	Q	Y	S	S	T	E	I	S	G	K	V	L	L	K	H	R	E	T	C	S	I	L	L	L	K	M	V	E	C	R	D	L	F	V	K	Q		
<i>A.gossypii</i>	N	P	V	L	I	A	K	K	L	I	D	V	Y	I	K	N	L	E	I	S	K	V	H	R	K	N	K	E	T	C	I	L	L	L	K	L	V	D	I	R	R	T	Y	I	A	R	
<i>S.cerevisiae</i>	N	P	V	L	L	A	R	R	M	A	S	I	Y	F	D	N	A	G	I	S	R	Q	I	H	V	K	N	K	E	I	C	M	L	L	L	N	I	S	S	I	R	E	L	Y	F	N	K
<i>S.pombe</i>	V	A	S	E	A	P	D	A	L	A	A	N	L	L	A	M	Y	E	S	N	P	K	K	S	A	K	V	S	A	T	N	K	K	A	L	K	V	L	L	K	V	V	K	V	Q	K	L	Y	G	Q	E	
<i>C.elegans</i>	I	A	D	.	L	V	H	V	A	E	Q	F	K	K	V	Q	R	G	C	Q	A	S	E	Y	A	T	L	S	L	L	V	D	L	A	V	L	F	D	H	C	R	N	E
<i>D.melanogaster</i>	L	G	D	I	I	N	R	L	D	A	A	L	V	V	R	K	S	D	V	E	V	Q	V	V	V	T	Y	T	V	L	T	K	V	M	K	F	F	D	H	Y	H	E	G
<i>D.erio</i>	L	K	N	M	A	V	A	I	A	E	R	Y	R	A	N	G	V	A	G	E	K	S	V	D	N	T	F	Y	L	L	L	D	L	M	T	F	F	D	E	Y	H	A	G
<i>X.laevis</i>	L	K	N	M	A	L	A	I	A	E	R	Y	K	S	Q	G	V	S	A	E	K	S	I	N	S	T	F	Y	L	L	L	D	L	I	T	F	F	D	E	Y	H	A	G
<i>H.sapiens</i>	L	K	N	M	A	L	S	I	A	E	R	Y	R	A	Q	G	I	S	A	N	K	F	V	D	S	T	F	Y	L	L	L	D	L	I	T	F	F	D	E	Y	H	S	G
949	960										970										980										990										999											

$\alpha 29$ $\alpha 30$ $\alpha 31$

<i>C.thermophilum</i>	R	W	A	E	C	L	D	K	I	R	A	L	D	I	L	P	L	T	A	R	G	D	P	G	T	I	R	S	Y	A	A	R	F	P	S	L	A	Q	P	V		
<i>A.nidulans</i>	K	W	T	A	A	L	D	T	I	N	E	L	G	I	L	P	L	R	A	N	G	S	V	P	Y	I	R	S	A	A	Q	A	F	S	S	L	S	S	L	I		
<i>N.crassa</i>	E	W	A	Q	A	I	D	V	I	R	S	L	E	I	L	P	T	D	D	C	M	G	D	P	A	K	I	R	S	Y	A	S	K	F	S	S	L	P	Q	P	E	V
<i>P.pastoris</i>	E	W	E	K	A	L	K	Q	I	G	Q	L	D	M	L	P	I	V	A	G	V	N	V	A	V	A	R	S	K	V	E	V	F	N	S	Y	D	E	S	V	
<i>A.gossypii</i>	Q	W	Q	N	T	L	Q	Q	I	E	E	L	D	L	L	P	S	V	E	D	S	S	P	R	K	K	A	Q	E	F	H	N	L	D	D	C	I			
<i>S.cerevisiae</i>	Q	W	Q	E	T	L	S	Q	M	E	L	L	D	L	L	P	F	S	D	E	L	S	A	R	K	K	A	Q	D	F	S	N	L	D	D	N	I			
<i>S.pombe</i>	K	W	E	V	L	Q	L	I	E	H	L	D	L	L	P	I	N	E	V	Q	A	E	F	E	P	N	E	Q	I	P	P	I	S	A	R	L	R	R	A	F	E	F	S	T	F	Q	D	E	V	
<i>C.elegans</i>	E	A	E	I	A	Y	G	I	S	T	H	L	R	L	I	P	T	E	P	D	Q	V	T	V	I	V	N	E	F	H	M	V	P	Q	K	V				
<i>D.melanogaster</i>	A	L	R	S	A	L	E	I	L	T	N	N	H	L	I	P	A	S	S	L	E	V	D	E	C	V	T	N	I	K	R	M	G	P	E	V				
<i>D.erio</i>	H	I	D	R	A	Y	D	V	I	E	R	L	K	L	V	P	L	S	Q	D	S	V	E	E	R	V	A	A	F	R	N	F	S	D	E	V				
<i>X.laevis</i>	H	I	D	L	S	F	D	V	I	E	R	L	K	L	V	P	L	S	Q	D	S	V	E	E	R	V	A	A	F	R	N	F	S	D	E	I				
<i>H.sapiens</i>	H	I	D	R	A	F	D	I	E	R	L	K	L	V	P	L	N	Q	E	S	V	E	E	R	V	A	A	F	R	N	F	S	D	E	I					
1000	1010										1020										1030										1039																			

$\alpha 32$ $\alpha 33$

<i>C.thermophilum</i>	A	I	N	V	P	N	L	L	M	W	T	V	L	C	C	M	R	Q	R	E	R	L	A	G	G	Q	F	A	G	N	E	S	T	A	R	L	M	M	D	E	L	K	Q	M		
<i>A.nidulans</i>	S	G	N	I	G	H	V	I	W	S	I	T	C	I	C	I	G	R	E	R	E	R	L	N	T	G	P	Y	.	.	E	N	E	M	R	O	G	L	A	E	E	L	L	V	M	
<i>N.crassa</i>	A	I	N	V	P	N	L	L	M	W	T	I	I	C	C	T	R	Q	R	E	R	E	R	L	N	T	G	Q	F	V	G	N	T	G	T	A	R	E	M	L	A	R	L	K	Q	I
<i>P.pastoris</i>	A	K	N	V	P	D	L	L	V	M	T	L	T	C	I	A	Q	L	T	Y	Q	L	T	S	S	E	F	.	.	N	G	L	V	K	S	D	K	I	K	Y	L	K	E	V
<i>A.gossypii</i>	I	K	N	V	P	N	L	L	I	I	A	M	T	C	V	S	N	L	I	K	Q	L	S	K	G	P	F	.	.	S	N	G	A	T	Q	A	Q	V	E	A	L	K	K	V
<i>S.cerevisiae</i>	V	K	N	I	P	N	L	L	I	I	T	L	S	C	I	S	N	M	I	H	I	L	N	E	S	K	Y	.	.	Q	S	S	T	K	G	Q	Q	I	D	S	L	K	N	V
<i>S.pombe</i>	L	S	V	I	P	S	L	M	Y	I	S	M	S	S	I	K	A	L	Y	R	T	I	S	K	L	P	V	.	.	V	N	E	E	S	K	K	L	Q	R	L	Q	F	K	
<i>C.elegans</i>	R	E	V	L	P	D	M	C	L	H	L	M	K	C	L	V	D	H	C	I	R	Q	S	T	T	Q	A	N	R	G	A	.	.	N	S	A	T	T	S	M	F	S	S	S	N	R	Y	V	K	Q		
<i>D.melanogaster</i>	I	K	V	L	P	D	I	L	L	A	S	M	D	I	V	Y	Q	E	Y	V	K	L	M	D	S	N	E	T	A	S	G	F	F	D	E	S	K	V	N	K	E	P	A	V	K	H	L	R	D	R		
<i>D.erio</i>	R	H	N	L	S	E	V																																													

Fig. S27.

Multispecies sequence alignment of Nic96^{SOL}. Sequences from twelve diverse species were aligned and colored by sequence similarity according to the BLOSUM62 matrix from white (less than 55 % similarity), to yellow (55 % similarity), to red (100 % identity). Numbering below alignment is relative to the *C. thermophilum* sequence. Secondary structure observed in the Nic96 structure is shown above the alignment: α -helices (red bars), β -sheets (blue bars), and unstructured regions (black lines). The secondary structure of R2 is unknown, but predicted to be helical, which is indicated by a red outline. Mutations that affect binding to Nup53, Nup188, or Nup192 found by mutational analysis (figs. S20 and S28) are indicated by circles above the alignment and colored according to the measured effect; weak effect (yellow), moderate effect (orange), and abolished binding (red). Disordered regions are indicated by gray dots.

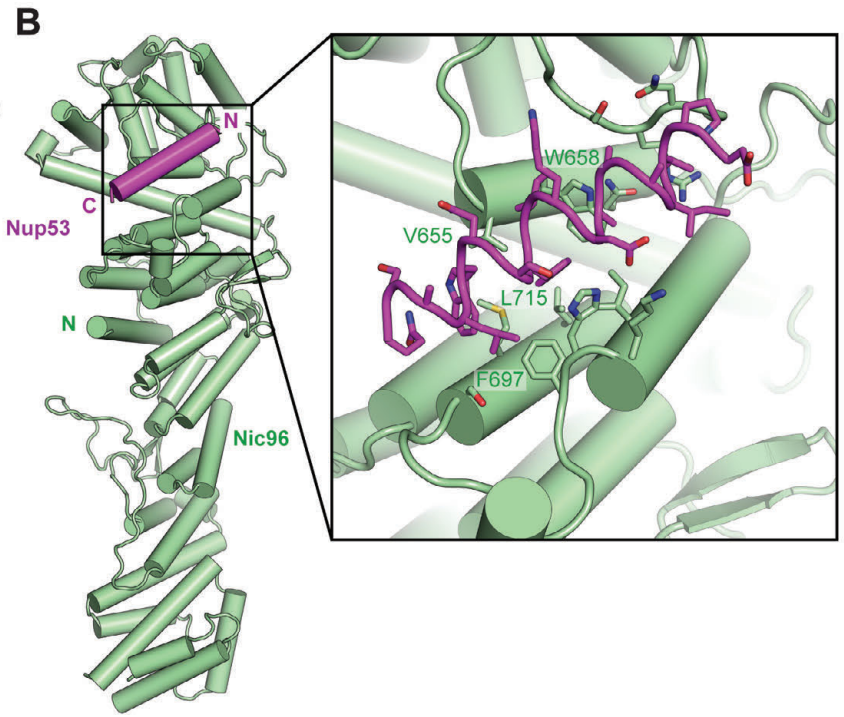
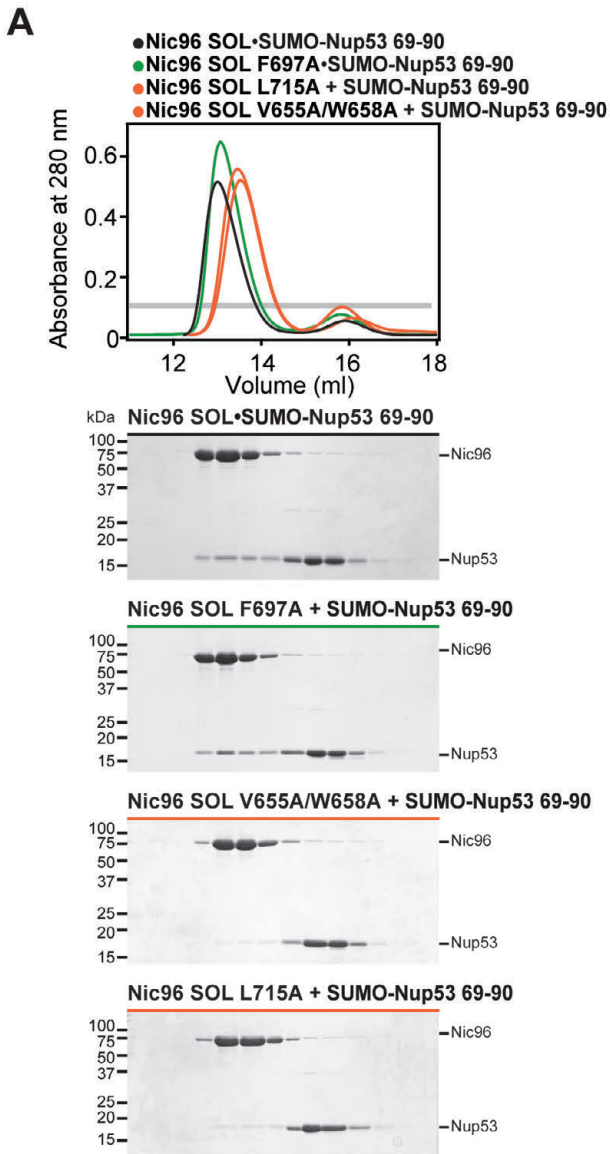


Fig. S28.

Identification of Nic96^{SOL} mutants that disrupt Nup53 binding. (A) SEC interaction analysis between Nic96^{SOL} mutants and SUMO-Nup53^{R2}. SEC profiles are colored according to the effect on SUMO-Nup53^{R2} binding; no effect (green), moderate effect (orange), or abolished binding (red). For reference, the SEC profile of the wild type Nic96^{SOL}•SUMO-Nup53^{R2} hetero-dimer (black) is shown. All SEC profiles were obtained using a Superdex 200 10/300 GL column. A gray bar indicates fractions that were resolved on SDS-PAGE gels and visualized by Coomassie staining. (B) The structure of Nic96^{SOL}•Nup53^{R2} is shown in cartoon representation. The inset illustrates the region that is expanded on the right with mutated residues labeled in green.

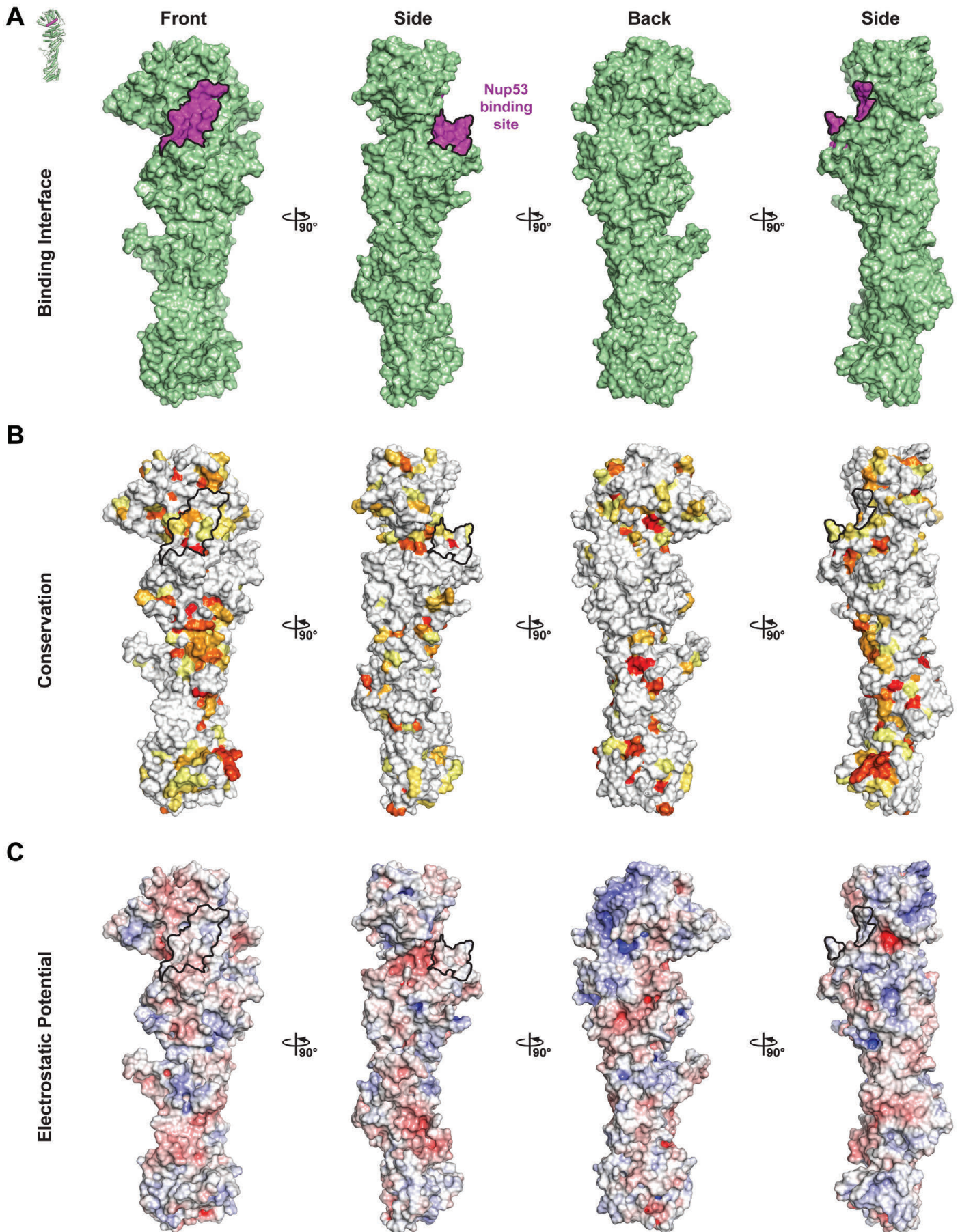


Fig. S29.

Surface properties of Nic96^{SOL}. Surface representations of Nic96^{SOL} are shown in four different orientations related by 90° rotations. The Nup53 binding interface is outlined in black. **(A)** Surface representation with the Nup53 binding site colored in purple. **(B)** Surface representation colored according to sequence identity based on the alignment in [fig. S27](#). **(C)** Surface representation colored according to electrostatic potential from -10 $k_B T/e$ (red) to +10 $k_B T/e$ (blue).

Nup192

- C.thermophilum
A.nidulans
N.crassa
P.pastoris
A.gossypii
S.cerevisiae
S.pombe
C.elegans
D.melanogaster
D.erio
X.laevis
H.sapiens

Table showing amino acid sequence for Nup192, residues 590-638. Helices alpha 26, alpha 27, and alpha 28 are indicated above the sequence.

- C.thermophilum
A.nidulans
N.crassa
P.pastoris
A.gossypii
S.cerevisiae
S.pombe
C.elegans
D.melanogaster
D.erio
X.laevis
H.sapiens

Table showing amino acid sequence for Nup192, residues 639-689. Helices alpha 29 and alpha 30 are indicated above the sequence.

- C.thermophilum
A.nidulans
N.crassa
P.pastoris
A.gossypii
S.cerevisiae
S.pombe
C.elegans
D.melanogaster
D.erio
X.laevis
H.sapiens

Table showing amino acid sequence for Nup192, residues 690-731. Helices alpha 31 and alpha 32 are indicated above the sequence.

- C.thermophilum
A.nidulans
N.crassa
P.pastoris
A.gossypii
S.cerevisiae
S.pombe
C.elegans
D.melanogaster
D.erio
X.laevis
H.sapiens

Table showing amino acid sequence for Nup192, residues 732-780. Helices alpha 33 and alpha 34 are indicated above the sequence.

- C.thermophilum
A.nidulans
N.crassa
P.pastoris
A.gossypii
S.cerevisiae
S.pombe
C.elegans
D.melanogaster
D.erio
X.laevis
H.sapiens

Table showing amino acid sequence for Nup192, residues 781-830. Helices alpha 34, alpha 35, and alpha 36 are indicated above the sequence.

Nup192

C.thermophilum
A.nidulans
N.crassa
P.pastoris
A.gossypii
S.cerevisiae
S.pombe
C.elegans
D.melanogaster
D.erio
X.laevis
H.sapiens

Sequence alignment for Nup192, residues 1019-1059. Helices alpha48 and alpha49 are highlighted in red. Conserved residues are in yellow.

C.thermophilum
A.nidulans
N.crassa
P.pastoris
A.gossypii
S.cerevisiae
S.pombe
C.elegans
D.melanogaster
D.erio
X.laevis
H.sapiens

Sequence alignment for Nup192, residues 1060-1107. Helices alpha50 and alpha51 are highlighted in red. Conserved residues are in yellow.

C.thermophilum
A.nidulans
N.crassa
P.pastoris
A.gossypii
S.cerevisiae
S.pombe
C.elegans
D.melanogaster
D.erio
X.laevis
H.sapiens

Sequence alignment for Nup192, residues 1108-1149. Helices alpha52 and alpha53 are highlighted in red. Conserved residues are in yellow.

C.thermophilum
A.nidulans
N.crassa
P.pastoris
A.gossypii
S.cerevisiae
S.pombe
C.elegans
D.melanogaster
D.erio
X.laevis
H.sapiens

Sequence alignment for Nup192, residues 1150-1200. Helices alpha54, alpha55, and beta3 are highlighted in red. Conserved residues are in yellow.

C.thermophilum
A.nidulans
N.crassa
P.pastoris
A.gossypii
S.cerevisiae
S.pombe
C.elegans
D.melanogaster
D.erio
X.laevis
H.sapiens

Sequence alignment for Nup192, residues 1201-1216. Helices beta4 and alpha56 are highlighted in red. Conserved residues are in yellow.

Fig. S30.

Multispecies sequence alignment of Nup192. Sequences from twelve diverse species were aligned and colored by sequence similarity according to the BLOSUM62 matrix from white (less than 55 % similarity), to yellow (55 % similarity), to red (100 % identity). Numbering below alignment is relative to the *C. thermophilum* sequence. Secondary structure observed in the Nup192 structure is shown above the alignment: α -helices (red bars), β -sheets (blue bars), and unstructured regions (black lines). A dashed line indicates the loop that was deleted for crystallization. Disordered regions are indicated by gray dots.

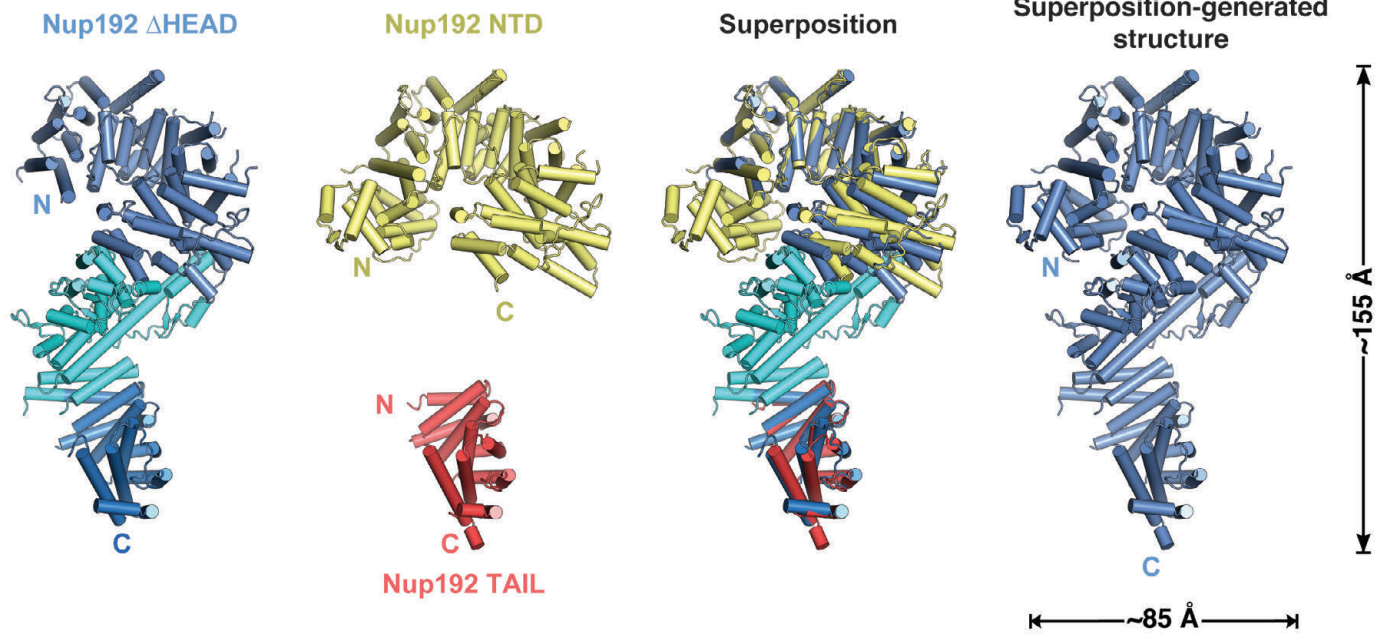


Fig. S31.

Superposition-generated structure of full-length Nup192. Cartoon representations of the crystal structures of Nup192^{ΔHEAD} (colored as in [Fig. 4F](#)), Nup192^{NTD} (yellow), and Nup192^{TAIL} (red) and their superposition are shown. A cartoon representation of the superposition-generated structure of full-length Nup192 (blue) generated from the superposition is shown on the right. See also [Movie 4](#).

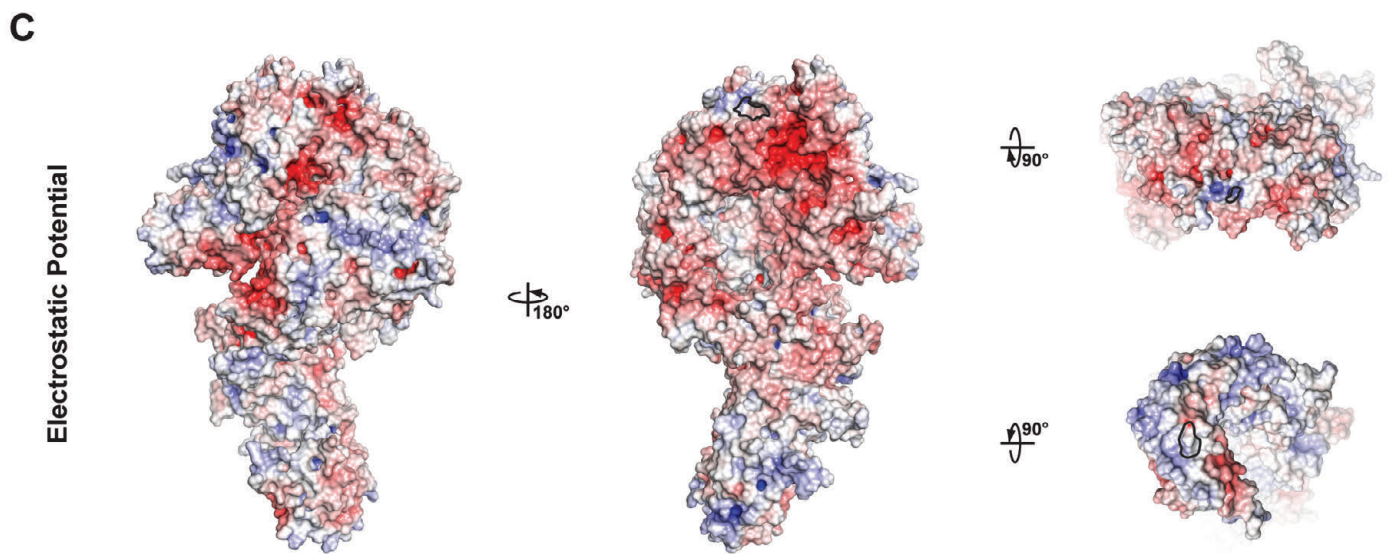
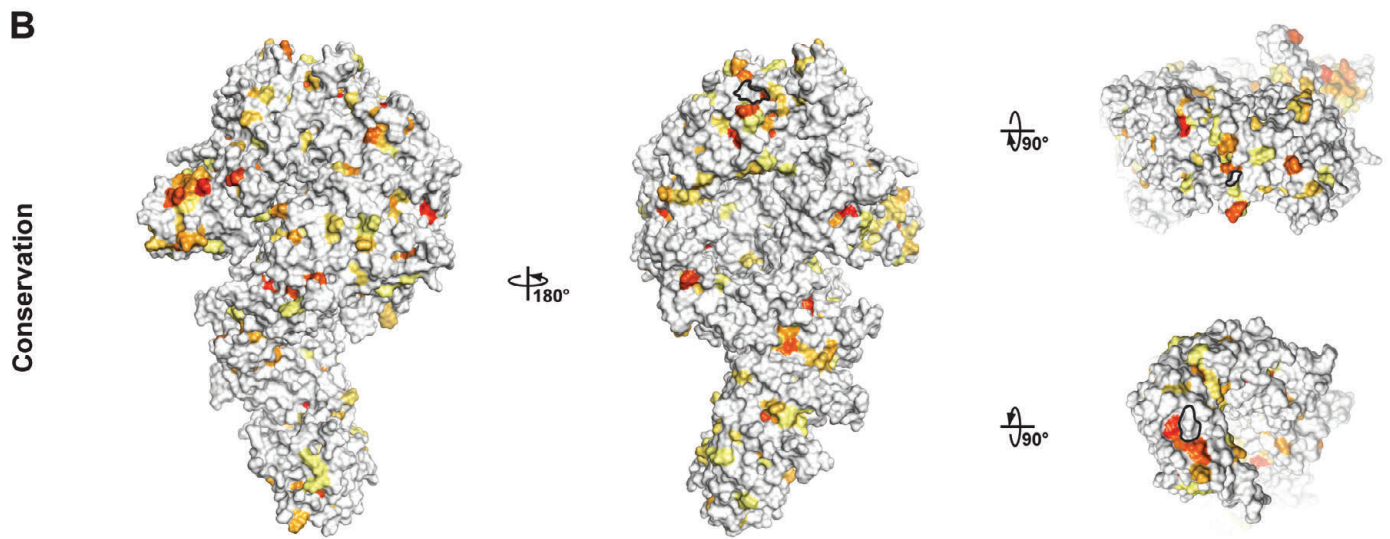
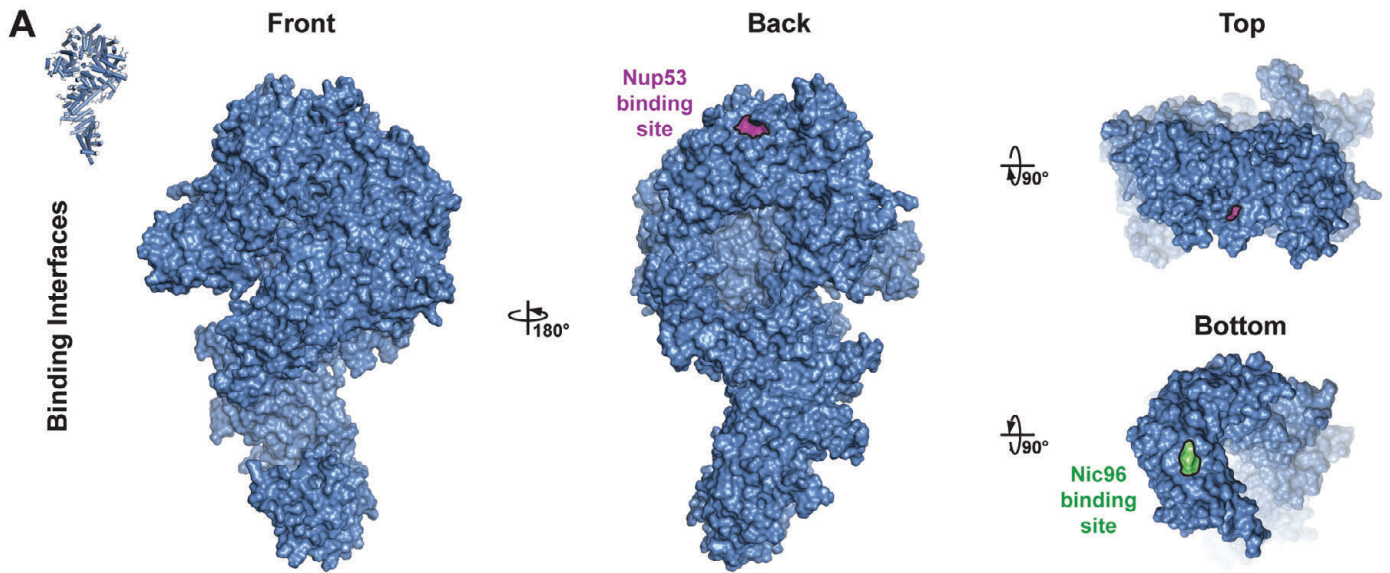
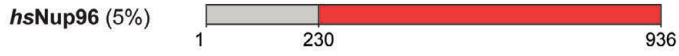
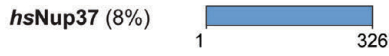
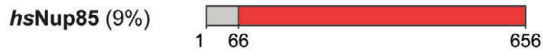
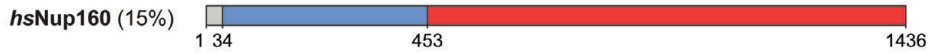


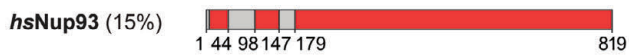
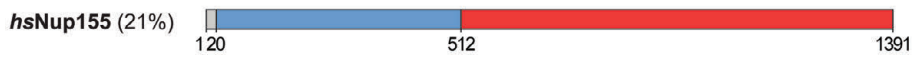
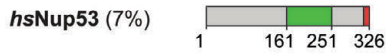
Fig. S32.

Surface properties of Nup192. Surface representations of Nup192 are shown in four different orientations. The surfaces corresponding to previously identified point mutations that disrupt interactions with Nup53 or Nic96 are outlined in black. **(A)** A surface representation of Nup192 with previously identified point mutations that disrupt interactions with Nup53 or Nic96 colored purple or green, respectively (15, 20). **(B)** Surface representation colored according to sequence identity based on the alignment in [fig. S30](#). **(C)** Surface representation colored according to electrostatic potential from $-10 k_B T/e$ (red) to $+10 k_B T/e$ (blue).

Coat nups



Adaptor nups



Channel nups

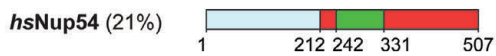


Fig. S33.

Domain structures of symmetric core nucleoporins are conserved between *H. sapiens* and *C. thermophilum*. Predicted domain boundaries are shown for the symmetric core nucleoporins from *H. sapiens* using *H. sapiens* nomenclature. Percent sequence identity to *C. thermophilum* is shown in parenthesis.

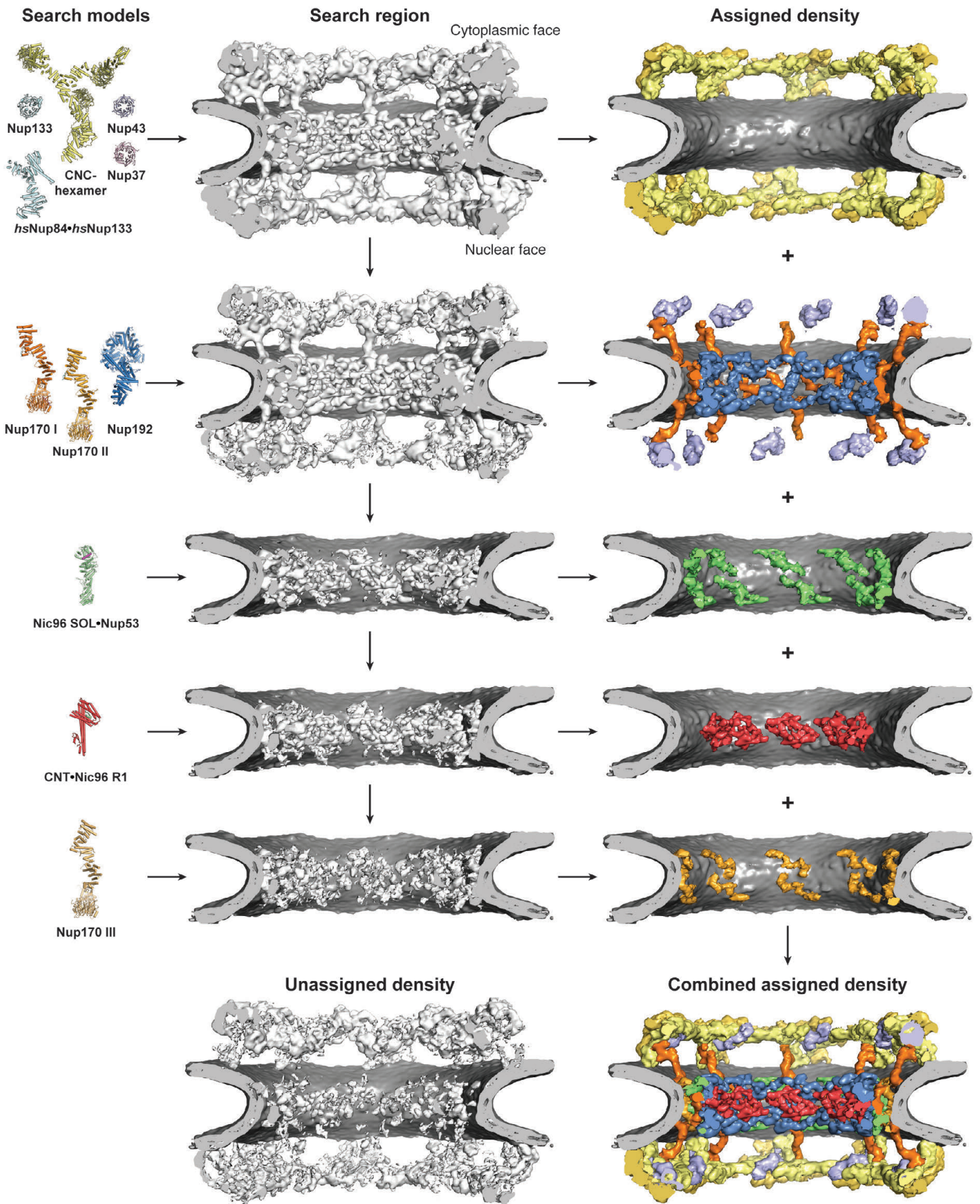


Fig. S34.

Flowchart of the incremental approach used to dock crystal structures into the cryoET reconstruction of the intact human NPC. For each docking step, the crystal structures used for global searches are shown on the left (search model) and the cryoET reconstruction the searches were performed with is shown in the middle (search region). Newly assigned density that was removed from the cryoET reconstruction in subsequent searches is shown on the right and colored as the crystal structure that was placed (assigned density). The remaining unassigned density and combined assigned density are shown at the bottom middle and right, respectively.

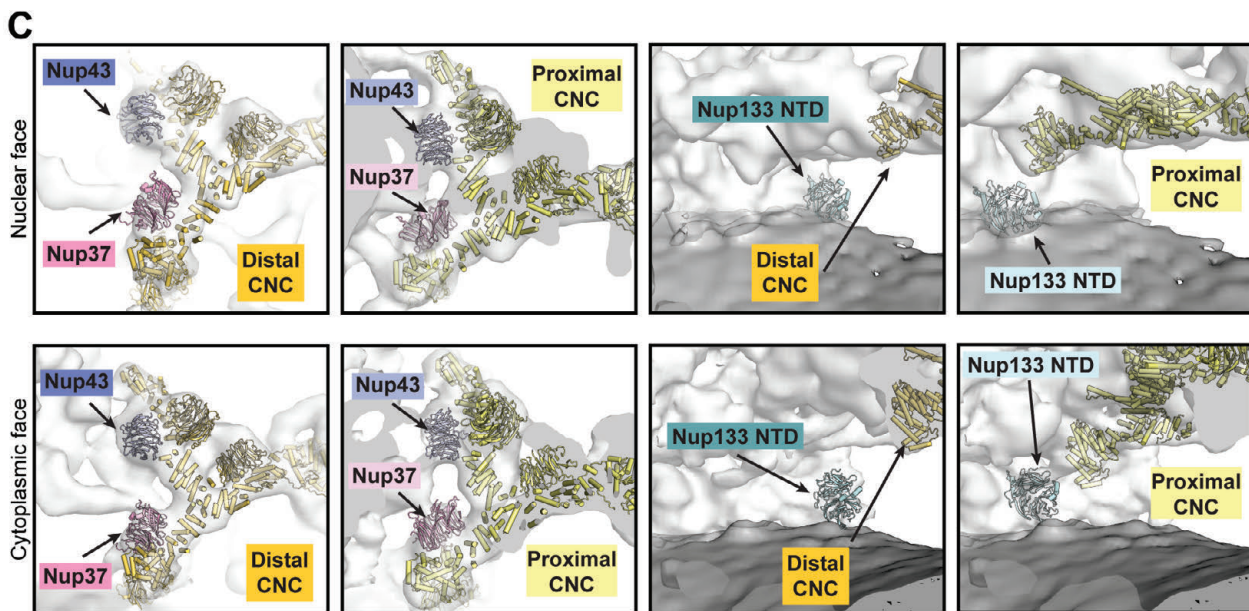
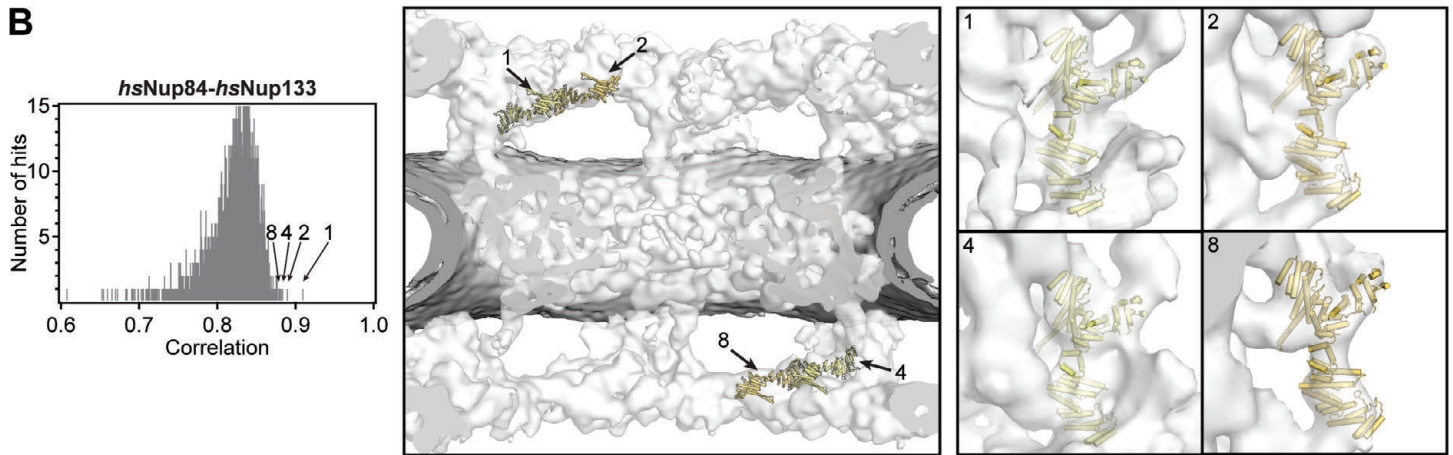
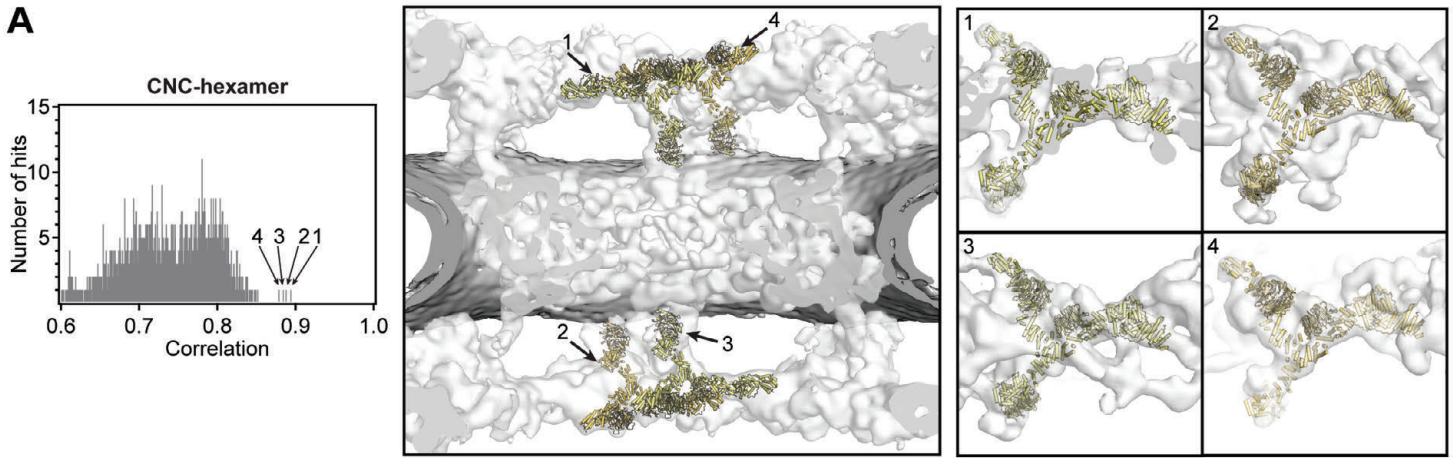


Fig. S35.

Docking of the CNC-hexamer and Nup84•Nup133 crystal structures into the cryoET reconstruction of the intact human NPC. On the left, histograms of the cross-correlation scores from a global search with 50,000 random initial placements are shown for (A) the yeast CNC-hexamer (PDB ID 4XMM) and (B) *hsNup84•hsNup133* hetero-dimer (PDB ID 3I4R) (14, 23). Arrows and corresponding numbers indicate the unique solutions that were accepted and the rank of the score, respectively. The arrangement of the unique solutions in one spoke is shown in the middle. The densities corresponding to the nuclear envelope and the NPC are colored in dark gray and white, respectively. Representative views illustrating the quality of the fits are shown on the right. The numbers on the top left of the box indicate which solution is depicted. (C) Manual docking of Nup43 (PDB ID 4I79; periwinkle), Nup37 (PDB ID 4FHM; pink), and Nup133^{NTD} (PDB ID 1XKS; turquoise) β -propellers into cryoET density guided by previously published biochemical and structural data (39-41, 63).

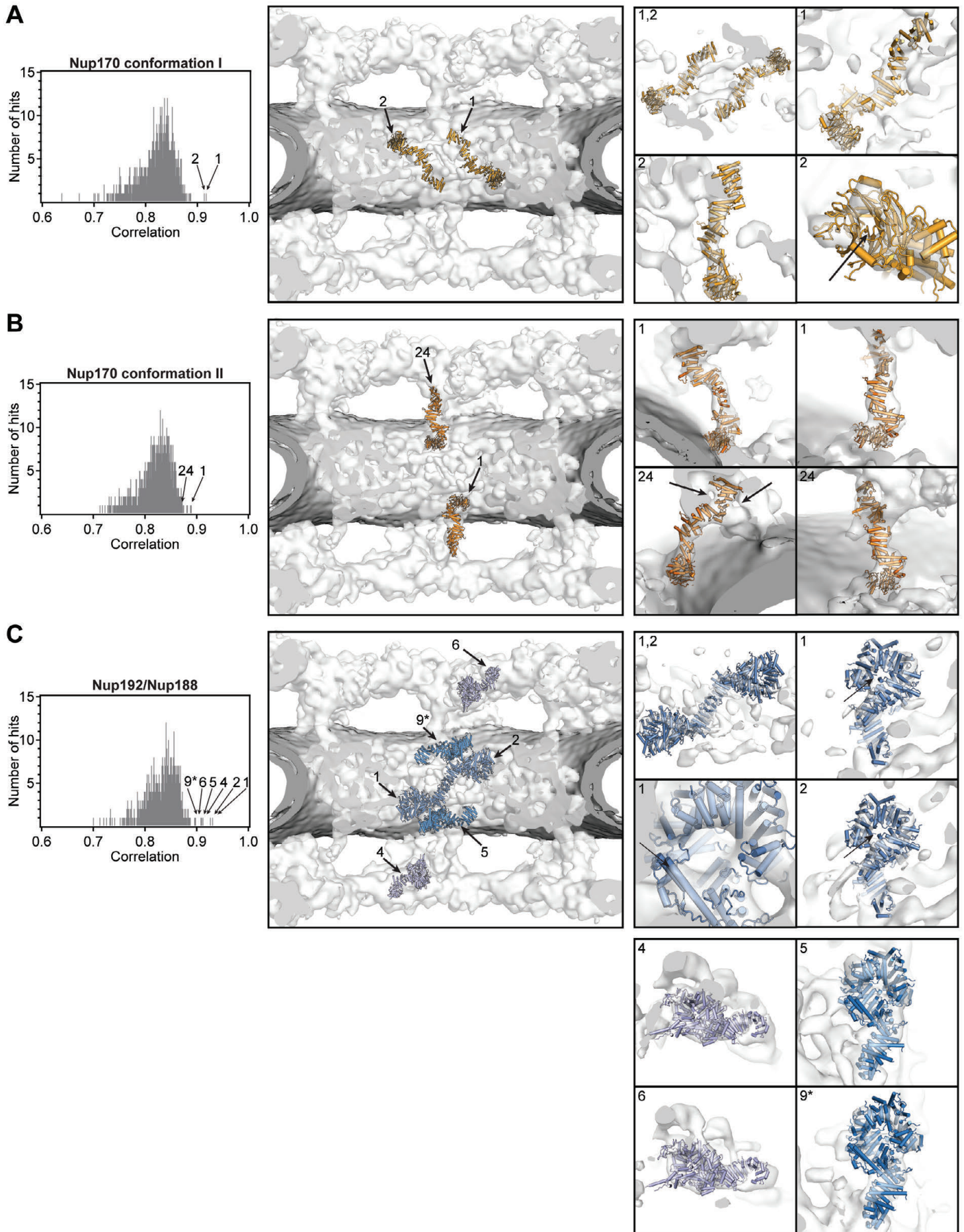


Fig. S36.

Docking of the superposition-generated full-length Nup170 and Nup192 structures into the cryoET reconstruction of the intact human NPC. On the left, histograms of the cross-correlation scores from a global search with 50,000 random initial placements are shown for (A) Nup170 conformation I (light orange), (B) Nup170 conformation II (dark orange), and (C) Nup192 (blue), Nup188 (purple). The Nup170 conformations I and II correspond to conformations 5 and 2, respectively, in [fig. S25](#). Arrows and corresponding numbers indicate the unique solutions that were accepted and the rank of the score, respectively. For Nup192, we accepted 5 placements from the global search results, two placements in the inner ring, two placements in the outer rings, and one placement on the nuclear peripheral side of the inner ring. A matching cytoplasmic peripheral placement was not found in global searches, but the manual placement on the cytoplasmic peripheral side of the inner ring generated a score which would rank as the 9th highest score (asterisk). The arrangement of the unique solutions in one spoke is shown in the middle. The densities corresponding to the nuclear envelope and the NPC are colored in dark gray and white, respectively. Representative views illustrating the quality of the fits are shown on the right. The numbers on the top left of the box indicate which solution is depicted.

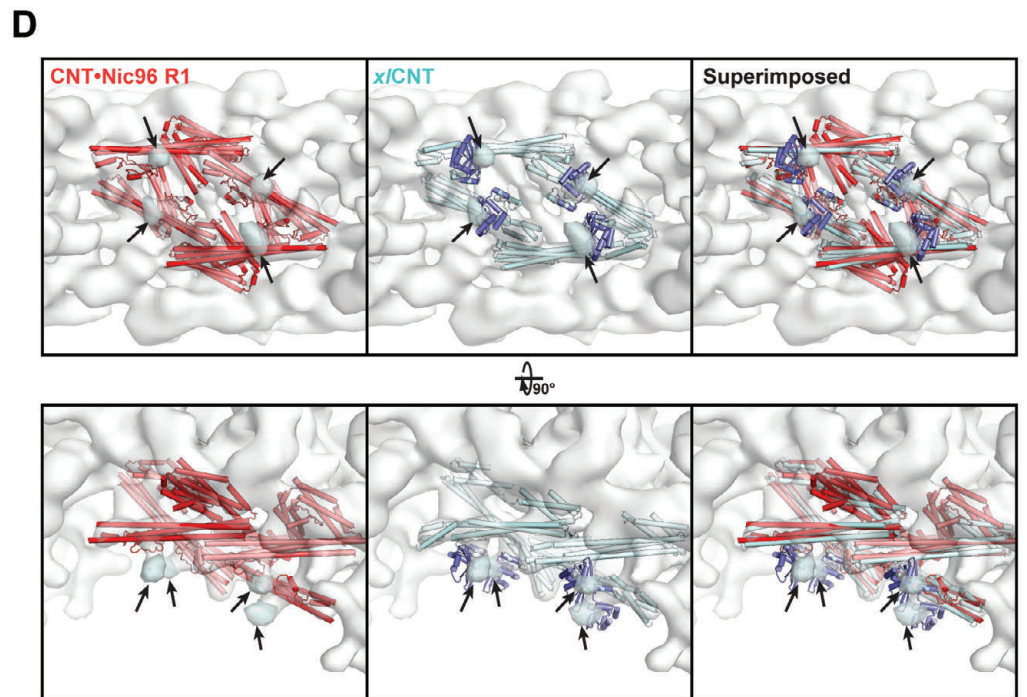
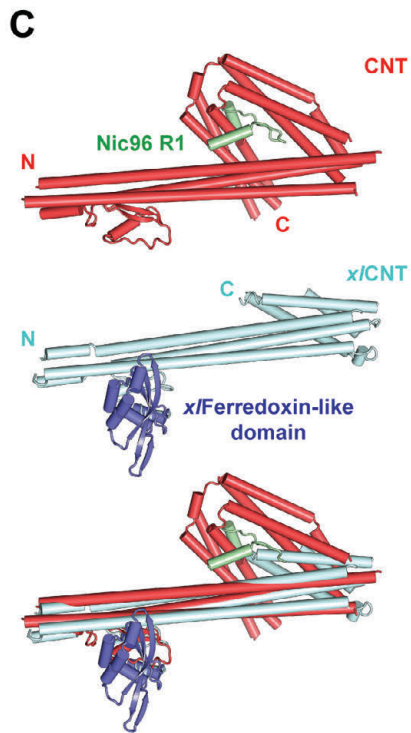
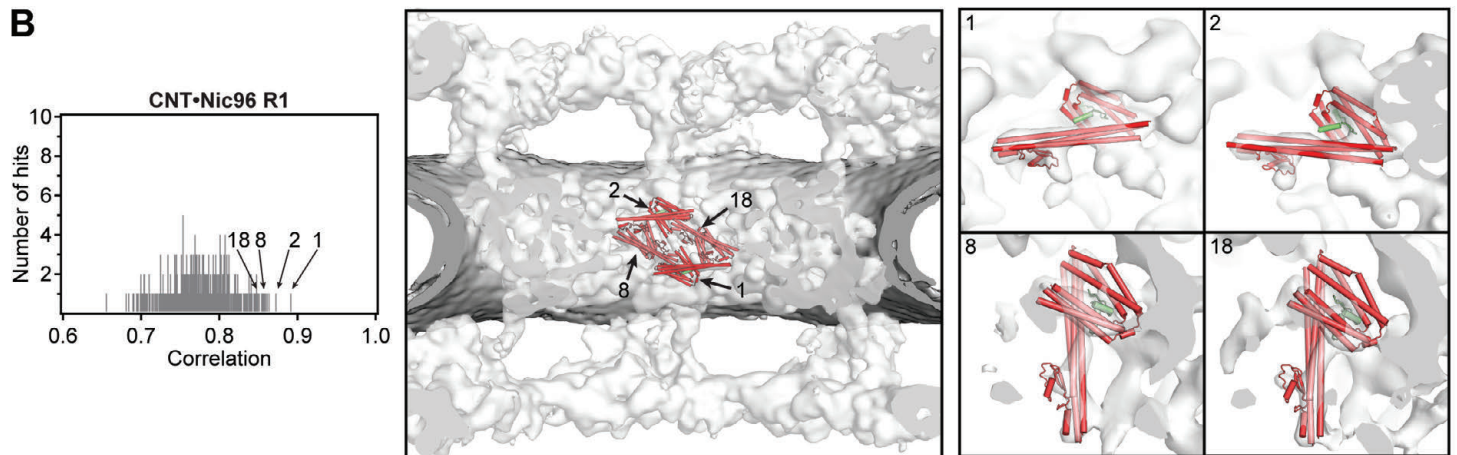
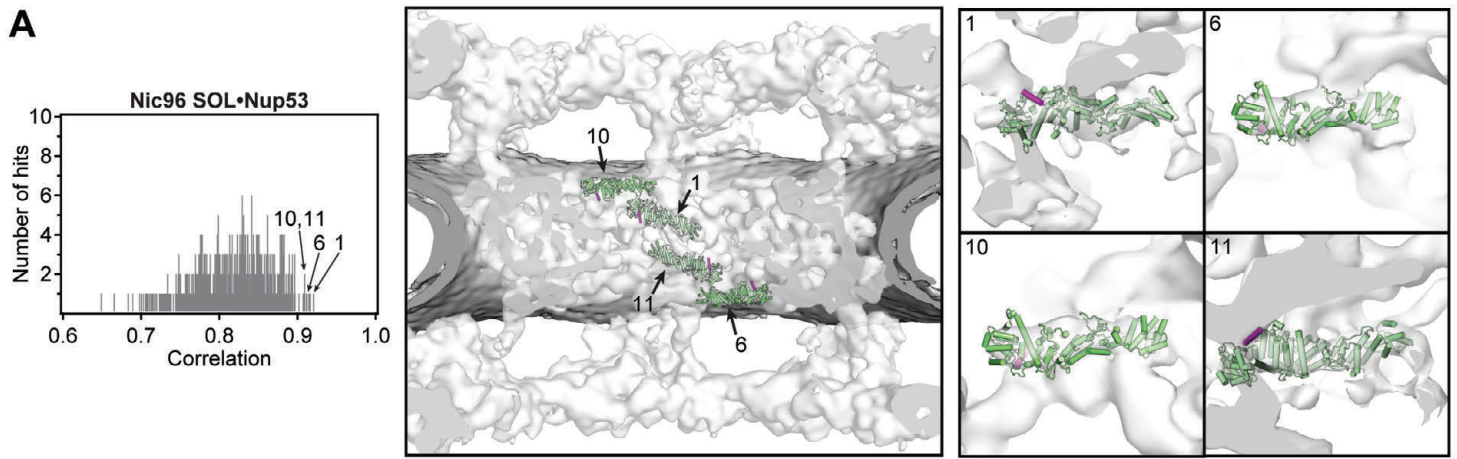
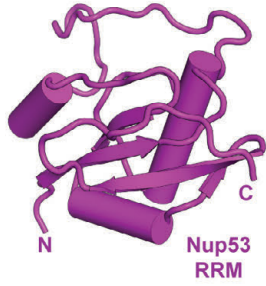
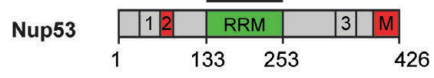
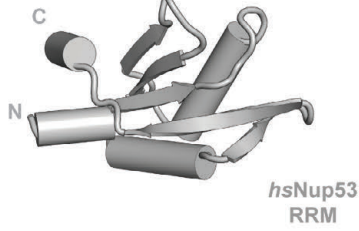
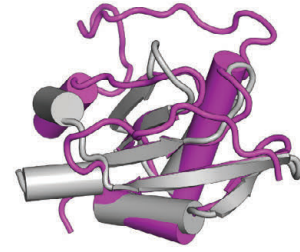


Fig. S37.

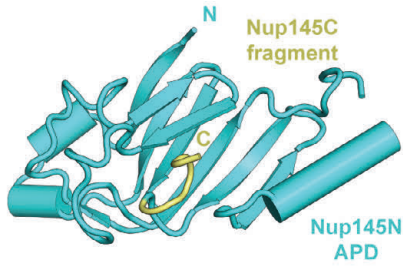
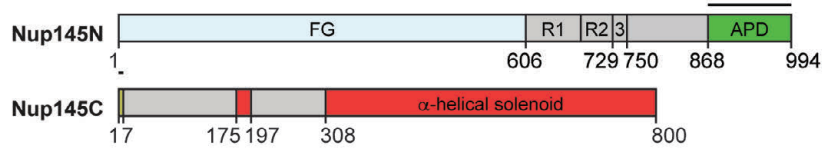
Docking of Nic96^{SOL} and CNT crystal structures into the cryoET reconstruction of the intact human NPC. On the left, histograms of the cross-correlation scores from a global search with 50,000 random initial placements are shown for **(A)** Nic96^{SOL}•Nup53^{R2} (green) and **(B)** CNT•Nic96^{R1} (PDB 5CWS; red). Arrows and corresponding numbers indicate the unique solutions that were accepted and the rank of the score, respectively. The arrangement of the unique solutions in one spoke is shown in the middle. The densities corresponding to the nuclear envelope and the NPC are colored in dark gray and white, respectively. Representative views illustrating the quality of the fits are shown on the right. The numbers on the top left of the box indicate which solution is depicted. **(C)** Crystal structures of the *C. thermophilum* CNT•Nic96^{R1} hetero-tetramer (PDB ID 5CWS; red and green; top), the *X. laevis* CNT hetero-trimer (PDB ID 5C3L; light cyan; middle) and ferredoxin-like domain (PDB ID 5C2U; purple; middle), and their superposition (bottom) are shown in cartoon representation (15, 16). **(D)** The four knobs of unexplained density directly adjacent to the docked CNT•Nic96^{R1} crystal structures (colored in cyan and marked with arrows) are readily explained by the presence of the ferredoxin-like domain, a metazoan-specific insertion in Nup57. Side views from within the central transport channel of the NPC (top) and top views from the cytoplasm (bottom) are shown of the cryoET reconstruction with the docked CNT•Nic96^{R1} crystal structures (left), the model of *X. laevis* CNT with ferredoxin-like domain (middle), and their superposition (right).

A

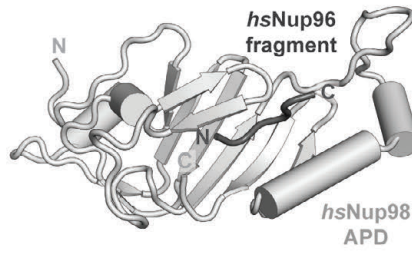
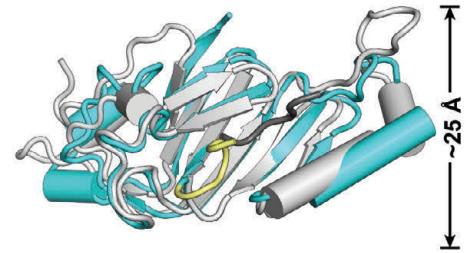
Nup53 RRM

*hsNup53* RRM

Superposition

B

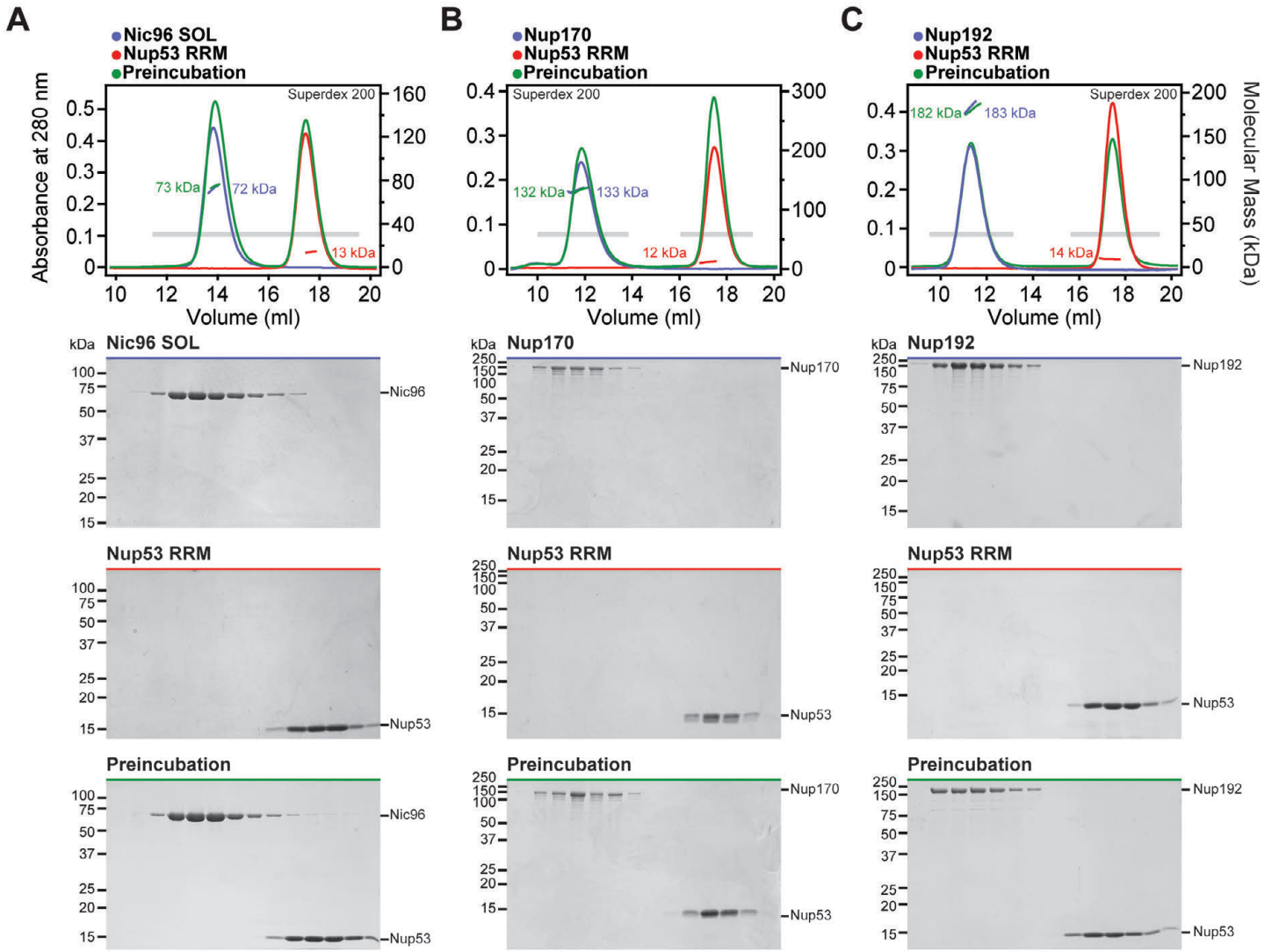
Nup145N APD

*hsNup98* APD

Superposition

Fig. S38.

Crystal structures of Nup53^{RRM} and Nup145N^{APD}•Nup145C^N. (A) Crystal structures of *C. thermophilum* Nup53^{RRM} (purple), *H. Sapiens* Nup53^{RRM} (PDB ID 4LIR; gray), and their superposition are shown in cartoon representation. The core fold is conserved, but there are minor alterations in the size of helices and loops. (B) Crystal structures of the *C. thermophilum* Nup145N^{APD}•Nup145C^N complex (cyan), the *H. sapiens* Nup98^{APD}•Nup96^N complex (PDB ID 1KO6; light gray), and their superposition are shown in cartoon representation. As previously observed for the *hsNup98*^{APD}•*hsNup96*^N hetero-dimer, fusion of the Nup145C^N peptide to Nup145N^{APD} and introduction of the catalytically inactive T994A mutation allowed for structure determination of the Nup145N^{APD}•Nup145C^N complex. Nup145C^N occupied the same binding groove as previously observed in the *hsNup98*•*hsNup96* complex (30). As references, the domain structures of Nup53, Nup145N, and Nup145C are shown above the crystal structures with black bars indicating the crystallized fragments.



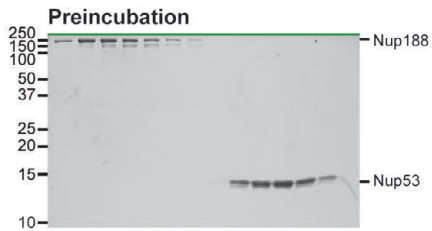
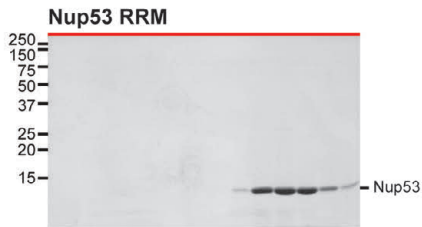
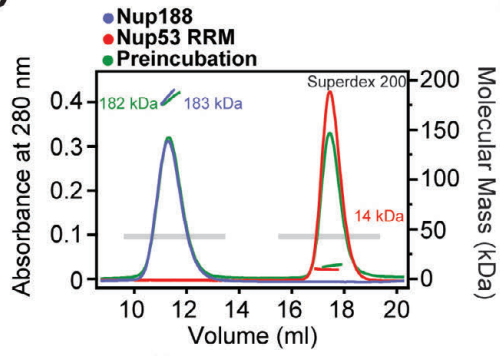
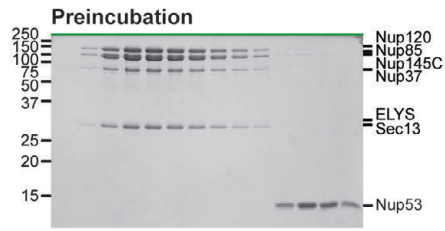
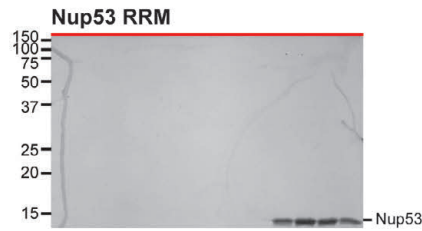
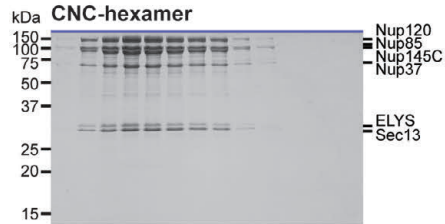
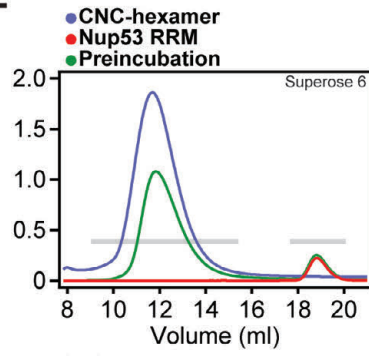
D**E**

Fig. S39.

Nup53^{RRM} does not interact with inner ring scaffold nucleoporins or the CNC-hexamer. (A-E) SEC-MALS profiles of nucleoporins or nucleoporin complexes are shown individually (blue and red) and after their preincubation (green). SEC profiles were obtained using a Superdex 200 10/300 column or Superose 6 10/300 column as indicated. Measured molecular masses are indicated for the peak fractions. Gray bars indicate fractions that were resolved on SDS-PAGE gels and visualized by Coomassie staining.

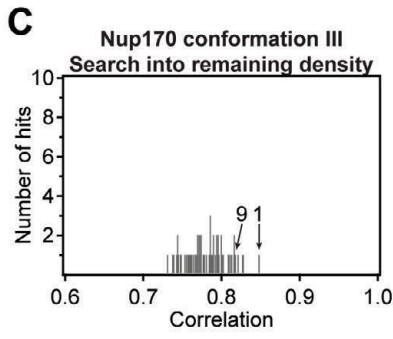
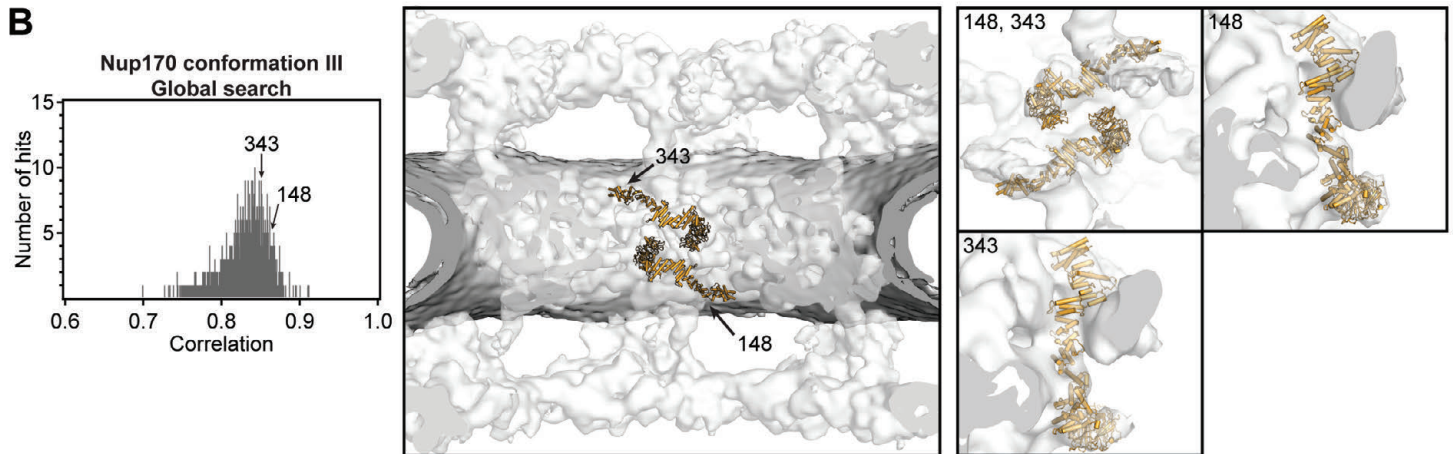
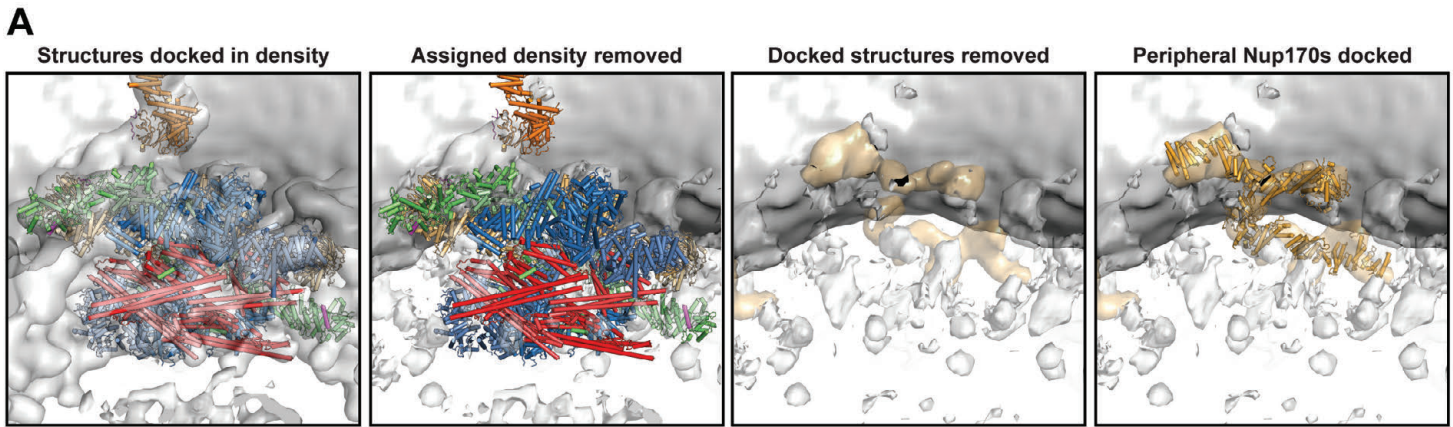


Fig. S40.

Identification of a third pair of Nup170 molecules in the inner ring of the cryoET reconstruction of the intact human NPC. (A) Views of the cryoET density in the inner ring illustrating all density and the docked proteins from the unbiased search (far left), the cryoET density remaining after removal of the assigned density and the docked proteins (middle left), the remaining cryoET density without the docked proteins from the unbiased search revealing density that is shaped like a Nup170 molecule colored in orange (middle right), and the same density with a third conformation of Nup170 docked (far right). (B) Search results for two additional Nup170 molecules fitted into a cryoET map from which the density for the CNCs had been removed. The histogram on the left shows the cross-correlation scores for a pair of Nup170 conformation III (light orange) from a global search with 50,000 random initial placements. Nup170 conformation III corresponds to conformation 8 in [fig. S25](#). Arrows and corresponding numbers indicate the unique solutions that were accepted and the rank of the score, respectively. The arrangement of the unique solutions in one spoke is shown in the middle. The densities corresponding to the nuclear envelope and the NPC are colored in dark gray and white, respectively. Representative views illustrating the quality of the fits are shown on the right. The numbers on the top left of the box indicate which solution is depicted. (C) A histogram illustrating the search results for fitting Nup170 conformation III into a cryoET map of the inner ring from which the density corresponding to all other components had been removed.

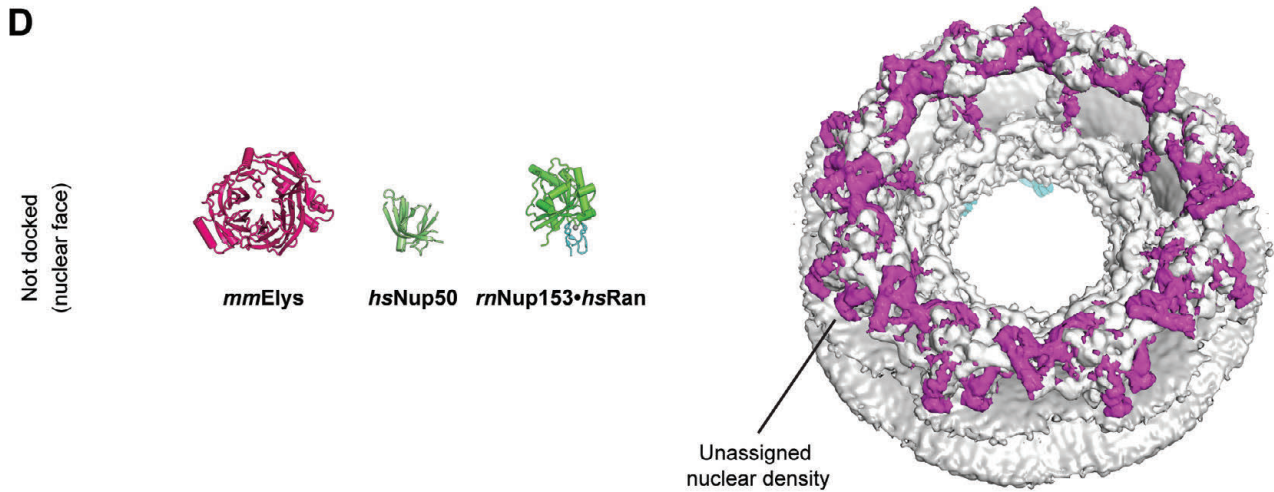
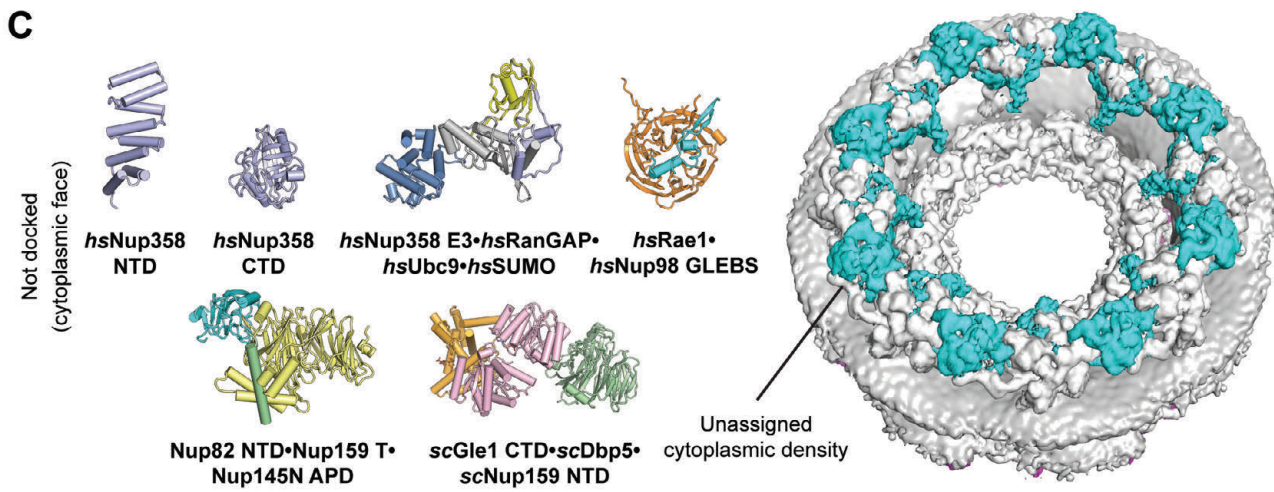
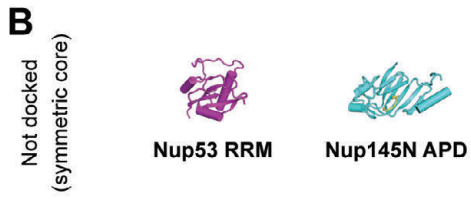
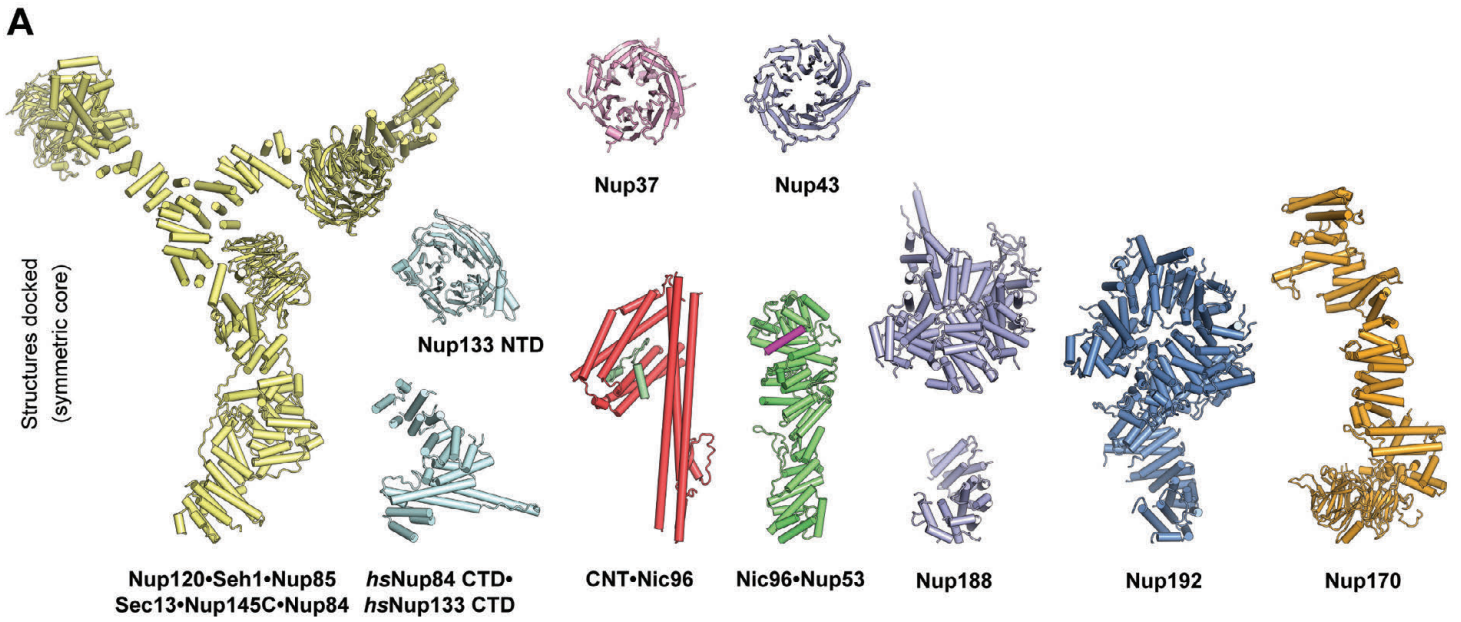
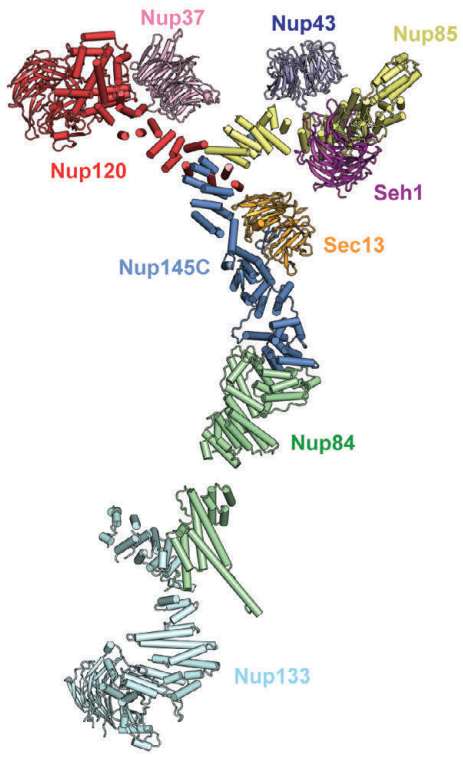


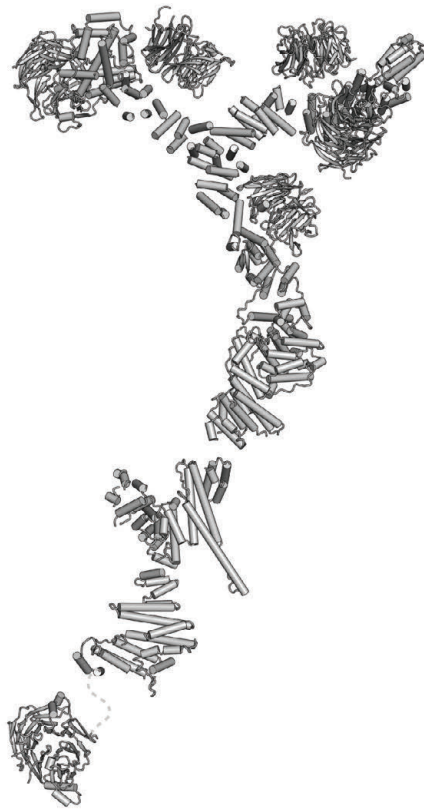
Fig. S41.

Summary of crystal structure docking into the cryoET reconstruction of the intact human NPC.

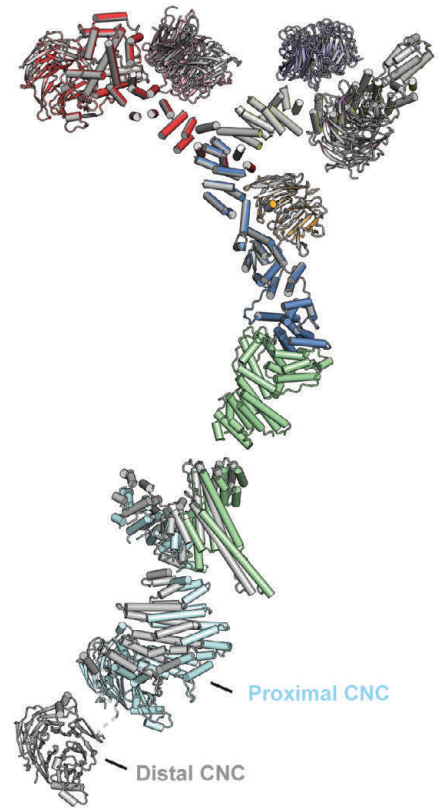
(A) Crystal structures of the symmetric core nucleoporins that could be successfully docked into a cryoET reconstruction of the intact human NPC. (B-D) Crystal structures of symmetric core nucleoporin domains, the cytoplasmic filament nucleoporins, and nuclear basket nucleoporins, which were not docked due to their small size, indistinctive shape, or lack of biochemical restraints. Cytoplasmic and nuclear views of the cryoET reconstruction of the intact human NPC are shown on the right. The assigned density of the symmetric NPC core is colored in gray and the unassigned densities on the cytoplasmic and nuclear faces are colored in cyan and purple, respectively. The volume of the unassigned density appears to be sufficient to accommodate the majority of the remaining structured protein mass of the asymmetric cytoplasmic filament and nuclear basket nucleoporins. All crystal structures are shown to scale in cartoon representation.



Proximal CNC



Distal CNC



Superposition

Fig. S42.

Comparison of the distal and proximal CNC docking solutions. Individual distal (multicolored; left) and proximal (gray; middle) CNCs are shown in cartoon representation. Their superposition reveals a dramatically different orientation for Nup133^{NTD} and slightly different orientations of the Nup133 and Nup84 solenoids (right).

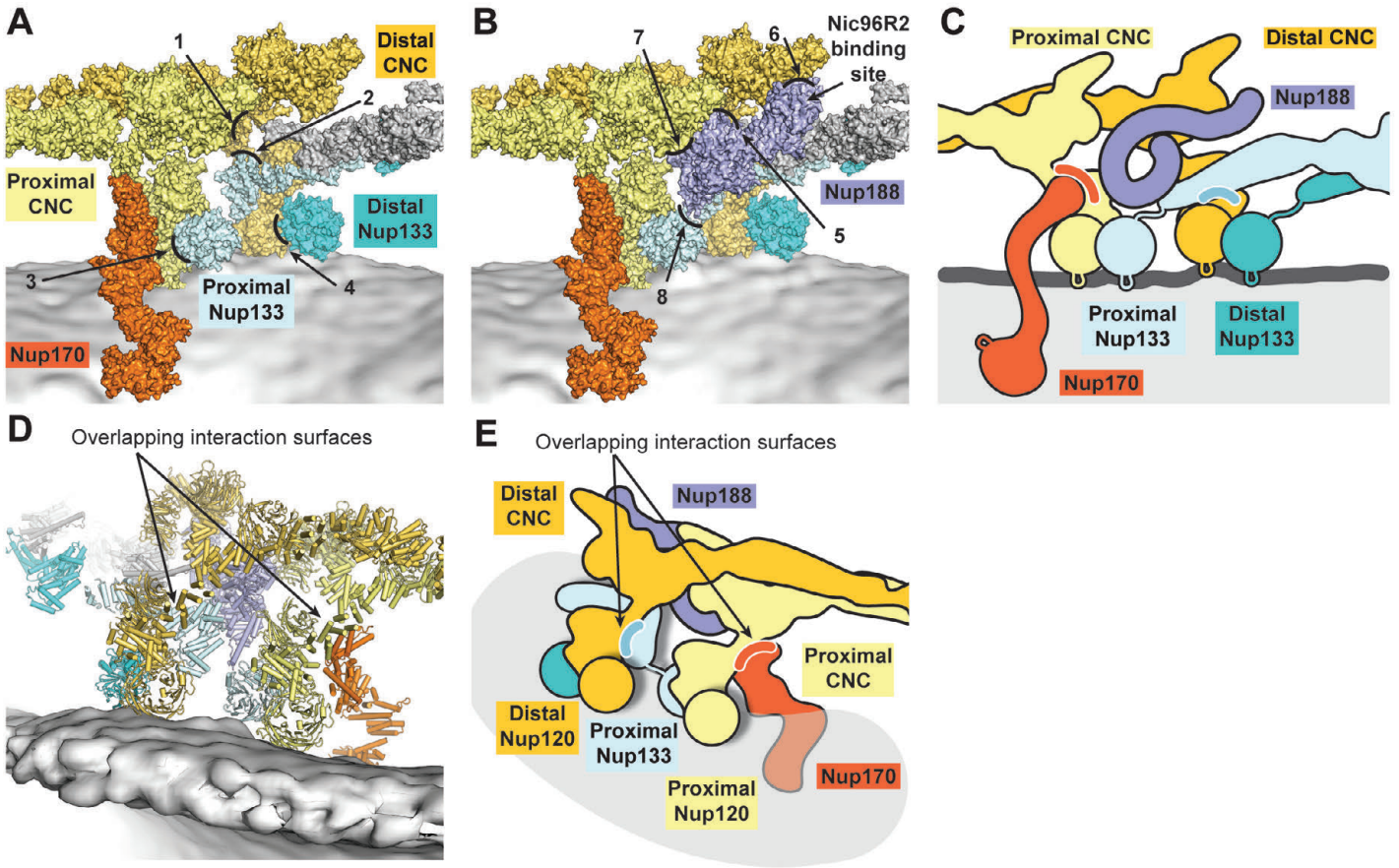
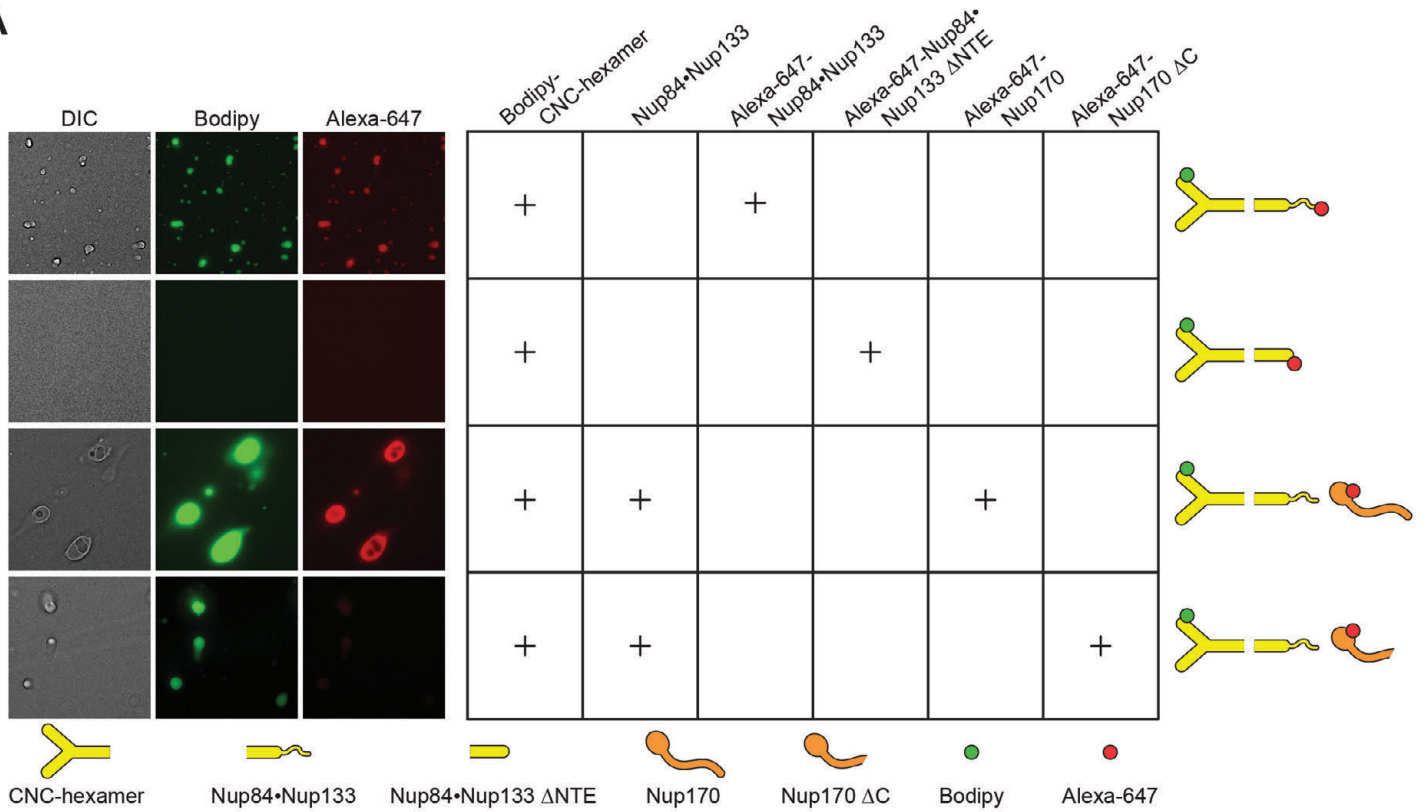


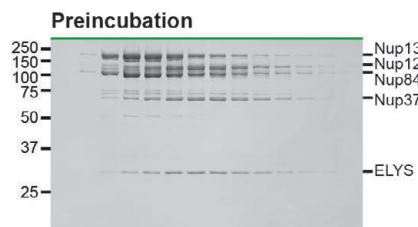
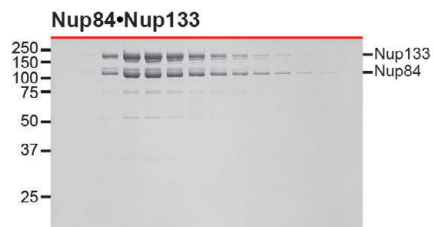
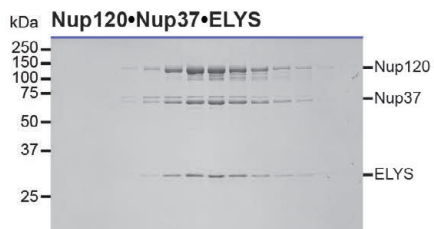
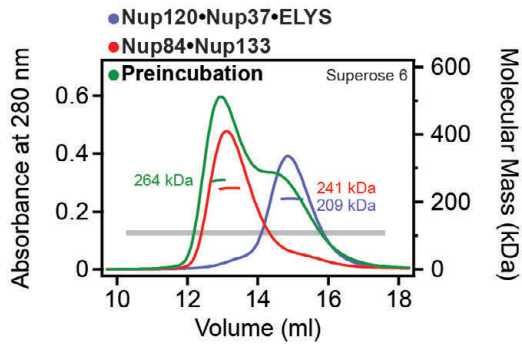
Fig. S43.

Interactions mediating inter-spoke assembly. (A) The outer ring inter-spoke interface is shown in surface representation, but with Nup188 removed for clarity. Contacts observed between CNCs from different spokes are indicated by arrows and numbered from 1 to 4, corresponding to the contacts described in the text. (B) The same view as in panel (A), but with Nup188 also shown in a surface representation. Contacts observed between Nup188 and the CNCs at the inter-spoke interface are indicated by arrows and numbered from 5 to 8, corresponding to the contacts described in the text. An arrow highlights the Nic96^{R2} binding site on Nup188. (C) Schematic of the inter-spoke interface, from the same view as in panel (A). (D) The outer ring inter-spoke interface, shown in cartoon representation, ~180° rotated from the view in panel (A). Nup170 and Nup133 contact overlapping interfaces on proximal and distal Nup120 molecules. (E) Schematic of the outer ring inter-spoke interface drawn in the same view as in panel (D).

A



B



C

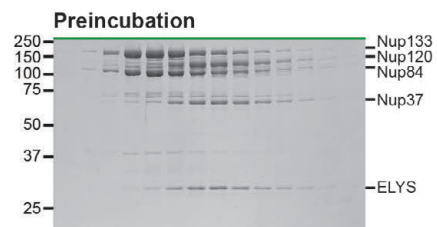
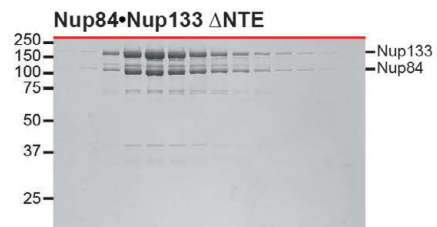
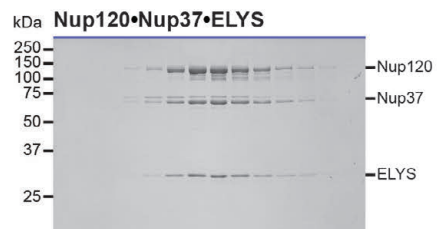
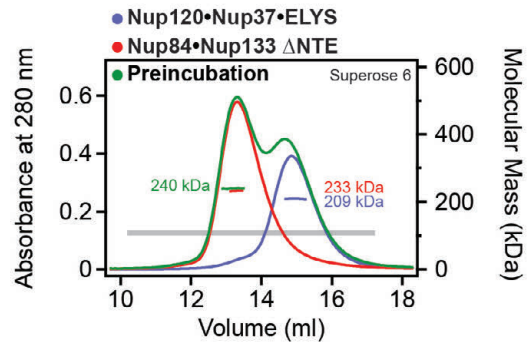


Fig. S44.

Oligomerization of the CNC. (A) The CNC forms oil droplets in the presence of the unstructured N-terminal extension (NTE) of Nup133. The CNC-hexamer was labeled with Bodipy and various other nucleoporins were labeled with Alexa-647 and tested for their ability to form oil droplets. Nup170 incorporates CNC oil droplets, but this incorporation is ablated by deletion of C-terminal helices. Tested protein combinations are indicated in the table and shown schematically on the right. All experiments were repeated at least three times. (B, C) SEC-MALS profiles of nucleoporin complexes are shown individually (blue or red) and after their preincubation (green). There is a weak interaction between Nup120•Nup37•ELYS and Nup84•Nup133 only in the presence of the NTE of Nup133. SEC profiles were obtained using a Superose 6 10/300 GL column. Measured molecular masses are indicated for the peak fractions. Gray bars indicate fractions that were resolved on SDS-PAGE gels and visualized by Coomassie staining.

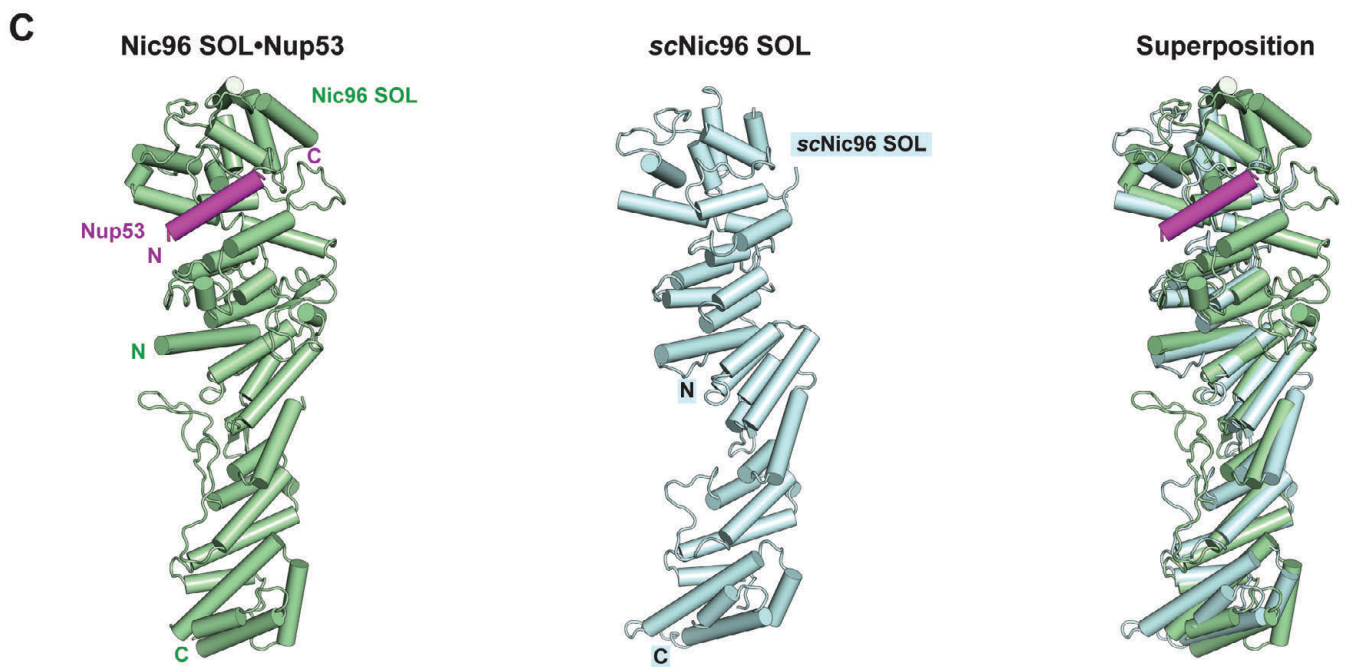
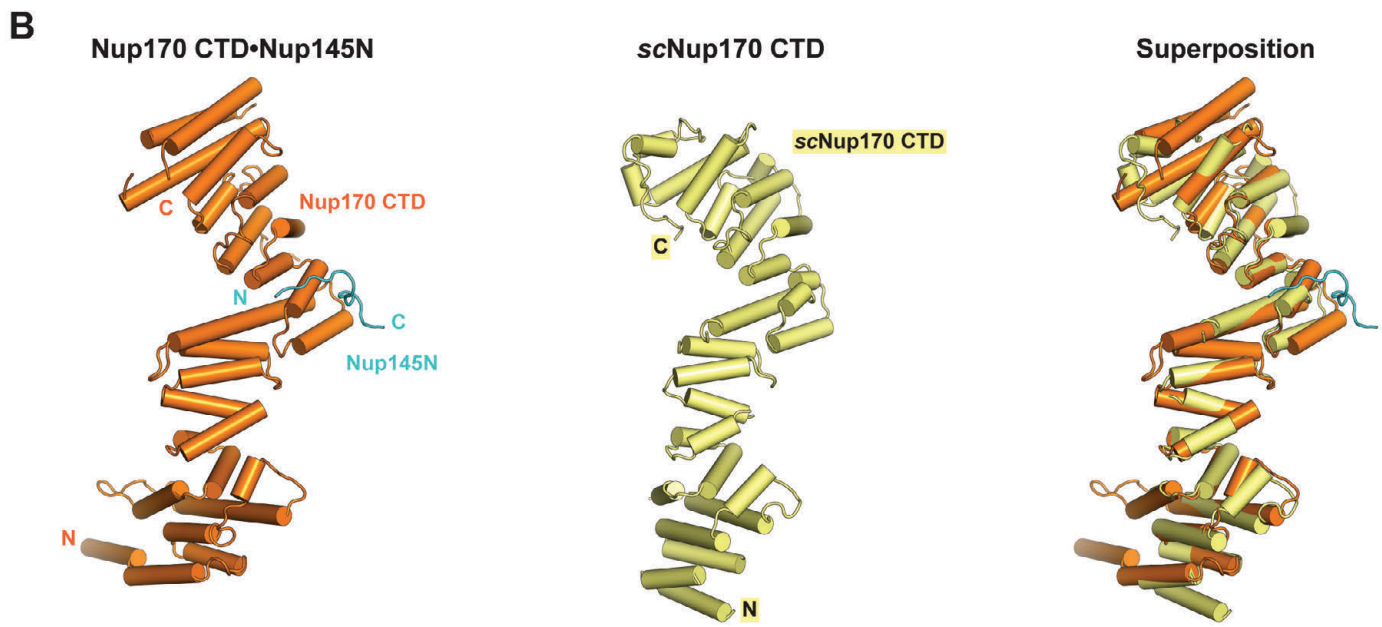
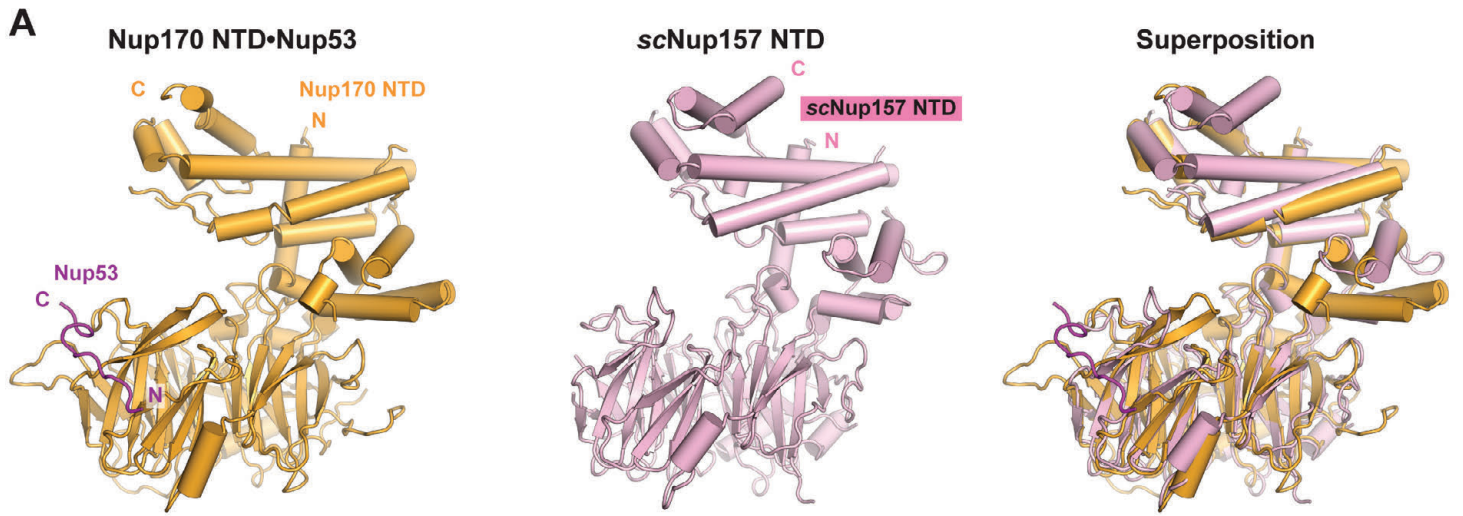


Fig. S45.

Overall nucleoporin folds are evolutionarily conserved. Structural comparison of *C. thermophilum* Nup170 and Nic96 complexes reported here and previously determined *apo S. cerevisiae* crystal structures, revealing extensive evolutionary conservation of the overall folds. **(A)** Nup170^{NTD}•Nup53^{R3} (left), scNup157^{NTD} (PDB ID 4MHC; middle), and their superposition (right) are shown in cartoon representation (21). **(B)** Nup170^{CTD}•Nup145N^{R3} (left), scNup170^{CTD} (PDB ID 3I5P; middle), and their superposition (right) are shown in cartoon representation (23). **(C)** Nic96^{SOL}•Nup53^{R2} (left), scNic96^{SOL} (PDB ID 2RFO; middle), and their superposition (right) are shown in cartoon representation (24).

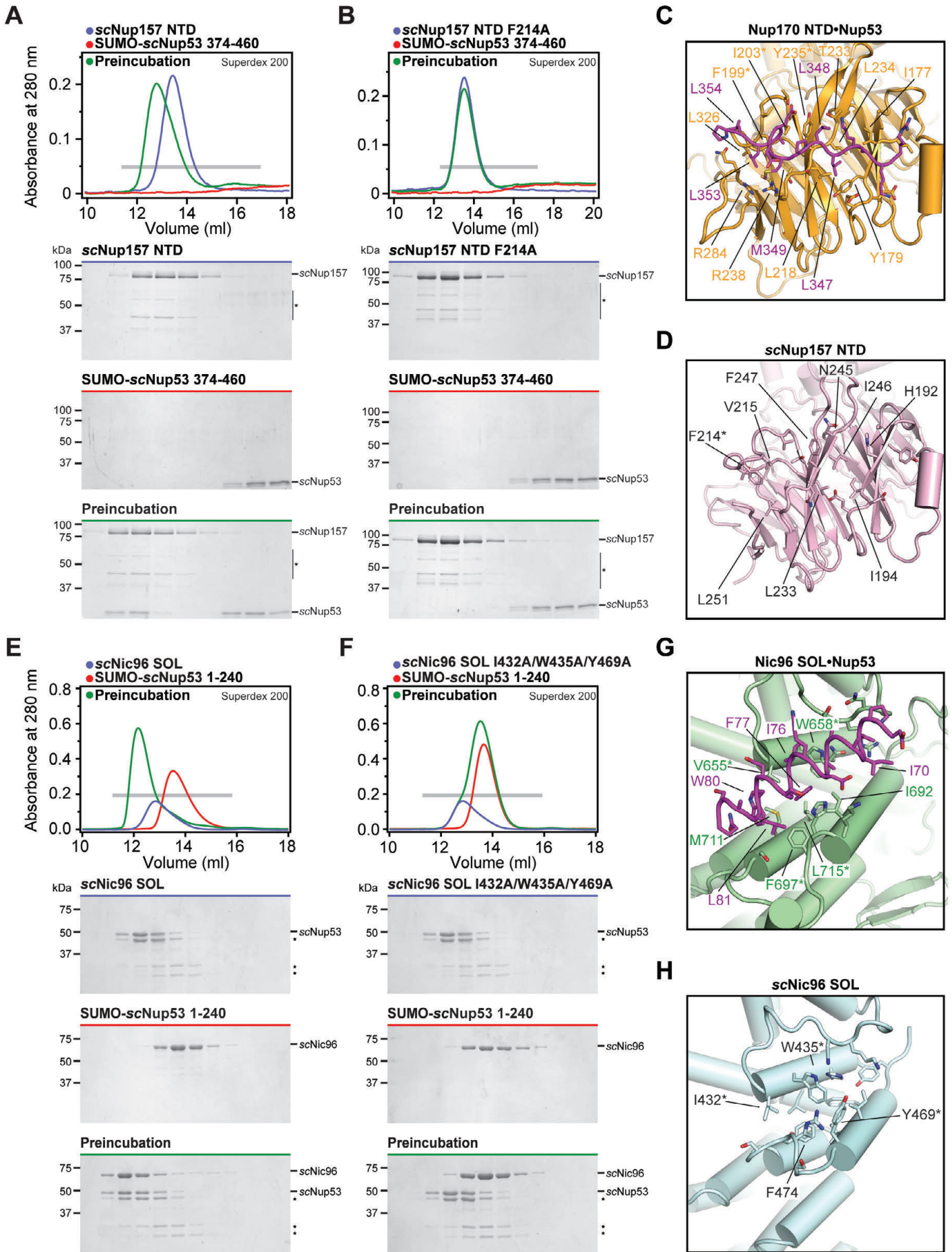


Fig. S46.

Binding pockets on scNup157 and scNic96 for scNup53 are evolutionarily conserved. (A, B) SEC interaction experiments were performed with constructs of *S. cerevisiae* Nup157^{NTD} and Nup53 homologous to the crystallized Nup170^{NTD}•Nup53^{R3} complex and with a mutant Nup157^{NTD} construct in which a conserved F214 residue in the Nup53 binding pocket was mutated to alanine. SEC profiles of nucleoporins are shown individually (blue and red) and after their preincubation (green). (C) A close-up view of the Nup170^{NTD}•Nup53^{R3} complex, same as Fig. 3C. (D) A close-up view of the corresponding surface of scNup157 (PDB ID 4MHC) reveals that the hydrophobic binding pocket for Nup53^{R3} is intact (21). An asterisk highlights the scNup157^{NTD} mutant that abolished the interaction with scNup53. (E, F) Interaction experiments were performed with fragments of *S. cerevisiae* Nic96^{SOL} and Nup53 homologous to the crystallized Nic96^{SOL}•Nup53^{R2} complex and with mutant scNic96^{SOL} in which conserved hydrophobic residues within the Nup53 binding pocket were mutated to alanine. SEC profiles of nucleoporins are shown individually (blue and red) and after their preincubation (green). (G) A close-up view of the Nic96^{SOL}•Nup53^{R2} complex, same as Fig. 4C. (H) A close-up view of the corresponding surface of scNic96^{SOL} (PDB ID 2RFO) reveals that the hydrophobic groove that recognizes Nup53^{R2} is intact (24). Asterisks highlight the scNic96^{SOL} mutants that abolished the interaction with scNup53. All SEC profiles were obtained using a Superdex 200 10/300 GL column. Gray bars indicate fractions that were resolved on SDS-PAGE gels and visualized by Coomassie staining.

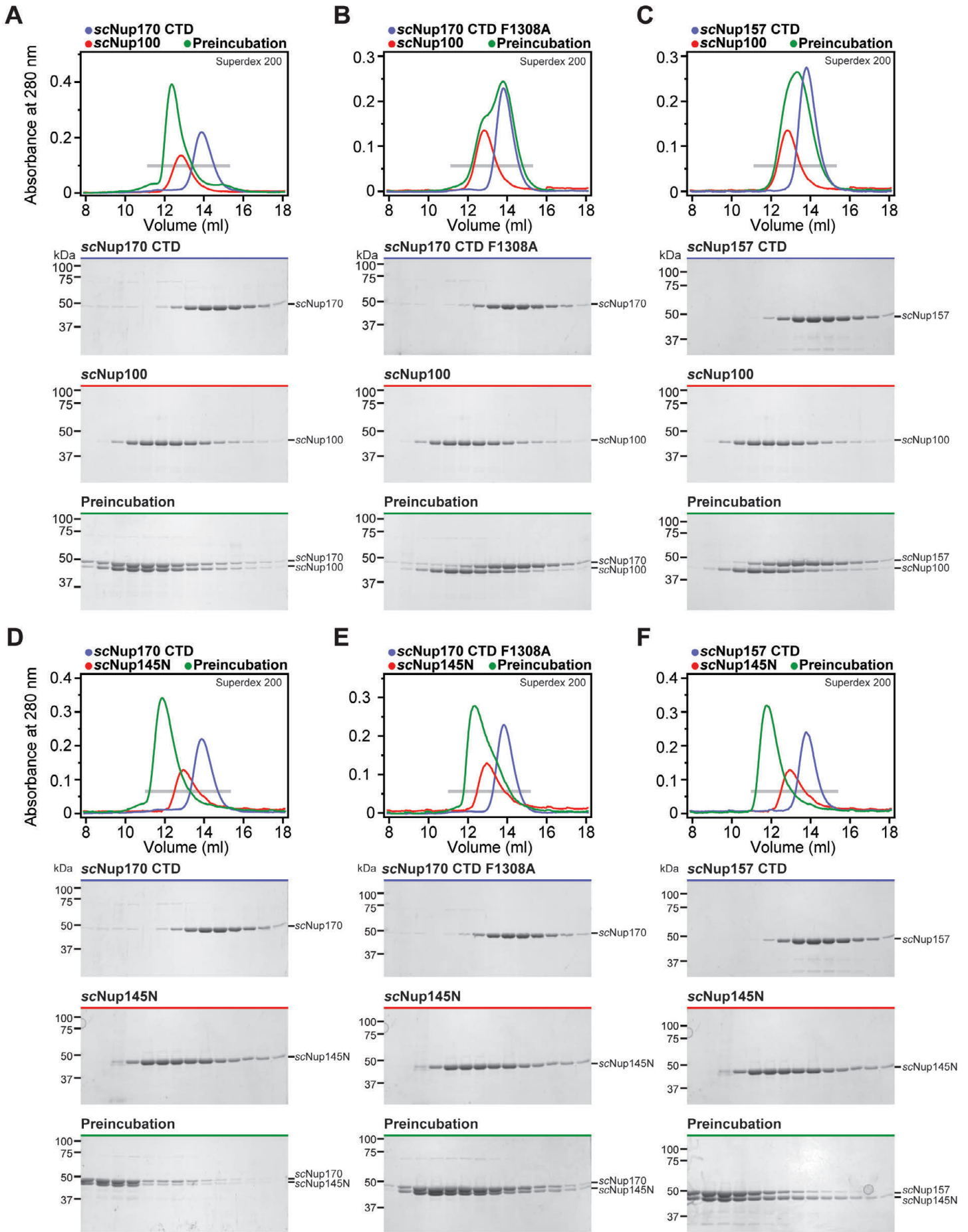


Fig. S47.

Binding pockets on scNup157 and scNup170 for the Nup145N paralogs scNup100 and scNup145N are conserved. (A-F) SEC profiles of nucleoporins or nucleoporin complexes are shown individually (blue and red) and after their preincubation (green). All SEC profiles were obtained using a Superdex 200 10/300 GL column. Gray bars indicate fractions that were resolved on SDS-PAGE gels and visualized by Coomassie staining.

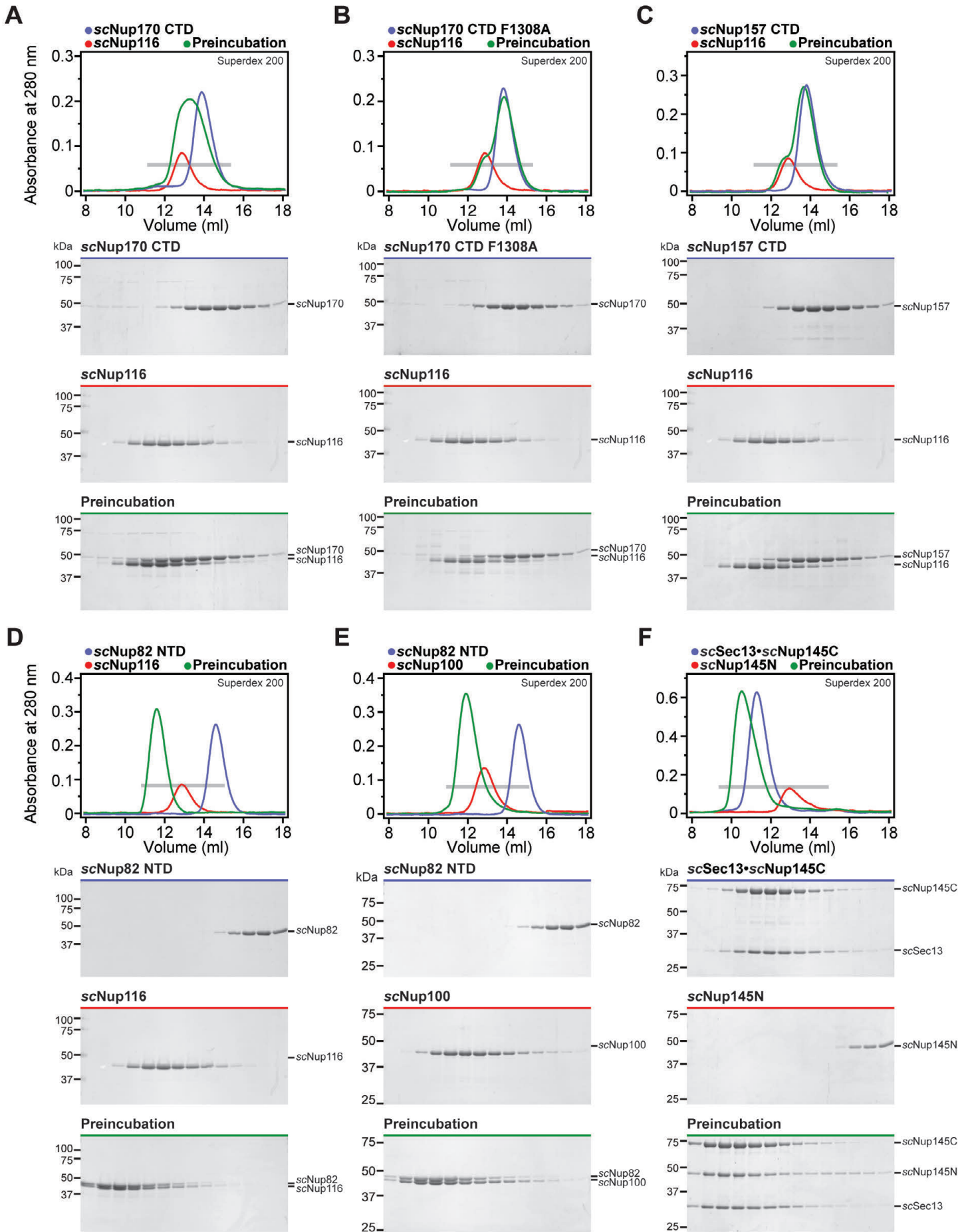


Fig. S48.

Other Nup145N interactions are conserved in the three *S. cerevisiae* paralogs scNup100, scNup145N, and scNup116, but scNup116 only binds very weakly to scNup170^{CTD} and scNup157^{CTD}. (A-F) SEC profiles of nucleoporins or nucleoporin complexes are shown individually (blue and red) and after their preincubation (green). All SEC profiles were obtained using a Superdex 200 10/300 GL column. Gray bars indicate fractions that were resolved on SDS-PAGE gels and visualized by Coomassie staining.

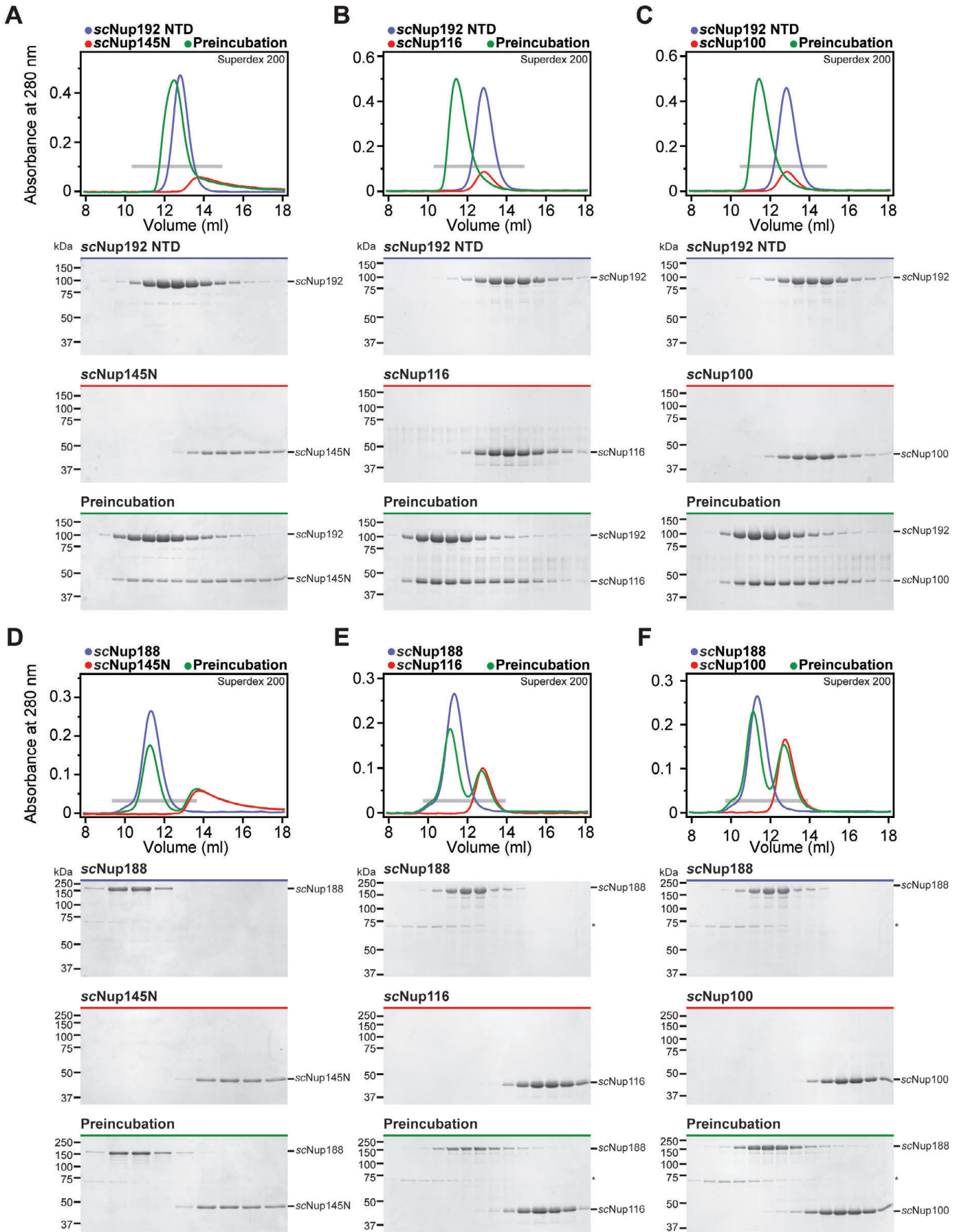


Fig. S49.

All three *S. cerevisiae* Nup145N paralogs bind to scNup192^{NTD}, but none bind to scNup188. (A-F) SEC profiles of nucleoporins or nucleoporin complexes are shown individually (blue and red) and after their preincubation (green). All SEC profiles were obtained using a Superdex 200 10/300 GL column. Gray bars indicate fractions that were resolved on SDS-PAGE gels and visualized by Coomassie staining.

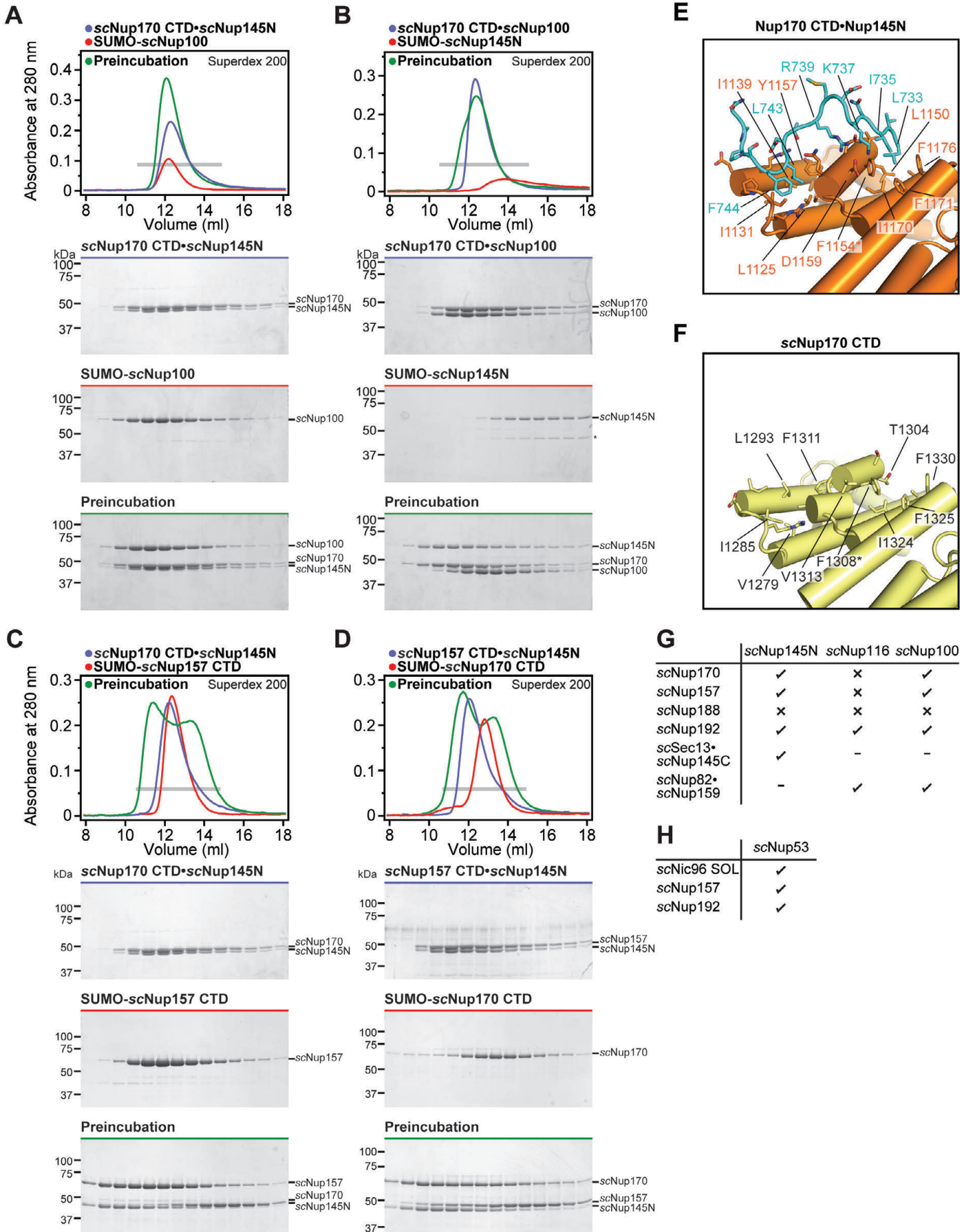


Fig. S50.

scNup145N and scNup100 bind to scNup170^{CTD} and scNup157^{CTD} in a mutually exclusive fashion. (A, B) scNup145N and scNup100 bind to scNup170^{CTD} in a mutually exclusive fashion and scNup145N outcompetes scNup100. (C, D) scNup157^{CTD} and scNup170^{CTD} bind to scNup145N in a mutually exclusive fashion. SEC profiles of nucleoporins or nucleoporin complexes are shown individually (blue and red) and after their preincubation (green). All SEC profiles were obtained using a Superdex 200 10/300 GL column. Gray bars indicate fractions that were resolved on SDS-PAGE gels and visualized by Coomassie staining. (E) Close-up view of the Nup170^{CTD}•Nup145N^{R3} complex. (F) Close-up view of the corresponding surface in scNup170^{CTD} (PDB ID 3I5P) revealed that both hydrophobic binding pockets for Nup145N^{R3} are conserved (23). The conserved residue, F1308, which was mutated in the interaction experiments in [figs. S47 and S48](#) is indicated by an asterisk. (G) Summary of the results of interaction experiments performed with *S. cerevisiae* Nup145N homologs. Check marks indicate complexes that can form in SEC experiments, crosses indicate complexes that do not form, and dashes indicate complexes that were not tested. (H) Summary of the results of interaction experiments performed with *S. cerevisiae* Nup53. Check marks indicate complexes that can form in SEC experiments, crosses indicate complexes that do not form, and dashes indicate complexes that were not tested.

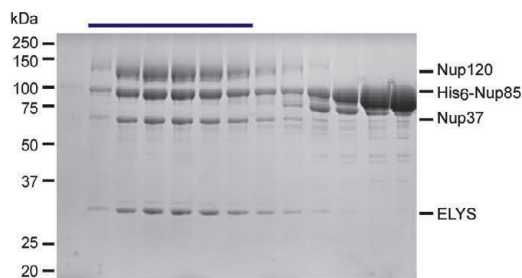
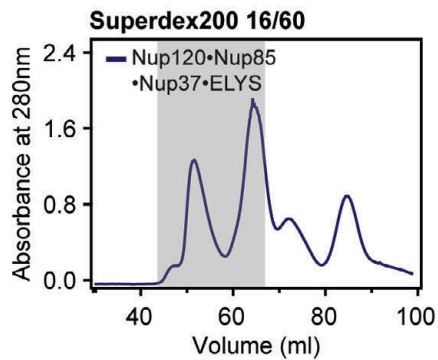
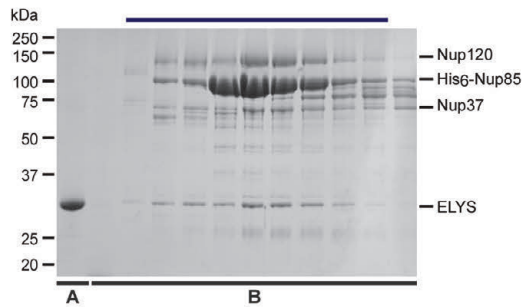
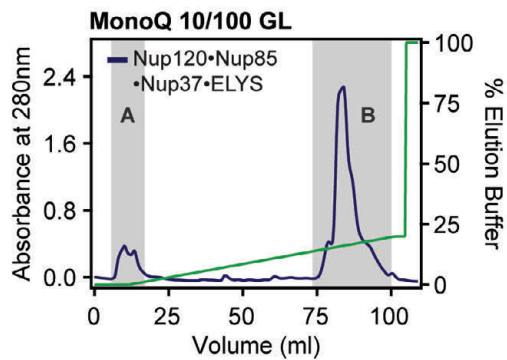
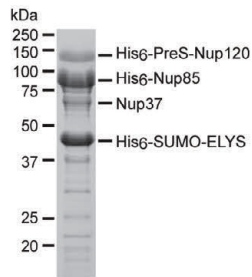
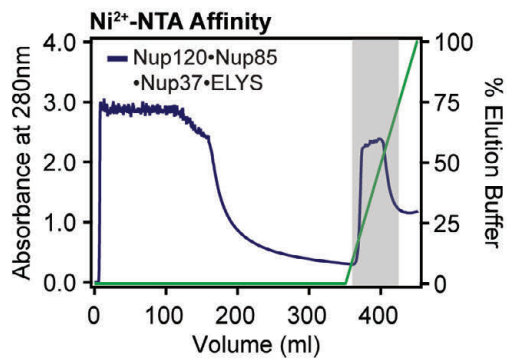
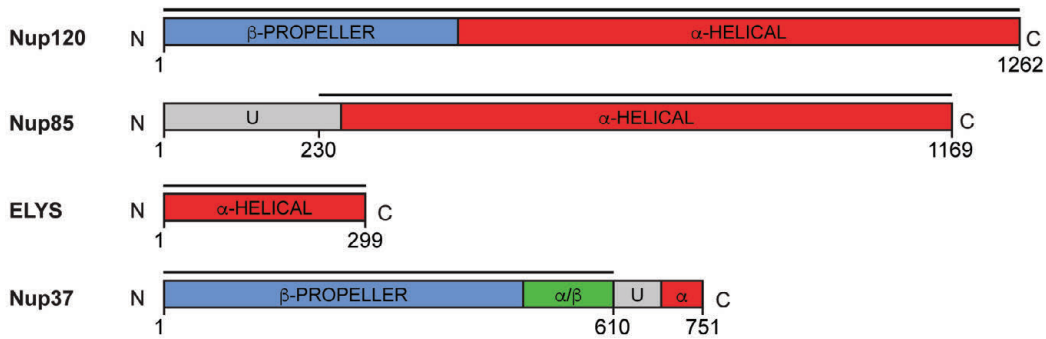


Fig. S51.

Purification protocol for Nup120•Nup37•ELYS•Nup85 hetero-tetramer. Domain boundaries of the purified nucleoporins are shown with black lines indicating the construct boundaries. Sequential chromatography purification steps are shown from top to bottom with the employed columns indicated. Gray bars indicate fractions that were resolved on SDS-PAGE gels and visualized by Coomassie staining. Pooled fractions are indicated with a black bar above the SDS-PAGE gels. For details of the buffer conditions see [Table S2](#).

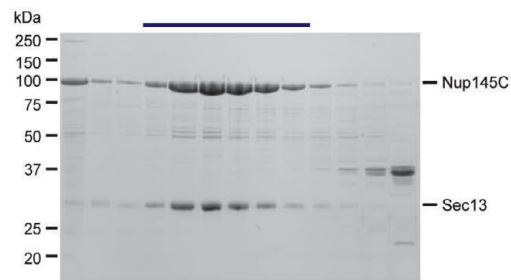
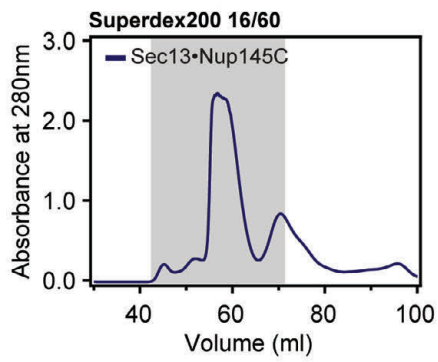
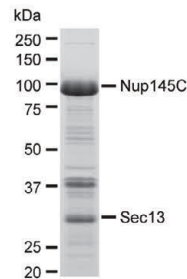
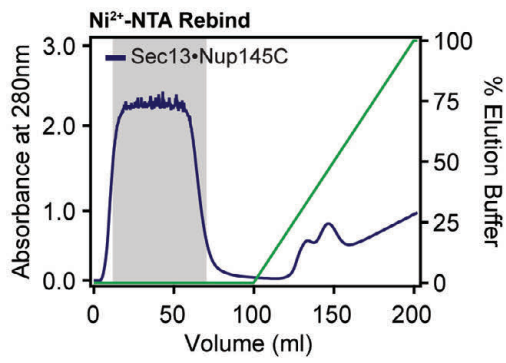
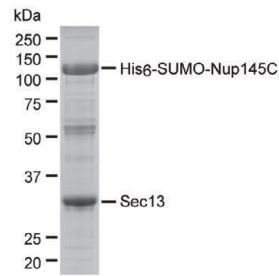
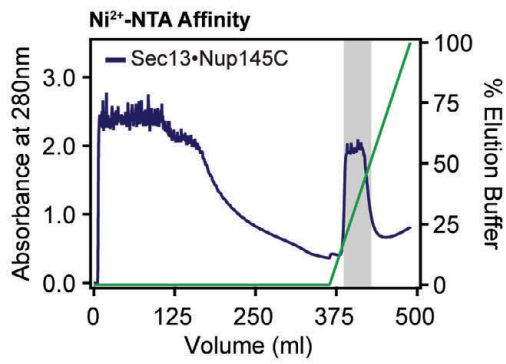
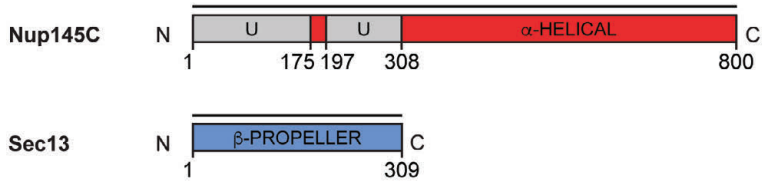


Fig. S52.

Purification protocol for the Sec13•Nup145C hetero-dimer. Domain boundaries of the purified nucleoporins are shown with black lines indicating the construct boundaries. Sequential chromatography purification steps are shown from top to bottom with the employed columns indicated. Gray bars indicate fractions that were resolved on SDS-PAGE gels and visualized by Coomassie staining. Pooled fractions are indicated with a black bar above the SDS-PAGE gels. For details of the buffer conditions see [Table S2](#).

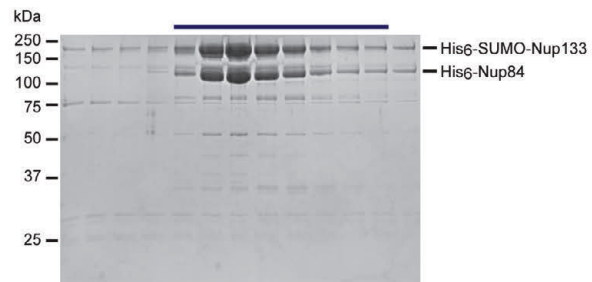
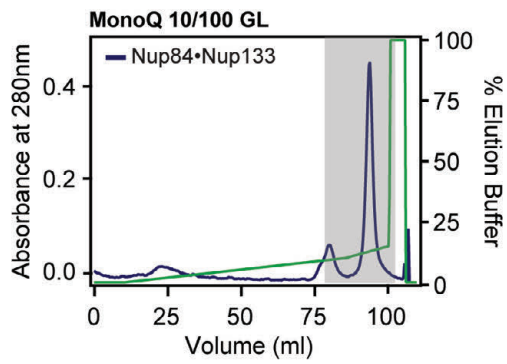
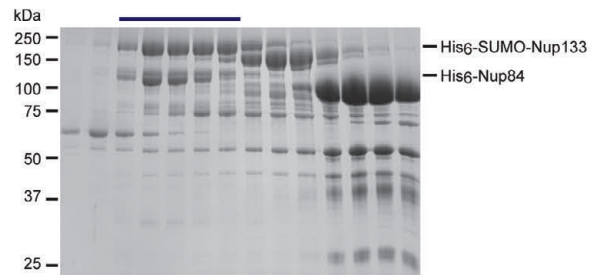
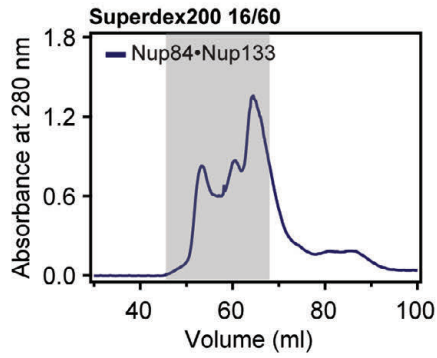
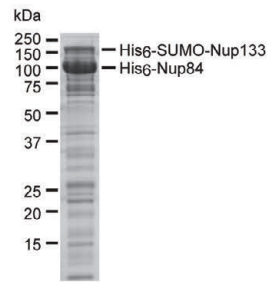
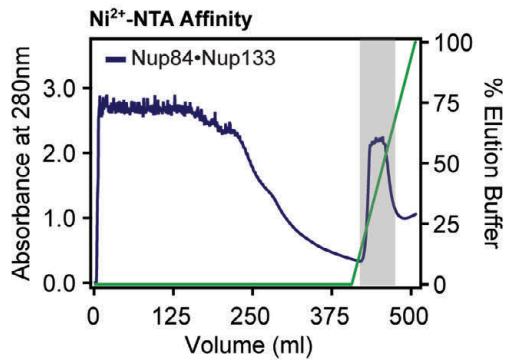
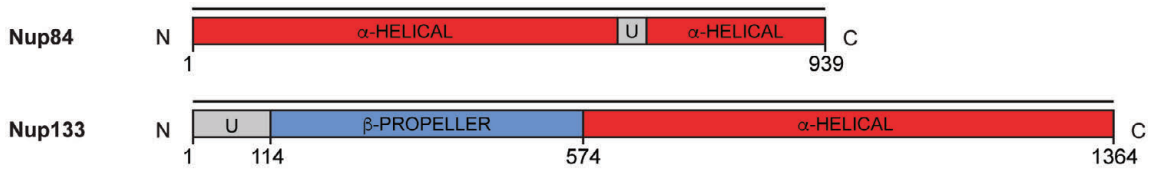


Fig. S53.

Purification protocol for the Nup84•Nup133 hetero-dimer. Domain boundaries for the purified proteins are shown above with black lines indicating the construct boundaries. Sequential steps of purification via chromatography are shown from top to bottom, with the fractions pooled for the subsequent step highlighted in grey. SDS-PAGE gels for each step of the purification are shown next to each chromatogram. Buffer conditions can be found in [Table S2](#).

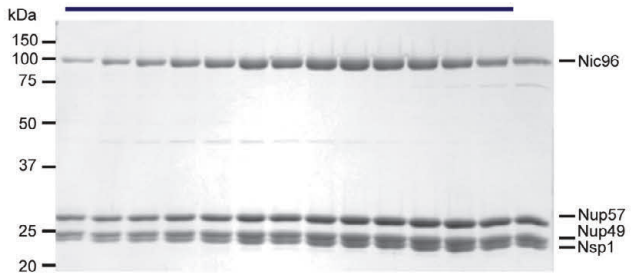
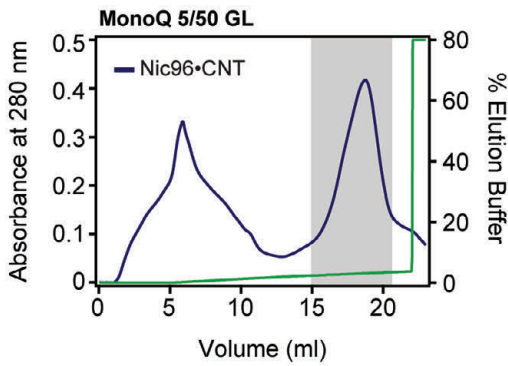
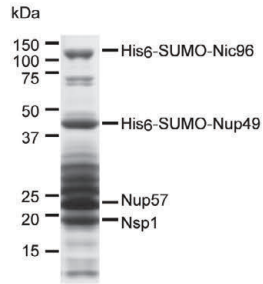
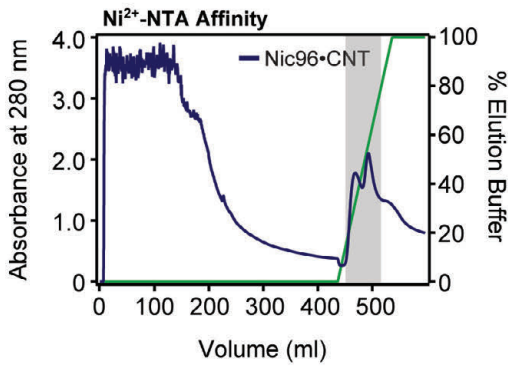
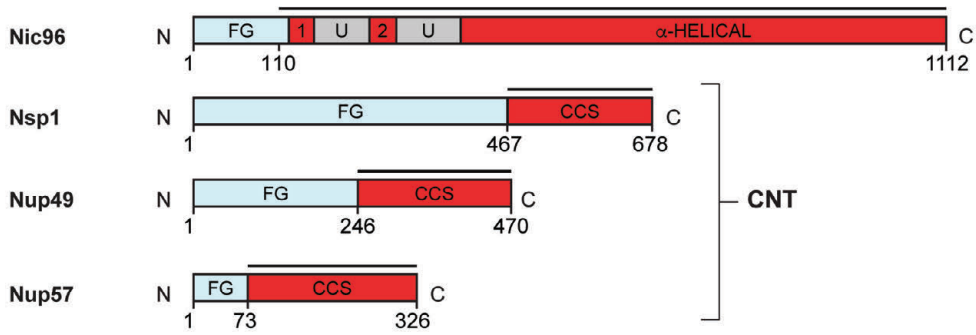


Fig. S54.

Purification protocol for the CNT•Nic96 hetero-tetramer. Domain boundaries of the purified nucleoporins are shown with black lines indicating the construct boundaries. Sequential chromatography purification steps are shown from top to bottom with the employed columns indicated. Gray bars indicate fractions that were resolved on SDS-PAGE gels and visualized by Coomassie staining. Pooled fractions are indicated with a black bar above the SDS-PAGE gels. For details of the buffer conditions see [Table S2](#).

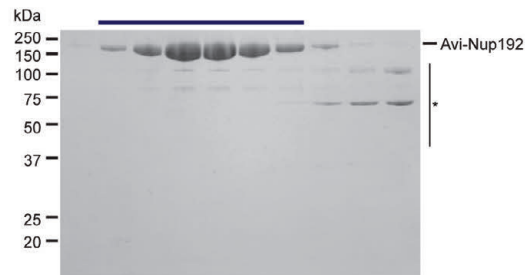
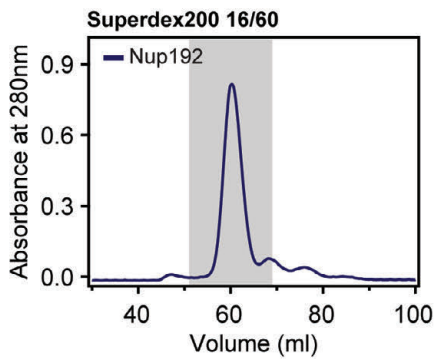
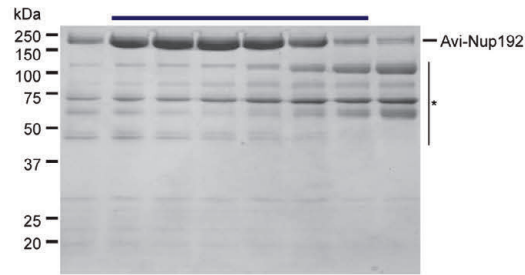
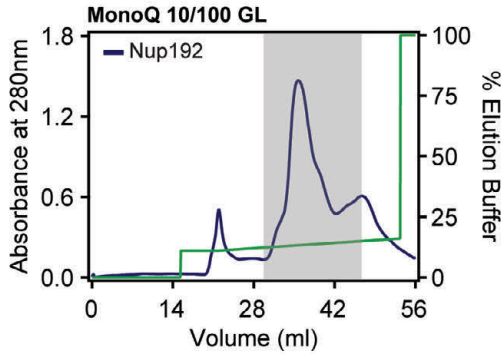
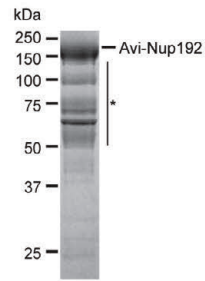
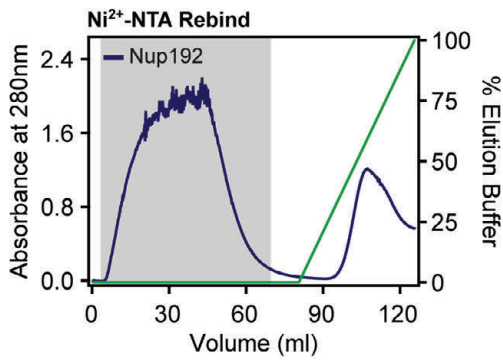
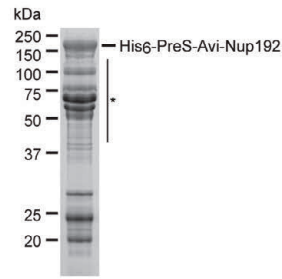
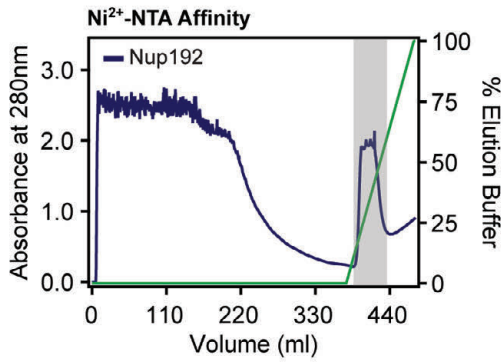


Fig. S55.

Purification protocol for Nup192. Domain boundaries of the purified nucleoporins are shown with black lines indicating the construct boundaries. Sequential chromatography purification steps are shown from top to bottom with the employed columns indicated. Gray bars indicate fractions that were resolved on SDS-PAGE gels and visualized by Coomassie staining. Pooled fractions are indicated with a black bar above the SDS-PAGE gels. For details of the buffer conditions see [Table S2](#).

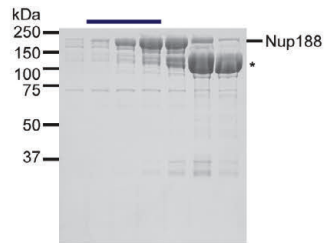
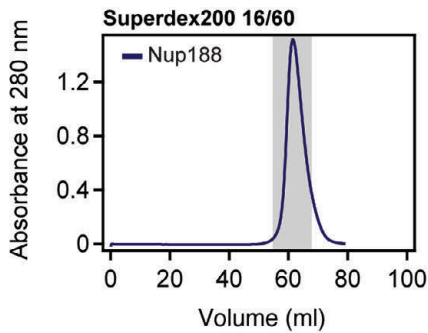
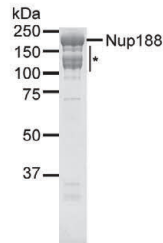
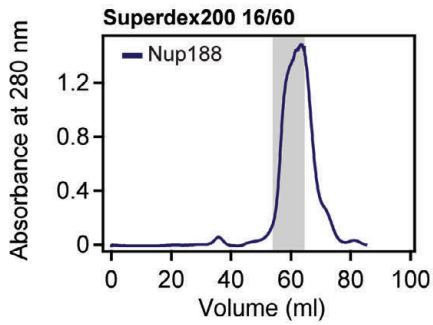
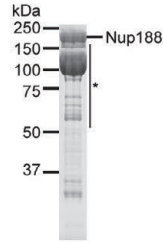
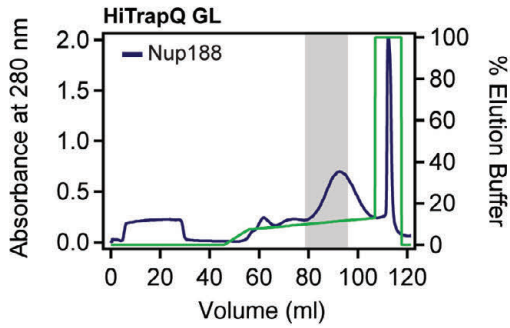
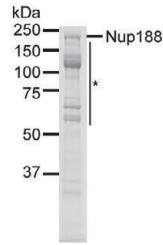
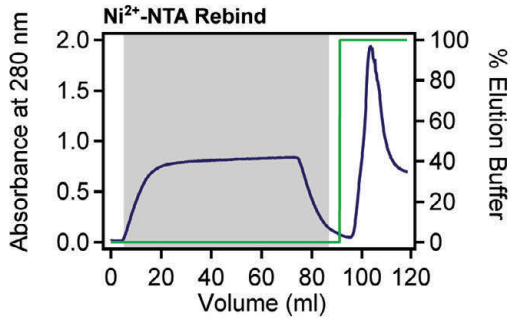
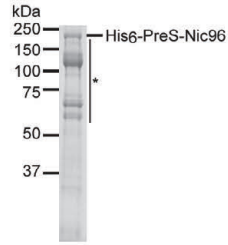
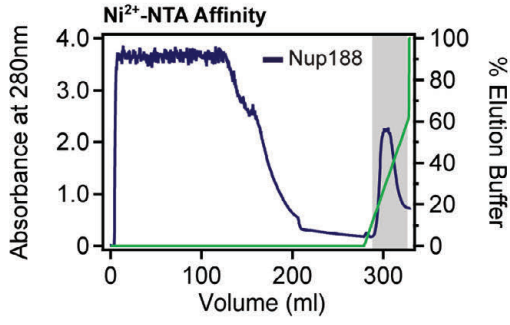
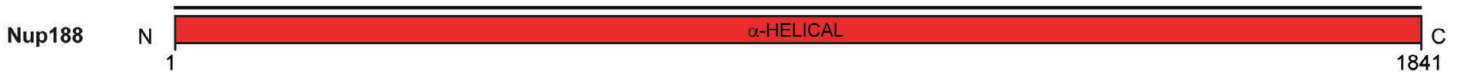


Fig. S56.

Purification protocol for Nup188. Domain boundaries of the purified nucleoporins are shown with black lines indicating the construct boundaries. Sequential chromatography purification steps are shown from top to bottom with the employed columns indicated. Gray bars indicate fractions that were resolved on SDS-PAGE gels and visualized by Coomassie staining. Pooled fractions are indicated with a black bar above the SDS-PAGE gels. For details of the buffer conditions see [Table S2](#).

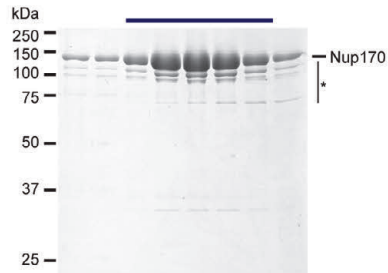
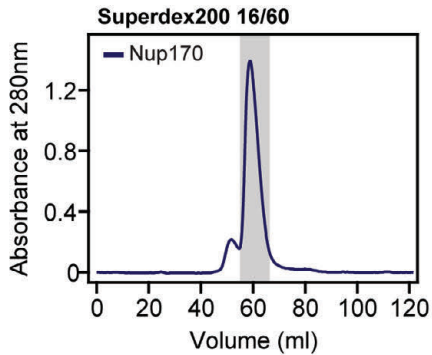
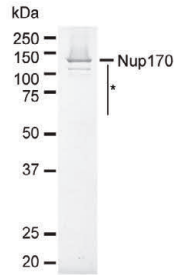
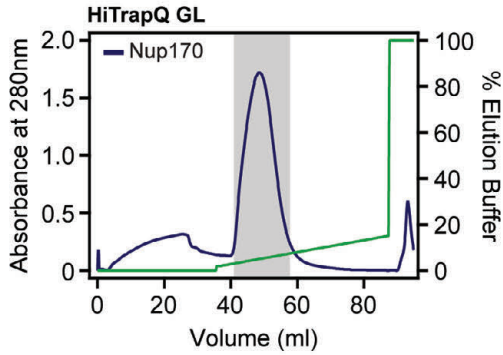
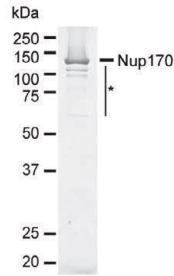
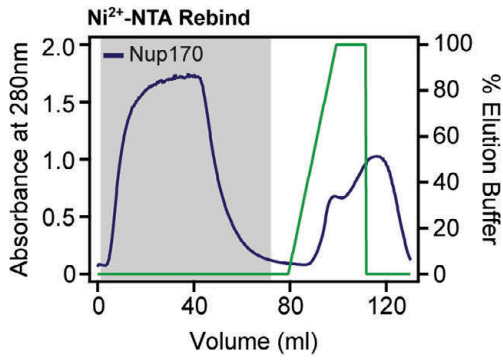
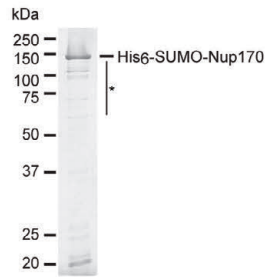
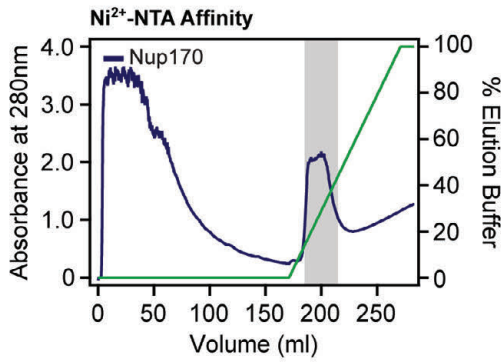
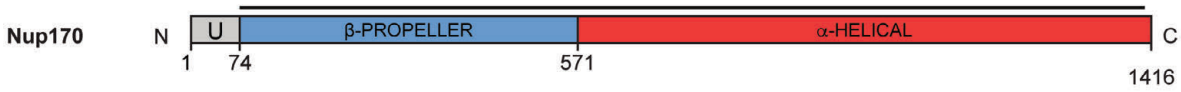


Fig. S57.

Purification protocol for Nup170. Domain boundaries of the purified nucleoporins are shown with black lines indicating the construct boundaries. Sequential chromatography purification steps are shown from top to bottom with the employed columns indicated. Gray bars indicate fractions that were resolved on SDS-PAGE gels and visualized by Coomassie staining. Pooled fractions are indicated with a black bar above the SDS-PAGE gels. For details of the buffer conditions see [Table S2](#).

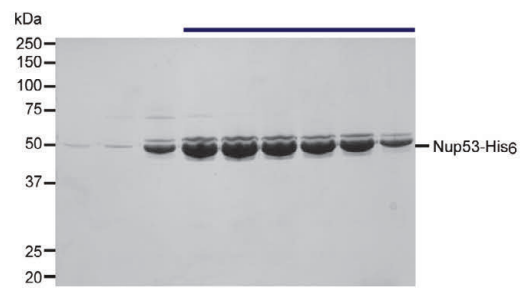
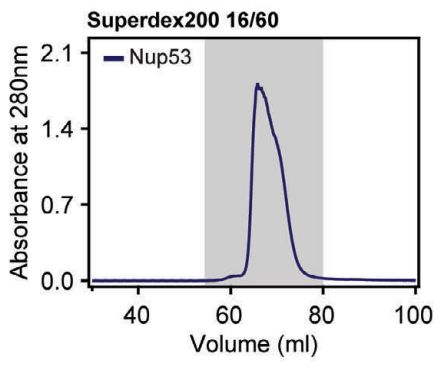
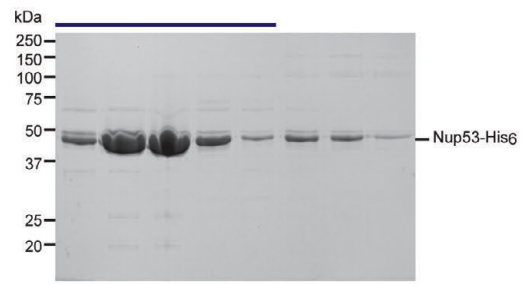
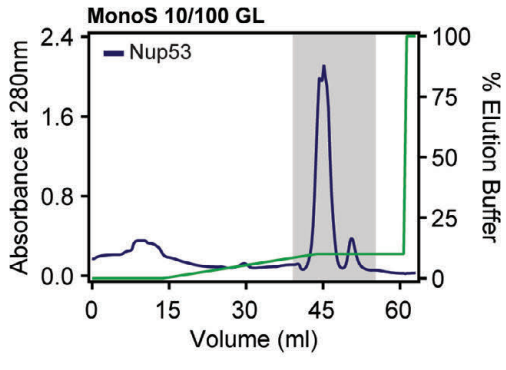
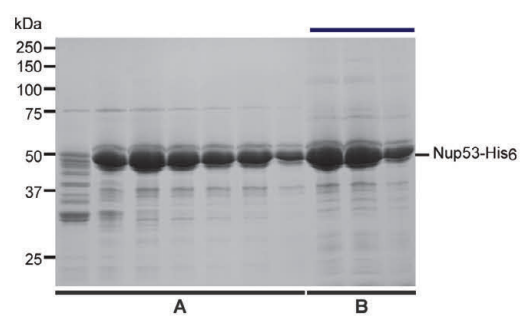
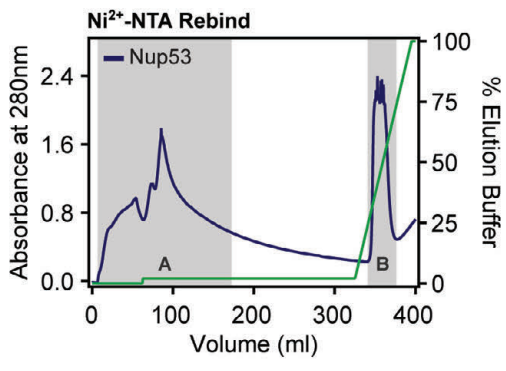
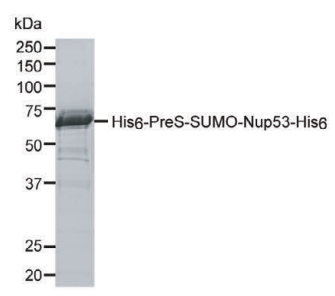
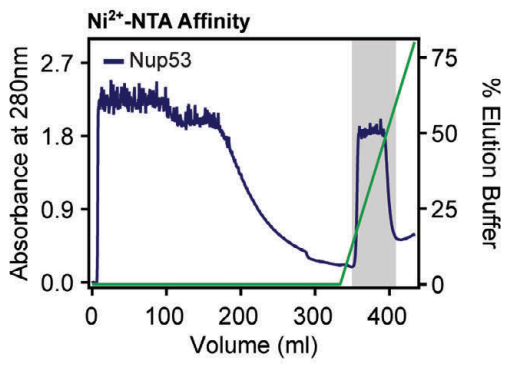
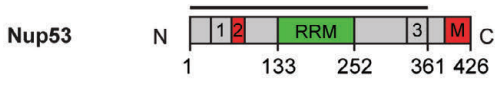


Fig. S58.

Purification protocol for Nup53. Domain boundaries of the purified nucleoporins are shown with black lines indicating the construct boundaries. Sequential chromatography purification steps are shown from top to bottom with the employed columns indicated. Gray bars indicate fractions that were resolved on SDS-PAGE gels and visualized by Coomassie staining. Pooled fractions are indicated with a black bar above the SDS-PAGE gels. For details of the buffer conditions see [Table S2](#).

Nup145N

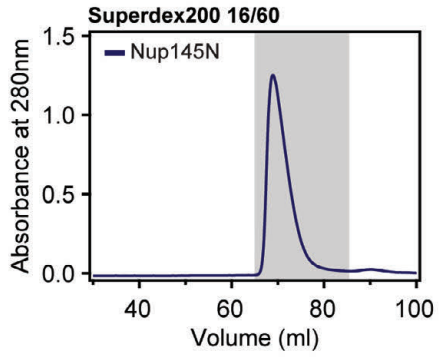
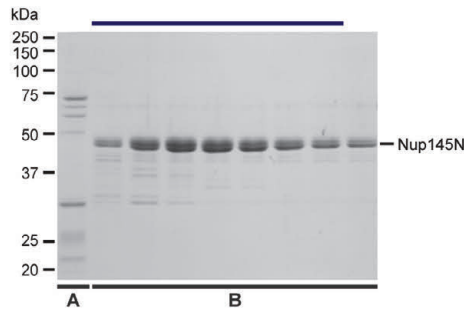
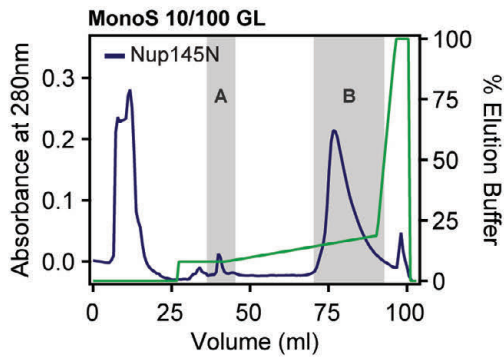
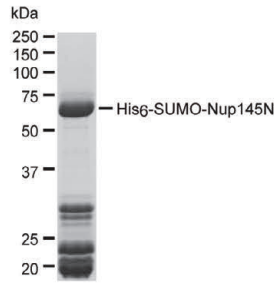
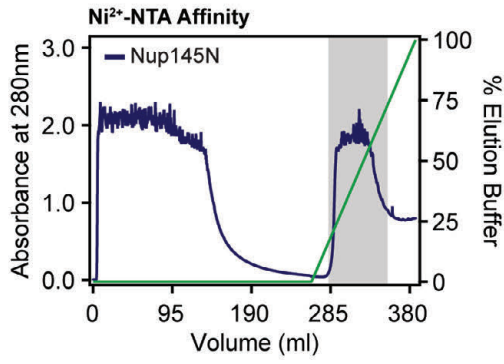


Fig. S59.

Purification protocol for Nup145N. Domain boundaries of the purified nucleoporins are shown with black lines indicating the construct boundaries. Sequential chromatography purification steps are shown from top to bottom with the employed columns indicated. Gray bars indicate fractions that were resolved on SDS-PAGE gels and visualized by Coomassie staining. Pooled fractions are indicated with a black bar above the SDS-PAGE gels. For details of the buffer conditions see [Table S2](#).

Table S1.**Bacterial expression constructs and expression conditions**

#	Protein	Residues	Expression vector	Restriction sites 5', 3'	N-terminal overhang	C-terminal overhang	Expression conditions
1	Nup82 NTD	1-595	pET28a-PreS	NdeI, NotI	GPH	none	18 °C / 18 hours
2	Nup159 T	1440-1481	pET28a-SUMO	BamHI, NotI	S	none	18 °C / 18 hours
3	Nup120 Nup37 ELYS	1-1262 1-610 1-299	pET-MCN-SUMO	NdeI, BamHI NdeI, BamHI BamHI, NotI	GPHMHSHHHH Q S	none none none	37 °C / 2 hours
4	Nup85	230-1169	pET24a	NdeI, BamHI	MGHSHHHH	none	37 °C / 2 hours
5	Sec13	1-309	pETMCN	NdeI, BamHI	Q	none	23 °C / 18 hours; coexpressed with Nup145C
6	Nup145C	1-800	pET-MCN-SUMO	NcoI, NotI	S	none	23 °C / 18 hours; coexpressed with Sec13
7	Nup84	1-939	pET24a	NdeI, BamHI	MGHSHHHH	none	23 °C / 18 hours; coexpressed with Nup133
8	Nup133	1-1364	pET-MCN-SUMO	EcoRI, HindIII	SEF	none	23 °C / 18 hours; coexpressed with Nup84
9	Nup133 ΔNTE	105-1364	pET-MCN-SUMO	EcoRI, HindIII	SEF	none	23 °C / 18 hours; coexpressed with Nup84
10	Nup53	1-361	pET28a-SUMO	BamHI, XhoI	S	LEHSHHHH	23 °C / 18 hours
11*	Nup53 RRM	133-253	pET28a-PreS	NdeI, XhoI	GPHM	none	23 °C / 18 hours
12	Nup53 R2	69-90	pET28a-SUMO	BamHI, NotI	S	none	37 °C / 2 hours
13*	Nup53	31-84	pET28a-SUMO	BamHI, NotI	S	none	37 °C / 2 hours
14	Nup53 R1	31-67	pET28a-SUMO	BamHI, NotI	S	none	37 °C / 2 hours
15	Nup53	1-90	pET28a-SUMO	BamHI, NotI	S	none	37 °C / 2 hours
16	Nup53 R3	329-361	pGEX-6P-1	BamHI, NotI	not cleaved	none	37 °C / 2 hours
17	Nup53 R3 (F334A)	329-361	pGEX-6P-1	BamHI, NotI	not cleaved	none	37 °C / 2 hours
18	Nup53 R3 (I338A)	329-361	pGEX-6P-1	BamHI, NotI	not cleaved	none	37 °C / 2 hours
19	Nup53 R3 (R342A)	329-361	pGEX-6P-1	BamHI, NotI	not cleaved	none	37 °C / 2 hours
20	Nup53 R3 (K343A)	329-361	pGEX-6P-1	BamHI, NotI	not cleaved	none	37 °C / 2 hours
21	Nup53 R3 (L346A)	329-361	pGEX-6P-1	BamHI, NotI	not cleaved	none	37 °C / 2 hours
22	Nup53 R3 (L347A)	329-361	pGEX-6P-1	BamHI, NotI	not cleaved	none	37 °C / 2 hours
23	Nup53 R3 (E350A)	329-361	pGEX-6P-1	BamHI, NotI	not cleaved	none	37 °C / 2 hours
24	Nup53 R3 (E351A)	329-361	pGEX-6P-1	BamHI, NotI	not cleaved	none	37 °C / 2 hours
25	Nup53 R3 (L353A)	329-361	pGEX-6P-1	BamHI, NotI	not cleaved	none	37 °C / 2 hours
26	Nup53 R3 (L354A)	329-361	pGEX-6P-1	BamHI, NotI	not cleaved	none	37 °C / 2 hours
27	Nup170	74-1402	pET28a-SUMO	BamHI, NotI	S	none	37 °C / 2 hours
28	Nup170 ΔC	74-1037	pET28a-SUMO	BamHI, NotI	S	none	37 °C / 2 hours
29*	Nup170 SOL	575-1402	pET28a-SUMO	BamHI, NotI	S	none	37 °C / 2 hours
30	Nup170 CTD	851-1402	pET28a-SUMO	BamHI, NotI	S	none	37 °C / 2 hours
31*	Nup170 CTD (ΔTLR)	851-1402 (Δ1375-1377)	pET28a-SUMO	BamHI, NotI	S	none	37 °C / 2 hours
32*	Nup170 NTD	74-827 (Δ293-305)	pET28a-SUMO	BamHI, NotI	S	none	37 °C / 2 hours
33*	Nup170 NTD	74-843 (Δ293-305)	pET28a-SUMO	BamHI, NotI	S	none	37 °C / 2 hours
34	Nup170 NTD (F199A)	74-843	pET28a-SUMO	BamHI, NotI	S	none	37 °C / 2 hours
35	Nup170 NTD (Y235A)	74-843	pET28a-SUMO	BamHI, NotI	S	none	37 °C / 2 hours
36	Nup170 NTD (V241A)	74-843	pET28a-SUMO	BamHI, NotI	S	none	37 °C / 2 hours
37	Nup170 NTD (W280A)	74-843	pET28a-SUMO	BamHI, NotI	S	none	37 °C / 2 hours
38*	Nup170 CTD	851-1416	pET28a-SUMO	BamHI, NotI	S	none	37 °C / 2 hours
39	Nup170 NTD (F281A)	74-843	pET28a-SUMO	BamHI, NotI	S	none	37 °C / 2 hours
40	Nup170 NTD (R284A)	74-843	pET28a-SUMO	BamHI, NotI	S	none	37 °C / 2 hours
41	Nup170 NTD (I203A)	74-843	pET28a-SUMO	BamHI, NotI	S	none	37 °C / 2 hours
42	Nup170 NTD (M239A)	74-843	pET28a-SUMO	BamHI, NotI	S	none	37 °C / 2 hours
43	Nup170 NTD (L218A)	74-843	pET28a-SUMO	BamHI, NotI	S	none	37 °C / 2 hours
44	Nup170 NTD (E214A)	74-843	pET28a-SUMO	BamHI, NotI	S	none	37 °C / 2 hours
45	Nup170 NTD (E181A)	74-843	pET28a-SUMO	BamHI, NotI	S	none	37 °C / 2 hours
46	Nup170 CTD (Y1050A)	851-1402	pET28a-SUMO	BamHI, NotI	S	none	37 °C / 2 hours
47	Nup170 CTD (V1062A)	851-1402	pET28a-SUMO	BamHI, NotI	S	none	37 °C / 2 hours
48	Nup170 CTD (L1066A)	851-1402	pET28a-SUMO	BamHI, NotI	S	none	37 °C / 2 hours
49	Nup170 CTD (E1110A)	851-1402	pET28a-SUMO	BamHI, NotI	S	none	37 °C / 2 hours
50	Nup170 CTD (L1111A)	851-1402	pET28a-SUMO	BamHI, NotI	S	none	37 °C / 2 hours
51	Nup170 CTD (I1131A)	851-1402	pET28a-SUMO	BamHI, NotI	S	none	37 °C / 2 hours
52	Nup170 CTD (I1147A)	851-1402	pET28a-SUMO	BamHI, NotI	S	none	37 °C / 2 hours
53	Nup170 CTD (Y1164A)	851-1402	pET28a-SUMO	BamHI, NotI	S	none	37 °C / 2 hours
54	Nup170 CTD (F1171A)	851-1402	pET28a-SUMO	BamHI, NotI	S	none	37 °C / 2 hours
55	Nup170 CTD (F1154A)	851-1402	pET28a-SUMO	BamHI, NotI	S	none	37 °C / 2 hours
56	Nup170 CTD (Y1157A)	851-1402	pET28a-SUMO	BamHI, NotI	S	none	37 °C / 2 hours
57*	Nup170 CTD (Y905M/ L1007M/L1183M/V1292M)	832-1416	pET28a-SUMO	BamHI, NotI	S	none	37 °C / 2 hours

#	Protein	Residues	Expression vector	Restriction sites 5', 3'	N-terminal overhang	C-terminal overhang	Expression conditions
58	Nup145N	606-993	pET28a-SUMO	BamHI, NotI	S	none	23 °C / 18 hours
59*	Nup145N APD	858-993	pET28a-PreS	NdeI, XhoI	GPHM	none	23 °C / 18 hours
60*	Nup145N APD (T994A) •Nup145C N	858-1000	pET28a-PreS	NdeI, XhoI	GPHM	none	23 °C / 18 hours
61	Nup145N R1	606-683	pET28a-SUMO	BamHI, NotI	S	AAALEHHHHHH	37 °C / 2 hours
62	Nup145N	606-750	pET28a-SUMO	BamHI, NotI	S	AAALEHHHHHH	37 °C / 2 hours
63	Nup145N	649-750	pET28a-SUMO	BamHI, NotI	S	AAALEHHHHHH	37 °C / 2 hours
64	Nup145N R3	729-750	pGEX-6P-1	BamHI, NotI	not cleaved	none	18 °C / 18 hours
65	Nup145N R3 (L733A)	729-750	pGEX-6P-1	BamHI, NotI	not cleaved	none	18 °C / 18 hours
66	Nup145N R3 (V734A)	729-750	pGEX-6P-1	BamHI, NotI	not cleaved	none	18 °C / 18 hours
67	Nup145N R3 (I735A)	729-750	pGEX-6P-1	BamHI, NotI	not cleaved	none	18 °C / 18 hours
68	Nup145N R3 (M739A)	729-750	pGEX-6P-1	BamHI, NotI	not cleaved	none	18 °C / 18 hours
69	Nup145N R3 (D742A)	729-750	pGEX-6P-1	BamHI, NotI	not cleaved	none	18 °C / 18 hours
70	Nup145N R3 (L743A)	729-750	pGEX-6P-1	BamHI, NotI	not cleaved	none	18 °C / 18 hours
71	Nup145N R3 (F744A)	729-750	pGEX-6P-1	BamHI, NotI	not cleaved	none	18 °C / 18 hours
72	Avi-Nup192	1-1756	pET28a-PreS	NdeI, NotI		GPLMSGSLNDIFEAQKI EWHEGSAGGSGH	37 °C / 2 hours
73*	Nup192 ΔHEAD	153-1756 (Δ167-184, replaced with GSGS)	pET28a-PreS	NdeI, NotI	GPHM	none	37 °C / 2 hours
74	Nup192 NTD	1-958	pET28a-PreS	NdeI, NotI	GPH	none	37 °C / 2 hours
75	Nup192 CTD	921-1756	pET28a-PreS	NdeI, NotI	GPHM	none	23 °C / 18 hours
76	Nup192 TAIL	1397-1756	pET28a-PreS	NdeI, NotI	GPHM	none	37 °C / 2 hours
77	Nic96	110-1112	pET28a-SUMO	BamHI, NotI	S	AAALEHHHHHH	18 °C / 18 hours
78*	Nic96 SOL	391-1112	pET28a-SUMO	BamHI, NotI	S	none	18 °C / 18 hours
79	Nic96 R2Δ2	274-301	pET-MCN-SUMO	BamHI, NotI	S	none	37 °C / 2 hours coexpressed with Nup188 TAIL
80	Nic96 R2Δ4	286-301	pET-MCN-SUMO	BamHI, NotI	S	none	37 °C / 2 hours
81	Nic96 R2	262-301	pET-MCN-SUMO	BamHI, NotI	S	none	37 °C / 2 hours
82	Nic96 R2 (F275A)	262-301	pET-MCN-SUMO	BamHI, NotI	S	none	37 °C / 2 hours
83	Nic96 R2 (D276A)	262-301	pET-MCN-SUMO	BamHI, NotI	S	none	37 °C / 2 hours
84	Nic96 R2 (F278A)	262-301	pET-MCN-SUMO	BamHI, NotI	S	none	37 °C / 2 hours
85	Nic96 R2 (N282A)	262-301	pET-MCN-SUMO	BamHI, NotI	S	none	37 °C / 2 hours
86	Nic96 R2 (L285A)	262-301	pET-MCN-SUMO	BamHI, NotI	S	none	37 °C / 2 hours
87	Nic96 R2 (W287A)	262-301	pET-MCN-SUMO	BamHI, NotI	S	none	37 °C / 2 hours
88	Nic96 R2 (I294A)	262-301	pET-MCN-SUMO	BamHI, NotI	S	none	37 °C / 2 hours
89	Nic96 R2 (F298A)	262-301	pET-MCN-SUMO	BamHI, NotI	S	none	37 °C / 2 hours
90	Nic96 SOL (L715A)	391-1112	pET28a-SUMO	BamHI, NotI	S	none	18 °C / 18 hours
91	Nic96 SOL (V655A/W658A)	391-1112	pET28a-SUMO	BamHI, NotI	S	none	18 °C / 18 hours
92	Nic96 SOL (F697A)	391-1112	pET28a-SUMO	BamHI, NotI	S	none	18 °C / 18 hours
93	Nup188	1-1858	pET28a-PreS	Asel, BamHI	GPHN	none	23 °C / 18 hours
94	Nup188 NTD	1-1134	pET28a-PreS	Asel, BamHI	GPHN	none	23 °C / 18 hours
95	Nup188 TAIL	1447-1858	pET28a-SUMO	BamHI, NotI	SM	none	18 °C / 18 hours
96	Nsp1 Nup57	467-674 74-319	pETDuet1	NcoI, NotI NdeI, XhoI	None M	none none	18 °C / 18 hours coexpressed with Nup49
97	Nup49	246-470	pET28a-SUMO	BamHI, NotI	S	none	18 °C / 18 hours coexpressed with Nsp1 and Nup57
98	hsNup155 CTD	870-1391	pET28a-PreS	NdeI, NotI	GPHM	none	37 °C / 2 hours
99	hsNup98	596-617	pGEX-6P-1	BamHI, NotI	not cleaved	none	23 °C / 18 hours
100	hsNup98 (S608E/S612E)	596-617	pGEX-6P-1	BamHI, NotI	not cleaved	none	23 °C / 18 hours
101	scNup159 T scNup82 NTD	1425-1460 1-452	pETDuet1	NcoI, NotI NdeI, XhoI	GPHM none	none none	18 °C / 16 hours
102	scNup145C scSec13	1-712 1-297	pETDuet1	BamHI, NotI NdeI, XhoI	MGSSHHHHHSQDP N/A	none none	18 °C / 16 hours
103	scNup53	374-460	pET28a-SUMO	BamHI, NotI	S	none	18 °C / 16 hours
104	scNup170 CTD	999-1502	pET28a-SUMO	SacI, NotI	SEFEL	none	18 °C / 8 hours
105	scNup170 CTD (F1308A)	999-1502	pET28a-SUMO	SacI, NotI	SEFEL	none	18 °C / 8 hours
106	scNup157 CTD	894-1391	pET28a-SUMO	BamHI, NotI	S	none	18 °C / 16 hours
107	scNup157 NTD	70-893	pGEX-6P-1	BamHI, NotI	GPLGS	none	18 °C / 8 hours
108	scNup157 NTD (F214A)	70-893	pGEX-6P-1	BamHI, NotI	GPLGS	none	18 °C / 8 hours
109	scNup100	571-959	pET28a-SUMO	BamHI, NotI	S	none	18 °C / 16 hours
110	scNup116	752-1113	pET28a-SUMO	BamHI, NotI	S	none	18 °C / 16 hours
111	scNup145N	210-605	pET28a-SUMO	BamHI, NotI	S	none	18 °C / 16 hours
112	scNup192 NTD	1-960	pET28a-PreS	NdeI, NotI	GPH	none	21 °C / 8 hours
113	scNic96 SOL (I432A/W435A/Y469A)	204-839	pET28a-SUMO	BamHI, NotI	S	none	18 °C / 16 hours
114	scNup53	1-240	pET28a-SUMO	BamHI, NotI	S	none	18 °C / 16 hours
115	scNup188	1-1655	pET28a-SUMO	BamHI, NotI	S	none	21 °C / 16 hours
116	Nup145N PreS	606-993	pET28a-SUMO	BamHI, NotI	S	none	23 °C / 18 hours

Proteins are from *C. thermophilum* unless otherwise noted

* Constructs that were used for crystallization

Table S2.**Protein purification protocols**

Protein(s)	Expression constructs	Purification step	Buffer A	Buffer B
Avi-Nup192*	Individual (#72)	1. Ni-NTA 2. Dialysis/Cleavage 3. Ni-NTA 4. MonoQ 10/100 GL 5. HiLoad Superdex 200 16/60 PG	1. Ni-A1, 5 mM β -ME 2. IEX-A2, pH 8.0, 5 mM β -ME / PreS 3. Ni-A2, 5 mM β -ME 4. IEX-A2, pH 8.0, 5 mM DTT 5. SEC-A, 5 mM DTT	1. Ni-B1, 5 mM β -ME 2. N/A 3. Ni-B1, 5 mM β -ME 4. IEX-B, pH 8.0, 5 mM DTT 5. N/A
Nup192 ΔHEAD*	Individual (#73)	1. Ni-NTA 2. Dialysis/Cleavage 3. Ni-NTA 4. MonoQ 10/100 GL 5. HiLoad Superdex 200 16/60 PG	1. Ni-A1, 5 mM β -ME 2. IEX-A2, pH 8.0, 5 mM β -ME / PreS 3. Ni-A2, 5 mM β -ME 4. IEX-A2, pH 8.0, 5 mM DTT 5. SEC-A, 5 mM DTT	1. Ni-B1, 5 mM β -ME 2. N/A 3. Ni-B1, 5 mM β -ME 4. IEX-B, pH 8.0, 5 mM DTT 5. N/A
Nup192 NTD	Individual (#74)	1. Ni-NTA 2. Dialysis/Cleavage 3. Ni-NTA 4. HiTrap Q HP 5. HiLoad Superdex 200 16/60 PG	1. Ni-A1, 5 mM β -ME 2. Ni-A2, 5 mM β -ME / PreS 3. Ni-A2, 5 mM β -ME 4. IEX-A2, pH 8.0, 5 mM DTT 5. SEC-A, 5 mM DTT	1. Ni-B1, 5 mM β -ME 2. N/A 3. Ni-B1, 5 mM β -ME 4. IEX-B, pH 8.0, 5 mM DTT 5. N/A
Nup192 CTD	Individual (#75)	1. Ni-NTA 2. Dialysis/Cleavage 3. Ni-NTA 4. MonoQ 10/100 GL 5. HiLoad Superdex 200 16/60 PG	1. Ni-A1, 5 mM β -ME 2. IEX-A2, pH 8.0, 5 mM β -ME / PreS 3. Ni-A2, 5 mM β -ME 4. IEX-A2, pH 8.0, 5 mM DTT 5. SEC-A, 5 mM DTT	1. Ni-B1, 5 mM β -ME 2. N/A 3. Ni-B1, 5 mM β -ME 4. IEX-B, pH 8.0, 5 mM DTT 5. N/A
Nup192 TAIL	Individual (#76)	1. Ni-NTA 2. Dialysis/Cleavage 3. Ni-NTA 4. HiLoad Superdex 200 16/60 PG	1. Ni-A1, 5 mM β -ME 2. Ni-A3, 5 mM β -ME / PreS 3. Ni-A3, 5 mM β -ME 4. SEC-C, 1 mM DTT	1. Ni-B1, 5 mM β -ME 2. N/A 3. Ni-B1, 5 mM β -ME 4. N/A
Nup188*	Individual (#93)	1. Ni-NTA 2. Dialysis/Cleavage 3. Ni-NTA 4. HiTrap Q HP 5. HiLoad Superdex 200 16/60 PG 6. HiLoad Superdex 200 16/60 PG	1. Ni-A1, 5 mM β -ME 2. IEX-A2, pH 8.0, 5 mM β -ME / PreS 3. Ni-A2, 5 mM β -ME 4. IEX-A2, pH 8.0, 5 mM DTT 5. SEC-A, 5 mM DTT 6. SEC-A, 5 mM DTT	1. Ni-B1, 5 mM β -ME 2. N/A 3. Ni-B1, 5 mM β -ME 4. IEX-B, pH 8.0, 5 mM DTT 5. N/A 6. N/A
Nup188 NTD	Individual (#94)	1. Ni-NTA 2. Dialysis/Cleavage 3. Ni-NTA 4. HiTrap Q HP 5. HiLoad Superdex 200 16/60 PG	1. Ni-A1, 5 mM β -ME 2. Ni-A2, 5 mM β -ME / PreS 3. Ni-A2, 5 mM β -ME 4. IEX-A2, pH 8.0, 5 mM DTT 5. SEC-A, 5 mM DTT	1. Ni-B1, 5 mM β -ME 2. N/A 3. Ni-B1, 5 mM β -ME 4. IEX-B, pH 8.0, 5 mM DTT 5. N/A
Nup188 TAIL	Individual (#95)	1. Ni-NTA 2. Dialysis/Cleavage 3. Ni-NTA 4. HiTrap Q HP 5. HiLoad Superdex 200 16/60 PG	1. Ni-A1, 5 mM β -ME 2. Ni-A2, 5 mM β -ME / ULP1 3. Ni-A2, 5 mM β -ME 4. IEX-A2, pH 8.0, 5 mM DTT 5. SEC-A, 5 mM DTT	1. Ni-B1, 5 mM β -ME 2. N/A 3. Ni-B1, 5 mM β -ME 4. IEX-B, pH 8.0, 5 mM DTT 5. N/A
Nic96 SOL* wild-type and mutants	Individual (#78, 82-92)	1. Ni-NTA 2. HiPrep 26/20 Desalting/Cleavage 3. Ni-NTA 4. HiLoad Superdex 200 16/60 PG	1. Ni-A1, 5 mM β -ME 2. IEX-A2, pH 8.0, 5 mM β -ME / ULP1 3. Ni-A2, 5 mM β -ME 4. SEC-A, 5 mM DTT	1. Ni-B1, 5 mM β -ME 2. N/A 3. Ni-B1, 5 mM β -ME 4. N/A
Nup170*	Individual (#27)	1. Ni-NTA 2. Dialysis/Cleavage 3. Ni-NTA 4. HiTrap Q HP 5. HiLoad Superdex 200 16/60 PG	1. Ni-A1, 5 mM β -ME, 5 % Glycerol 2. Ni-A3, 5 mM β -ME, 5 % Glycerol / ULP1 3. Ni-A3, 5 mM β -ME, 5 % Glycerol 4. IEX-A4, pH 8.0, 5 mM DTT, 5 % Glycerol 5. SEC-C, 5 mM DTT, 5 % Glycerol	1. Ni-B1, 5 mM β -ME, 5 % Glycerol 2. N/A 3. Ni-B1, 5 mM β -ME, 5 % Glycerol 4. IEX-B, pH 8.0, 5 mM DTT, 5 % Glycerol 5. N/A
Nup170 SOL*	Individual (#29)	1. Ni-NTA 2. Dialysis/Cleavage (48 hr) 3. Ni-NTA 4. HiTrap Q HP 5. HiLoad Superdex 200 16/60 PG	1. Ni-A1, 5 mM β -ME, 2. Ni-A3, 5 mM β -ME / ULP1 3. Ni-A3, 5 mM β -ME 4. IEX-A4, pH 8.0, 5 mM DTT 5. SEC-C, 5 mM DTT	1. Ni-B1, 5 mM β -ME 2. N/A 3. Ni-B1, 5 mM β -ME 4. IEX-B, pH 8.0, 5 mM DTT 5. N/A
Nup170 NTD* wild-type and mutants	Individual (#32-47, 39-45)	1. Ni-NTA 2. Dialysis/Cleavage 3. Ni-NTA 4. HiTrap Q HP 5. HiLoad Superdex 200 16/60 PG	1. Ni-A1, 5 mM β -ME, 5 % Glycerol 2. Ni-A3, 5 mM β -ME, 5 % Glycerol / ULP1 3. Ni-A3, 5 mM β -ME, 5 % Glycerol 4. IEX-A2, pH 8.0, 5 mM DTT, 5 % Glycerol 5. SEC-C, 5 mM DTT, 5 % Glycerol	1. Ni-B1, 5 mM β -ME, 5 % Glycerol 2. N/A 3. Ni-B1, 5 mM β -ME, 5 % Glycerol 4. IEX-B, pH 8.0, 5 mM DTT, 5 % Glycerol 5. N/A
Nup170 CTD* wild-type and mutants	Individual (#30-31, 38, 46-57)	1. Ni-NTA 2. HiPrep 26/20 Desalting/Cleavage 3. Ni-NTA 4. HiTrap Q HP 5. HiLoad Superdex 200 16/60 PG	1. Ni-A1, 5 mM β -ME 2. Ni-A2, 5 mM β -ME / ULP1 3. Ni-A2, 5 mM β -ME 4. IEX-A2, pH 8.0, 5 mM DTT 5. SEC-A, 5 mM DTT	1. Ni-B1, 5 mM β -ME 2. N/A 3. Ni-B1, 5 mM β -ME 4. IEX-B, pH 8.0, 5 mM DTT 5. N/A
hsNup155 CTD	Individual (#98)	1. Ni-NTA 2. HiPrep 26/20 Desalting/Cleavage 3. Ni-NTA 4. HiTrap Q HP 5. HiLoad Superdex 200 16/60 PG	1. Ni-A1, 5 mM β -ME, 5 % Glycerol 2. Ni-A3, 5 mM β -ME, 5 % Glycerol / PreS 3. Ni-A3, 5 mM β -ME, 5 % Glycerol 4. IEX-A3, pH 8.0, 5 mM DTT, 5 % Glycerol 5. SEC-B, 5 mM DTT, 5 % Glycerol	1. Ni-B1, 5 mM β -ME, 5 % Glycerol 2. N/A 3. Ni-B1, 5 mM β -ME, 5 % Glycerol 4. IEX-B, pH 8.0, 5 mM DTT, 5 % Glycerol 5. N/A
Nup120•Nup37•ELYS*	Co-expression (#3)	1. Ni-NTA 2. Dialysis/Cleavage 3. HiTrap Q HP 4. HiLoad Superdex 200 16/60 PG	1. Ni-A1, 5 mM β -ME, 5 % Glycerol 2. Ni-A3, 5 mM DTT, 5 % Glycerol / ULP1-PreS 3. IEX-A4, pH 8.0, 5 mM DTT, 5 % Glycerol 4. SEC-A, 5 mM DTT	1. Ni-B1, 5 mM β -ME, 5 % Glycerol 2. N/A 3. IEX-B, pH 8.0, 5 mM DTT, 5 % Glycerol 4. N/A
Nup85*	Individual (#4)	1. Ni-NTA 2. Dialysis/Cleavage 3. HiTrap Q HP 4. HiLoad Superdex 200 16/60 PG	1. Ni-A1, 5 mM β -ME 2. Ni-A2, 5 mM DTT / PreS 3. IEX-A2, pH 8.0, 5 mM DTT 4. SEC-A, 5 mM DTT	1. Ni-B1, 5 mM β -ME, 5 % Glycerol 2. N/A 3. IEX-B, pH 8.0, 5 mM DTT 4. N/A
Sec13•Nup145C*	Co-expression (#5, 6)	1. Ni-NTA 2. HiPrep 26/20 Desalting /Cleavage 3. Ni-NTA 4. HiLoad Superdex 200 16/60 PG	1. Ni-A1, 5 mM β -ME 2. Ni-A2, 5 mM β -ME / ULP1 3. Ni-A2, 5 mM β -ME 4. SEC-A, 5 mM DTT	1. Ni-B1, 5 mM β -ME 2. N/A 3. Ni-B2, 5 mM β -ME 4. N/A

Protein(s)	Expression constructs	Purification step	Buffer A	Buffer B
Nup84-Nup133*	Co-expression (#7, 8)	1. Ni-NTA 2. Dialysis 3. HiLoad Superdex 200 16/60 PG 4. MonoQ 10/100 GL	1. Ni-A1, 5 mM β -ME 2. SEC-A, 5 mM DTT 3. SEC-A, 5 mM DTT 4. IEX-A2, pH 8.0, 5 mM DTT	1. Ni-B1, 5 mM β -ME 2. N/A 3. N/A 4. IEX-B, pH 8.0, 5 mM DTT
Nup84-Nup133 ΔNTE	Co-expression (#7, 9)	1. Ni-NTA 2. Dialysis 3. HiLoad Superdex 200 16/60 PG 4. MonoQ 10/100 GL	1. Ni-A1, 5 mM β -ME 2. SEC-A, 5 mM DTT 3. SEC-A, 5 mM DTT 4. IEX-A2, pH 8.0, 5 mM DTT	1. Ni-B1, 5 mM β -ME 2. N/A 3. N/A 4. IEX-B, pH 8.0, 5 mM DTT
Nup145N* wild-type and PreS	Individual (#58, 116)	1. Ni-NTA 2. HiPrep 26/20 Desalting/Cleavage 3. MonoS 5/50 GL 4. HiLoad Superdex 75 16/60 PG	1. Ni-A1, 5 mM β -ME 2. IEX-A2, pH 7.0, 5 mM DTT / ULP1 3. IEX-A2, pH 7.0, 5 mM DTT 4. SEC-A, 5 mM DTT	1. Ni-B1, 5 mM β -ME 2. N/A 3. IEX-B, pH 7.0, 5 mM DTT 4. N/A
Nup145N APD*	Individual (#59)	1. Ni-NTA 2. Dialysis/cleavage 3. Ni-NTA 4. HiLoad Superdex 75 16/60 PG	1. Ni-A1, 5 mM β -ME 2. Ni-A2, pH 8.0, 5 mM β -ME / PreS 3. Ni-A2, 5 mM β -ME 4. SEC-A, 5 mM DTT	1. Ni-B1, 5 mM β -ME 2. N/A 3. Ni-B1, 5 mM β -ME 4. N/A
GST-Nup145N wild-type and mutants	Individual (#64, 65-71)	1. GST Affinity 2. HiTrap Q HP 3. HiLoad Superdex 200 16/60 PG	1. GST-A, 5 mM DTT 2. IEX-A2, pH 8.0, 5 mM DTT 3. SEC-A, 5 mM DTT	1. GST-B, 5mM DTT 2. IEX-B, pH 8.0, 5 mM DTT 3. N/A
GST-hsNup98 wild-type and mutant	Individual (#99, 100)	1. GST Affinity 2. HiTrap Q HP 3. HiLoad Superdex 200 16/60 PG	1. GST-A, 5 mM DTT 2. IEX-A2, pH 8.0, 5 mM DTT 3. SEC-A, 5 mM DTT	1. GST-B, 5mM DTT 2. IEX-B, pH 8.0, 5 mM DTT 3. N/A
SUMO-Nup145N various fragments	Individual (#61-63)	1. Ni-NTA 2. HiPrep 26/20 Desalting /Cleavage 3. Ni-NTA 4. HiLoad Superdex 200 16/60 PG	1. Ni-A1, 5 mM β -ME 2. Ni-A2, 5 mM β -ME / ULP1 3. Ni-A2, 5 mM β -ME 4. SEC-A, 5 mM DTT	1. Ni-B1, 5 mM β -ME 2. N/A 3. Ni-B2, 5 mM β -ME 4. N/A
Nup53*	Individual (#10)	1. Ni-NTA 2. HiPrep 26/20 Desalting/Cleavage 3. Ni-NTA 4. HiPrep 26/20 Desalting 5. MonoS 5/50 GL 6. HiLoad Superdex 75 16/60 PG	1. Ni-A1, 5 mM β -ME 2. Ni-A1, 5 mM β -ME / ULP1 3. Ni-A1, 5 mM β -ME 4. IEX-A2, pH 7.0, 5 mM DTT 5. IEX-A2, pH 7.0, 5 mM DTT 6. SEC-A, 5 mM DTT	1. Ni-B1, 5 mM β -ME 2. N/A 3. Ni-B1, 5 mM β -ME 4. N/A 5. EX-B, pH 7.0, 5 mM DTT 6. N/A
Nup53 RRM*	Individual (#11)	1. Ni-NTA 2. Desalting/Cleavage 3. Ni-NTA 4. HiLoad Superdex 75 16/60 PG	1. Ni-A1, 5 mM β -ME 2. Ni-A2, pH 8.0, 5 mM β -ME / PreS 3. Ni-A2, 5 mM β -ME 4. SEC-A, 5 mM DTT	1. Ni-B1, 5 mM β -ME 2. N/A 3. Ni-B1, 5 mM β -ME 4. N/A
SUMO-Nup53 various fragments	Individual (#12-15)	1. Ni-NTA 2. HiPrep 26/20 Desalting 3. HiLoad Superdex 75 16/60 PG	1. Ni-A1, 5 mM β -ME 2. SEC-A, 5 mM DTT 3. SEC-A, 5 mM DTT	1. Ni-B1, 5 mM β -ME 2. N/A 3. N/A
GST-Nup53 R3 wild-type and mutants	Individual (#16, 17-26)	1. GST Affinity 2. HiTrap Q HP 3. HiLoad Superdex 200 16/60 PG	1. GST-A, 5 mM DTT 2. IEX-A2, pH 8.0, 5 mM DTT 3. SEC-A, 5 mM DTT	1. GST-B, 5mM DTT 2. IEX-B, pH 8.0, 5 mM DTT 3. N/A
CNT	Co-expression (#96, 97)	1. Ni-NTA 2. HiPrep 26/20 Desalting/Cleavage 3. Ni-NTA 4. HiTrap Q HP 5. HiLoad Superdex 200 16/60 PG	1. Ni-A1, 4 mM β -ME 2. Ni-A2, 4 mM β -ME / ULP1 3. Ni-A2, 4 mM β -ME 4. IEX-A2, pH 8.0, 5 mM DTT 5. SEC-A, 5 mM DTT	1. Ni-B1, 4 mM β -ME 2. N/A 3. Ni-B1, 4 mM β -ME 4. IEX-B, pH 8.0, 5 mM DTT 5. N/A
Nup82 NTD* SUMO-Nup159 T	Individual (#1, 2) co-lysis ratio 1:1	1. Ni-NTA 2. Dialysis/Cleavage 3. Ni-NTA 4. HiLoad Superdex 200 16/60 PG	1. Ni-A1, 5 mM β -ME 2. Ni-A1, 5 mM β -ME / PreS / ULP1 3. Ni-A1, 5 mM β -ME 4. SEC-A, 5 mM DTT	1. Ni-B1, 4 mM β -ME 2. N/A 3. Ni-B1, 4 mM β -ME 4. N/A
His₆-Nup192 TAIL	Individual (#76)	1. Ni-NTA 2. Dialysis 3. HiTrap Q HP 4. HiLoad Superdex 200 16/60 PG	1. Ni-A1, 5 mM β -ME 2. IEX-A1, pH 9.0, 1 mM DTT 3. IEX-A1, pH 9.0, 1 mM DTT 4. SEC-C, 1 mM DTT	1. Ni-B1, 5 mM β -ME 2. N/A 3. IEX-B, pH 9.0, 1 mM DTT 4. N/A
SUMO-Nup188 TAIL	Individual (#95)	1. Ni-NTA 2. Dialysis 3. MonoQ 10/100 GL 4. HiLoad Superdex 200 16/60 PG	1. Ni-A1, 5 mM β -ME 2. IEX-A2, pH 8.0, 1 mM DTT 3. IEX-A2, pH 8.0, 1 mM DTT 4. SEC-C, 1 mM DTT	1. Ni-B1, 5 mM β -ME 2. N/A 3. IEX-B, pH 8.0, 1 mM DTT 4. N/A
SUMO-Nup188 TAIL* SUMO-Nic96-R2Δ2	Co-expression (#95, 79)	1. Ni-NTA 2. Dialysis 3. HiTrap Q HP 4. HiLoad Superdex 200 16/60 PG	1. Ni-A1, 5 mM β -ME 2. IEX-A2, pH 8.0, 1 mM DTT 3. IEX-A2, pH 8.0, 1 mM DTT 4. SEC-C, 1 mM DTT	1. Ni-B1, 5 mM β -ME 2. N/A 3. IEX-B, pH 8.0, 1 mM DTT 4. N/A
SUMO-Nic96 R2	Individual (#81)	1. Ni-NTA 2. Dialysis 3. HiTrap Q HP 4. HiLoad Superdex 75 16/60 PG	1. Ni-A1, 5 mM β -ME 2. IEX-A2, pH 8.0, 1 mM DTT 3. IEX-A2, pH 8.0, 1 mM DTT 4. SEC-C, 1 mM DTT	1. Ni-B1, 5 mM β -ME 2. N/A 3. IEX-B, pH 8.0, 1 mM DTT 4. N/A
SUMO-Nic96 R2Δ4	Individual (#80)	1. Ni-NTA 2. Dialysis 3. HiTrap Q HP 4. HiLoad Superdex 75 16/60 PG	1. Ni-A1, 5 mM β -ME 2. IEX-A2, pH 8.0, 5 mM β -ME 3. IEX-A2, pH 8.0, 1 mM DTT 4. SEC-C, 1 mM DTT	1. Ni-B1, 5 mM β -ME 2. N/A 3. IEX-B, pH 8.0, 1 mM DTT 4. N/A
SUMO-scNup53	Individual (#103)	1. Ni-NTA 2. Dialysis 3. HiTrap Q HP 4. HiLoad Superdex 200 16/60 PG	1. Ni-A4, 4 mM β -ME, 5 % Glycerol 2. IEX-A3, pH 8.0, 4 mM β -ME, 5 % Glycerol 3. IEX-A3, pH 8.0, 4 mM β -ME, 5 % Glycerol 4. SEC-B, 5 mM DTT, 5 % Glycerol	1. Ni-B1, 4 mM β -ME 2. N/A 3. IEX-B, pH 8.0, 4 mM β -ME 4. N/A
scNup100	Individual (#109)	1. Ni-NTA 2. Dialysis/Cleavage 3. Ni-NTA 4. HiTrap Q HP 5. HiLoad Superdex 200 16/60 PG	1. Ni-A4, 4 mM β -ME, 5 % Glycerol 2. IEX-A3, pH 8.0, 4 mM β -ME, 5 % Glycerol / ULP1 3. IEX-A3, pH 8.0, 4 mM β -ME 5 % Glycerol 4. IEX-A3, pH 8.0, 4 mM β -ME 5 % Glycerol 5. SEC-B, 5 mM DTT, 5 % Glycerol	1. Ni-B1, 4 mM β -ME 2. N/A 3. Ni-B1, 4 mM β -ME 4. IEX-B, pH 8.0, 4 mM β -ME 5. N/A
SUMO-scNup100	Individual (#109)	1. Ni-NTA 2. Dialysis 3. HiTrap Q HP 4. HiLoad Superdex 200 16/60 PG	1. Ni-A4, 4 mM β -ME, 5 % Glycerol 2. IEX-A3, pH 8.0, 4 mM β -ME, 5 % Glycerol 3. IEX-A3, pH 8.0, 4 mM β -ME, 5 % Glycerol 4. SEC-B, 5 mM DTT, 5 % Glycerol	1. Ni-B1, 4 mM β -ME 2. N/A 3. IEX-B, pH 8.0, 4 mM β -ME 4. N/A

Protein(s)	Expression constructs	Purification step	Buffer A	Buffer B
scNup116	Individual (#110)	1. Ni-NTA 2. Dialysis/Cleavage 3. Ni-NTA 4. HiTrap Q HP 5. HiLoad Superdex 200 16/60 PG	1. Ni-A4, 4 mM β -ME, 5 % Glycerol 2. IEX-A3, pH 8.0, 4 mM β -ME, 5 % Glycerol / ULP1 3. IEX-A3, pH 8.0, 4 mM β -ME 5 % Glycerol 4. IEX-A3, pH 8.0, 4 mM β -ME 5 % Glycerol 5. SEC-B, 5 mM DTT, 5 % Glycerol	1. Ni-B1, 4 mM β -ME 2. N/A 3. Ni-B1, 4 mM β -ME 4. IEX-B, pH 8.0, 4 mM β -ME 5. N/A
scNup145N	Individual (#111)	1. Ni-NTA 2. Dialysis/Cleavage 3. Ni-NTA 4. HiTrap Q HP 5. HiLoad Superdex 200 16/60 PG	1. Ni-A4, 4 mM β -ME, 5 % Glycerol 2. IEX-A3, pH 8.0, 4 mM β -ME, 5 % Glycerol / ULP1 3. IEX-A3, pH 8.0, 4 mM β -ME 5 % Glycerol 4. IEX-A3, pH 8.0, 4 mM β -ME 5 % Glycerol 5. SEC-B, 5 mM DTT, 5 % Glycerol	1. Ni-B1, 4 mM β -ME 2. N/A 3. Ni-B1, 4 mM β -ME 4. IEX-B, pH 8.0, 4 mM β -ME 5. N/A
SUMO-scNup145N	Individual (#111)	1. Ni-NTA 2. Dialysis 3. HiTrap Q HP 4. HiLoad Superdex 200 16/60 PG	1. Ni-A4, 4 mM β -ME, 5 % Glycerol 2. IEX-A3, pH 8.0, 4 mM β -ME, 5 % Glycerol 3. IEX-A3, pH 8.0, 4 mM β -ME, 5 % Glycerol 4. SEC-B, 5 mM DTT, 5 % Glycerol	1. Ni-B1, 4 mM β -ME 2. N/A 3. IEX-B, pH 8.0, 4 mM β -ME 4. N/A
scNup188	Individual (#115)	1. Ni-NTA 2. Dialysis/Cleavage 3. Ni-NTA 4. HiTrap Q HP 5. HiLoad Superdex 200 16/60 PG	1. Ni-A4, 4 mM β -ME, 5 % Glycerol 2. IEX-A2, pH 8.0, 4 mM β -ME, 5 % Glycerol / ULP1 3. IEX-A2, pH 8.0, 4 mM β -ME 5 % Glycerol 4. IEX-A2, pH 8.0, 4 mM β -ME 5 % Glycerol 5. SEC-A, 5 mM DTT, 5 % Glycerol	1. Ni-B1, 4 mM β -ME 2. N/A 3. Ni-B1, 4 mM β -ME 4. IEX-B, pH 8.0, 4 mM β -ME 5. N/A
scNup192 NTD	Individual (#112)	1. Ni-NTA 2. Dialysis/Cleavage 3. Ni-NTA 4. HiTrap Q HP 5. HiLoad Superdex 200 16/60 PG	1. Ni-A4, 4 mM β -ME, 5 % Glycerol 2. IEX-A2, pH 8.0, 4 mM β -ME, 5 % Glycerol / PreS 3. IEX-A2, pH 8.0, 4 mM β -ME 5 % Glycerol 4. IEX-A2, pH 8.0, 4 mM β -ME 5 % Glycerol 5. SEC-A, 5 mM DTT, 5 % Glycerol	1. Ni-B1, 4 mM β -ME 2. N/A 3. Ni-B1, 4 mM β -ME 4. IEX-B, pH 8.0, 4 mM β -ME 5. N/A
scNup170 CTD wild-type and mutant	Individual (#104, 105)	1. Ni-NTA 2. Dialysis/Cleavage 3. Ni-NTA 4. HiTrap Q HP 5. HiLoad Superdex 200 16/60 PG	1. Ni-A4, 4 mM β -ME, 5 % Glycerol 2. IEX-A4, pH 8.0, 4 mM β -ME, 5 % Glycerol / ULP1 3. IEX-A4, pH 8.0, 4 mM β -ME 5 % Glycerol 4. IEX-A4, pH 8.0, 4 mM β -ME 5 % Glycerol 5. SEC-C, 5 mM DTT, 5 % Glycerol	1. Ni-B1, 4 mM β -ME 2. N/A 3. Ni-B1, 4 mM β -ME 4. IEX-B, pH 8.0, 4 mM β -ME 5. N/A
SUMO-scNup170 CTD	Individual (#104)	1. Ni-NTA 2. Dialysis 3. HiTrap Q HP 4. HiLoad Superdex 200 16/60 PG	1. Ni-A4, 4 mM β -ME, 5 % Glycerol 2. IEX-A4, pH 8.0, 4 mM β -ME, 5 % Glycerol 3. IEX-A4, pH 8.0, 4 mM β -ME 5 % Glycerol 4. SEC-C, 5 mM DTT, 5 % Glycerol	1. Ni-B1, 4 mM β -ME 2. N/A 3. IEX-B, pH 8.0, 4 mM β -ME 4. N/A
scNup157 CTD	Individual (#106)	1. Ni-NTA 2. Dialysis/Cleavage 3. Ni-NTA 4. HiTrap Q HP 5. HiLoad Superdex 200 16/60 PG	1. Ni-A4, 4 mM β -ME, 5 % Glycerol 2. IEX-A4, pH 8.0, 4 mM β -ME, 5 % Glycerol / ULP1 3. IEX-A4, pH 8.0, 4 mM β -ME 5 % Glycerol 4. IEX-A4, pH 8.0, 4 mM β -ME 5 % Glycerol 5. SEC-C, 5 mM DTT, 5 % Glycerol	1. Ni-B1, 4 mM β -ME 2. N/A 3. Ni-B1, 4 mM β -ME 4. IEX-B, pH 8.0, 4 mM β -ME 5. N/A
SUMO-scNup157 CTD	Individual (#106)	1. Ni-NTA 2. Dialysis 3. HiTrap Q HP 4. HiLoad Superdex 200 16/60 PG	1. Ni-A4, 4 mM β -ME, 5 % Glycerol 2. IEX-A4, pH 8.0, 4 mM β -ME, 5 % Glycerol 3. IEX-A4, pH 8.0, 4 mM β -ME 5 % Glycerol 4. SEC-C, 5 mM DTT, 5 % Glycerol	1. Ni-B1, 4 mM β -ME 2. N/A 3. IEX-B, pH 8.0, 4 mM β -ME 4. N/A
scNup82 NTD+ scNup159 T	Co-expression (#101)	1. Ni-NTA 2. Dialysis/Cleavage 3. Ni-NTA 4. HiTrap Q HP 5. HiLoad Superdex 200 16/60 PG	1. Ni-A4, 4 mM β -ME, 5 % Glycerol 2. IEX-A2, pH 8.0, 4 mM β -ME, 5 % Glycerol / ULP1 3. IEX-A2, pH 8.0, 4 mM β -ME 5 % Glycerol 4. IEX-A2, pH 8.0, 4 mM β -ME 5 % Glycerol 5. SEC-A, 5 mM DTT, 5 % Glycerol	1. Ni-B1, 4 mM β -ME 2. N/A 3. Ni-B1, 4 mM β -ME 4. IEX-B, pH 8.0, 4 mM β -ME 5. N/A
scSec13+scNup145C	Co-expression (#103)	1. Ni-NTA 2. Dialysis/Cleavage 3. Ni-NTA 4. HiTrap Q HP 5. HiLoad Superdex 200 16/60 PG	1. Ni-A4, 4 mM β -ME, 5 % Glycerol 2. IEX-A2, pH 8.0, 4 mM β -ME, 5 % Glycerol / ULP1 3. IEX-A2, pH 8.0, 4 mM β -ME 5 % Glycerol 4. IEX-A2, pH 8.0, 4 mM β -ME 5 % Glycerol 5. SEC-A, 5 mM DTT, 5 % Glycerol	1. Ni-B1, 4 mM β -ME 2. N/A 3. Ni-B1, 4 mM β -ME 4. IEX-B, pH 8.0, 4 mM β -ME 5. N/A
scNic96 SOL triple mutant	Individual (#113)	1. Ni-NTA 2. HiPrep 26/20 Desalting/Cleavage 3. HiLoad Superdex 200 16/60 PG	1. Ni-A1, 4 mM β -ME 2. SEC-A, 5 mM DTT / ULP1 3. SEC-A, 5 mM DTT	1. Ni-B1, 4 mM β -ME 2. N/A 3. N/A
SUMO-scNup53	Individual (#114)	1. Ni-NTA 2. Dialysis 3. HiTrap Q HP 4. HiLoad Superdex 75 16/60 PG	1. Ni-A1, 4 mM β -ME 2. IEX-A1, pH 8.0, 5 mM DTT 3. IEX-A1, pH 8.0, 5 mM DTT 4. SEC-A, 5 mM DTT	1. Ni-B1, 4 mM β -ME 2. N/A 3. IEX-B, pH 8.0, 5 mM DTT 4. N/A
scNup157 NTD wild-type and mutant	Individual (#107-108)	Detailed description in SI methods		
Nic96-CNT	Individual (#77, 96, 97) co-lysis	Detailed description in SI methods		

♦ Constructs that were used for crystallization

* Detailed purification provided in supplementary figures

Ni-A1: 20 mM TRIS (pH 8.0), 500 mM NaCl, 20 mM imidazole
Ni-A2: 20 mM TRIS (pH 8.0), 100 mM NaCl, 20 mM imidazole
Ni-A3: 20 mM TRIS (pH 8.0), 200 mM NaCl, 20 mM imidazole
Ni-A4: 75 mM TRIS (pH 8.0), 500 mM NaCl, 20 mM imidazole
Ni-B1: 20 mM TRIS (pH 8.0), 500 mM NaCl, 500 mM imidazole
Ni-B2: 20 mM TRIS (pH 8.0), 100 mM NaCl, 500 mM imidazole

GST-A: 20 mM TRIS (pH 8.0), 200 mM NaCl
GST-B: 20 mM TRIS (pH 8.0), 200 mM NaCl, 20 mM glutathione

IEX-A1: 20 mM TRIS, 50 mM NaCl
IEX-A2: 20 mM TRIS, 100 mM NaCl
IEX-A3: 20 mM TRIS, 150 mM NaCl
IEX-A4: 20 mM TRIS, 200 mM NaCl
IEX-B: 20 mM TRIS, 2.0 M NaCl

SEC-A: 20 mM TRIS (pH 8.0), 100 mM NaCl
SEC-B: 20 mM TRIS (pH 8.0), 150 mM NaCl
SEC-C: 20 mM TRIS (pH 8.0), 200 mM NaCl

Table S3.

SEC-MALS analysis

Figure	Nucleoporin or nucleoporin complex	Experimental mass (kDa)	Theoretical mass (kDa)	Stoichiometry
fig. S3A	Nup192•Nup145N•Nup53	250	278	
	Nic96•CNT (Nic96•Nup57•Nup49•Nsp1)	160	187	
	IRC•Nup53 (Nup192•Nic96•Nup145N•Nup53•CNT)	380	465	conc. dependent
fig. S3B	IRC•Nup53 (Nup192•Nic96•Nup145N•Nup53•CNT)	335	423	
	Nup188	180	204	
	IRC•Nup53 + Nup188	341 / 220	627	no interaction
Fig. 1D fig. S4A	CNC-hexamer•Nup145N (Nup120•Nup37•ELYS•Nup85•Sec13•Nup145C•Nup145N)	482	507	
	Nup192•Nic96•Nup53•CNT	335	423	
	CNC-hexamer•IRC•Nup53	654	930	conc. dependent
Fig. 1E fig. S4B	CNC-hexamer (Nup120•Nup37•ELYS•Nup85•Sec13•Nup145C)	438	465	
	Nup192•Nic96•Nup53•CNT	335	423	
	CNC-hexamer + IRC•Nup53	430	888	no interaction
Fig. 1F fig. S4C	CNC-hexamer•Nup145N	466	507	
	Nup188•Nic96•Nup53•CNT	523	431	
	CNC-hexamer•Nup188•Nic96•Nup145N•Nup53•CNT	1220	938	superstoichiometric
Fig. 1G fig. S4D	CNC-hexamer	428	465	
	Nup188•Nic96•Nup53•CNT	523	431	
	CNC-hexamer + Nup188•Nic96•Nup53•CNT	507	896	no interaction
fig. S5A	CNC-hexamer	428	465	
	Nup145N	40	42	
	CNC-hexamer•Nup145N	508	507	stoichiometric
fig. S5B	CNC-hexamer	428	465	
	Nup145N APD	17	15	
	CNC-hexamer•Nup145N APD	447	480	stoichiometric
fig. S5C	CNC-hexamer	428	465	
	Nup145N PreS	36 / 15	27 / 15	
	CNC-hexamer•Nup145N APD + Nup145N MID	690	480	superstoichiometric
fig. S6A	CNC-hexamer	428	465	
	Nup82 NTD•Nup159 T•Nup145N	112	122	
	CNC-hexamer•Nup145N + Nup82 NTD•Nup159 T	579	587	stoichiometric
fig. S6B	Nup188•Nic96•Nup53•CNT	523	431	
	Nup82 NTD•Nup159 T•Nup145N	126	122	
	Nup188•Nic96•Nup145N•Nup53•CNT + Nup82 NTD•Nup159 T	670	553	superstoichiometric
Fig. 2A fig. S7A	Nup192	176	196	
	Nup188	180	204	
	Nup170	132	147	
	Nic96 SOL	73	81	
	Nup192 + Nup188 + Nup170 + Nic96 SOL	174	628	no interaction
Fig. 2B fig. S7B	Nup192 + Nup170 + Nic96 SOL	161 / 93	172 ^a / 81	
	Nup53 + Nup145N	52	41 ^a	
	Nup192•Nup170•Nic96 SOL•Nup53•Nup145N	528	506	stoichiometric
Fig. 2C fig. S7C	Nup188 + Nup170 + Nic96 SOL	165 / 87	176 ^a / 81	
	Nup53 + Nup145N	52	41 ^a	
	Nup188 + Nup170 + Nic96 SOL + Nup53 + Nup145N	242	512	weak interaction
Fig. 2D fig. S8A	Nic96 SOL	72	81	
	Nup53	40	40	
	Nic96 SOL•Nup53	146	121	superstoichiometric
Fig. 2D fig. S8B	Nup170	145	147	
	Nup53	35	40	
	Nup170•Nup53	197	187	stoichiometric
Fig. 2D fig. S8C	Nup188	188	204	
	Nup53	40	40	
	Nup188 + Nup53	188	244	weak interaction
Fig. 2D fig. S8D	Nup192	178	196	
	Nup53	40	40	
	Nup192•Nup53	223	236	stoichiometric
Fig. 2D fig. S8E	CNT (Nup57, Nup49, Nsp1)	70	77	
	Nup53	38	40	
	CNT + Nup53	73	117	weak interaction
Fig. 2E fig. S9A	Nup170	145	147	
	Nup145N	42	42	
	Nup170•Nup145N	196	189	stoichiometric
Fig. 2E fig. S9B	Nup188	189	204	
	Nup145N	40	42	
	Nup188•Nup145N	216	246	stoichiometric
Fig. 2E fig. S9C	Nup192	178	196	
	Nup145N	40	42	
	Nup192•Nup145N	265	238	superstoichiometric

Figure	Nucleoporin or nucleoporin complex	Experimental mass (kDa)	Theoretical mass (kDa)	Stoichiometry
Fig. 2D fig. S10A	Nup170•Nup53	154	187	
	Nic96 SOL	70	81	
	Nup170•Nup53•Nic96 SOL	208	268	stoichiometric
Fig. 2D fig. S10B	Nup170•Nup53	154	187	
	Nup188	194	204	
	Nup170•Nup53 + Nup188	188	391	no interaction
Fig. 2D fig. S10C	Nup170•Nup53	154	187	
	Nup192	196	196	
	Nup170•Nup53•Nup192	259	383	conc. dependent
Fig. 2D fig. S10D	Nup192•Nup53	215	236	
	Nic96 SOL	70	81	
	Nup192•Nup53•Nic96 SOL	252	317	conc. dependent
fig. S10E	Nup170•Nup53•Nup192	255	383	
	Nic96 SOL	70	81	
	Nup170•Nup53•Nup192•Nic96 SOL	286	464	conc. dependent
Fig. 2E fig. S11A	Nup170•Nup145N	178	189	
	Nup188	184	204	
	Nup170•Nup145N + Nup188•Nup145N	227	393	partial exchange
Fig. 2E fig. S11B	Nup170•Nup145N	178	189	
	Nup192	178	196	
	Nup170•Nup145N•Nup192	305	385	conc. dependent
Fig. 2E fig. S11C	Nup188•Nup145N	203	246	
	Nup170	137	147	
	Nup188•Nup145N + Nup170•Nup145N	193	393	partial exchange
Fig. 2E fig. S11D	Nup192•Nup145N	227	238	
	Nup170	137	147	
	Nup192•Nup145N•Nup170	276	385	conc. dependent
Fig. 2E fig. S11E	Nup192•Nup145N	233	238	
	Nup188	190	204	
	Nup192•Nup145N + Nup188•Nup145N	223	442	partial exchange
Fig. 2E fig. S11F	Nup188•Nup145N	215	246	
	Nup192	180	196	
	Nup188•Nup145N + Nup192•Nup145N	224	442	partial exchange
Fig. 2E fig. S11G	Avi-Nup192	178	194	
	Nup188	178	204	
	Nup145N	52	42	
	Avi-Nup192•Nup145N + Nup188•Nup145N	223	440	partial exchange
fig. S12A	Nup170•Nup145N	178	189	
	Nup53	38	40	
	Nup170•Nup145N•Nup53	*inconclusive	229	stoichiometric
fig. S12B	Nup192	179	196	
	Nup53	38	40	
	Nup145N	40	42	
	Nup192•Nup53•Nup145N	280	278	stoichiometric
fig. S12C	Nup170•Nup53•Nup145N	183	229	
	Nup192	176	196	
	Nup170•Nup53•Nup145N•Nup192	416	425	stoichiometric
Fig. 2F fig. S13A	Nup192	183	196	
	SUMO-Nup53 31-67	16	14	
	Nup192•SUMO-Nup53 31-67	197	210	stoichiometric
Fig. 2F fig. S14A	Nic96 SOL	70	81	
	SUMO-Nup53 1-90	21	21	
	Nic96 SOL•SUMO-Nup53 1-90	88	102	stoichiometric
Fig. 2F fig. S14B	Nic96 SOL	81	81	
	SUMO-Nup53 69-90	16	14	
	Nic96 SOL•SUMO-Nup53 69-90	88	95	stoichiometric
Fig. 2F fig. S14C	Nup192	176	196	
	Nic96 SOL•SUMO-Nup53 1-90	81	102	
	Nup192•Nic96 SOL•SUMO-Nup53 1-90	220	298	conc. dependent
Fig. 2F fig. S17A	Nup192	178	196	
	SUMO-Nup145N 606-683	20	19	
	Nup192•SUMO-Nup145N 606-683	189	215	stoichiometric
Fig. 2F fig. S17B	Nup192	176	196	
	Nup145N PreS	28 / 14	27 / 15	
	Nup192•Nup145N MID + Nup145N APD	223	223	stoichiometric
Fig. 2F fig. S17C	Nup192 NTD	100	109	
	Nup145N	53	42	
	Nup192 NTD•Nup145N	151	151	stoichiometric
Fig. 2F fig. S17D	Nup192 CTD	127	91	
	Nup145N	40	42	
	Nup192 CTD + Nup145N	137	133	stoichiometric
Fig. 2F fig. S17E	Nup192 TAIL	38	41	
	Nup145N	46	42	
	Nup192 TAIL + Nup145N	45 / 40	83	stoichiometric

Figure	Nucleoporin or nucleoporin complex	Experimental mass (kDa)	Theoretical mass (kDa)	Stoichiometry
fig. S18A	Nup170	125	147	
	SUMO-Nup53 31-67	16	14	
	Nup170 + SUMO-Nup53 31-67	129	161	no interaction
fig. S18B	Nup170	125	147	
	SUMO-Nup53 69-90	14	14	
	Nup170 + SUMO-Nup53 69-90	129	161	no interaction
fig. S18C	Nup170	125	147	
	SUMO-Nup145N 606-683	15	19	
	Nup170+ SUMO-Nup145N 606-683	133	166	no interaction
fig. S18D	Nup192	176	196	
	SUMO-Nup53 69-90	14	14	
	Nup192 + SUMO-Nup53 69-90	174	210	no interaction
fig. S18E	Nup192	176	196	
	GST-Nup53 329-361	55	61	
	Nup192 + GST-Nup53 329-361	172	257	no interaction
fig. S18F	Nup192	176	196	
	GST-Nup145N 729-750	55	59	
	Nup192 + GST-Nup145N 729-750	172	255	no interaction
fig. S18G	Nic96 SOL	70	81	
	SUMO-Nup53 31-67	16	14	
	Nic96 + SUMO-Nup53 31-67	74	95	no interaction
fig. S18H	Nic96 SOL	70	81	
	GST-Nup53 329-361	55	61	
	Nic96 + GST-Nup53 329-361	66	142	no interaction
Fig. 2F fig. S19B	Nup188	181	204	
	Nup145N PreS	28 / 14	27 / 15	
	Nup188•Nup145N MID + Nup145N APD	213	231	stoichiometric
Fig. 2F fig. S19C	Nup188	178	204	
	SUMO-Nup145N 606-750	37	27	
	Nup188•SUMO-Nup145N 606-750	202	231	stoichiometric
Fig. 2F fig. S19D	Nup188	179	204	
	SUMO-Nup145N 606-683	21	19	
	Nup188 + SUMO-Nup145N 606-683	173	223	no interaction
Fig. 2F fig. S19E	Nup188	178	204	
	GST-Nup145N 729-750	55	59	
	Nup188 + GST-Nup145N 729-750	188	263	weak interaction
fig. S39A	Nic96 SOL	72	81	
	Nup53 RRM	13	13	
	Nic96 SOL + Nup53 RRM	73	94	no interaction
fig. S39B	Nup170	133	147	
	Nup53 RRM	12	13	
	Nup170 + Nup53 RRM	132	160	no interaction
fig. S39C	Nup192	183	196	
	Nup53 RRM	14	13	
	Nup192 + Nup53 RRM	182	209	no interaction
fig. S39D	Nup188	183	204	
	Nup53 RRM	14	13	
	Nup188 + Nup53 RRM	182	209	no interaction
fig. S44B	Nup120•Nup37•ELYS	209	239	
	Nup84•Nup133	241	258	
	Nup120•Nup37•ELYS•Nup84•Nup133	264	497	weak interaction
fig. S44C	Nup120•Nup37•ELYS	209	239	
	Nup84•Nup133 ΔNTE	233	246	
	Nup120•Nup37•ELYS +Nup84•Nup133 ΔNTE	240	485	no interaction

Table S4.

Crystallization and cryoprotection conditions

Protein(s)	Concentration	Crystallization condition	Cryo protection condition
Nup170 ^{NTD} •Nup53 ^{R3}	20 mg/ml Nup170 ^{NTD} 3-fold molar excess Nup53 ^{R3}	1.0 M Na/K phosphate (pH 6.9)	Mother liquor gradually supplemented to 25 % (v/v) ethylene glycol in 5 % steps
Nup170 ^{CTD} •Nup145N ^{R3}	20 mg/ml Nup170 ^{CTD} 3-fold molar excess Nup145N ^{R3}	12 % (w/v) PEG 3,350 0.2 M lithium acetate	Mother liquor gradually supplemented to 25 % (v/v) ethylene glycol in 5 % steps
Nup170 ^{CTD} SeMet	15 mg/ml	0.1 M MES (pH 6.3) 10 % PEG 20,000 10 % (v/v) ethylene glycol 0.2 M potassium thiocyanate	Mother liquor gradually supplemented to 25 % (v/v) ethylene glycol in 5 % steps
Nup170 ^{CTD}	30 mg/ml	0.1 M HEPES (pH 7.0) 1.0 M sodium acetate	Mother liquor gradually supplemented to 25 % (v/v) ethylene glycol in 5 % steps
Nup170 ^{SOL}	7 mg/ml	0.1 M HEPES (pH 7.1) 0.5 M ammonium sulfate	Mother liquor gradually supplemented to 25 % (v/v) ethylene glycol in 5 % steps
Nic96 ^{SOL} •Nup53 ^{R2}	12 mg/ml	0.1 M TRIS (pH 7.0) 12 % (w/v) PEG 6,000 1.2 M sodium chloride	Paratone N
Nic96 ^{SOL}	12 mg/ml	4 % Tacsimate (pH 7.4) 14 % (w/v) PEG 3,350	Paratone N
Nup192 ^{HEAD}	7 mg/ml	0.1 M TRIS (pH 7.9) 6 % (w/v) PEG 4,000 5 % (v/v) polypropylene glycol	Stabilized in 0.1 M TRIS (pH 7.9) 7 % (w/v) PEG 4,000 6 % (v/v) polypropylene glycol Solution gradually supplemented to 25 % (v/v) polypropylene glycol in 5 % steps
Nup53 ^{RRM}	15 mg/ml	0.1 M HEPES (pH 7.0) 24 % (w/v) PEG 3,350 0.2 M potassium iodide	Mother liquor supplemented to 25 % ethylene glycol
Nup53 ^{RRM}	15 mg/ml	4 % Tacsimate (pH 4.1) 15 % (w/v) PEG 3,350	32 % Tacsimate (pH 4.1) 19 % (w/v) PEG 3,350
Nup145N ^{APD}	10 mg/ml	0.1 M citric acid (pH 3.0) 25 % (w/v) PEG 3,350	Mother liquor supplemented to 25 % ethylene glycol
Nup145N ^{APD} •Nup145C ^N	10 mg/ml	0.1 M TRIS (pH 8.8) 32 % (w/v) PEG 4,000 0.2 M lithium sulfate	Mother liquor supplemented to 10 % glycerol

Table S5.X-ray crystallography analysis of Nup170^{NTD}•Nup53^{R3} and Nup170^{SOL}

Data collection					
Protein	Nup170 ^{NTD} •Nup53 ^{R3}	Nup170 ^{NTD} •Nup53 ^{R3}	Nup170 ^{SOL}	Nup170 ^{SOL g}	Nup170 ^{SOL g}
PDB ID		5HAX		5HB1	
Synchrotron	APS ^a	APS	SSRL ^b	SSRL	SSRL
Beamline	23-ID-D	23-ID-D	BL12-2	BL12-2	BL12-2
Space group	P2 ₁ 2 ₁ 2 ₁	P2 ₁ 2 ₁ 2 ₁	P2 ₁ 2 ₁ 2	P2 ₁ 2 ₁ 2	P2 ₁ 2 ₁ 2
Cell dimensions					
<i>a</i> , <i>b</i> , <i>c</i> (Å)	68.7, 104.0, 119.0	69.2, 106.2, 120.1	93.2, 136.9, 89.0	96.0, 138.5, 89.2	96.0, 138.5, 89.2
α , β , γ (°)	90.0, 90.0, 90.0	90.0, 90.0, 90.0	90.0, 90.0, 90.0	90.0, 90.0, 90.0	90.0, 90.0, 90.0
	<i>Se Peak</i>		<i>Se Peak</i>		
Wavelength	0.9792	1.0332	0.9791	1.0330	
Resolution (Å)	50.0 – 2.5	50.0 – 2.1	50.0 – 4.5	40.0 – 4.0	40.0 – 4.3
<i>R</i> _{meas} (%) ^c	8.5 (127.7)	8.0 (188.5)	13.1 (290.0)	5.7 (353.7)	5.1 (121.5)
<i>R</i> _{pim} (%) ^c	1.7 (24.9)	2.2 (51.1)	3.7 (85.0)	1.7 (98.5)	1.5 (33.0)
<i>CC</i> _{1/2} ^c	100.0 (86.6)	100.0 (68.1)	99.9 (56.0)	100.0 (55.5)	100.0 (92.2)
<i>< I / σ I ></i> ^c	30.4 (2.4)	20.3 (1.8)	11.6 (1.0)	18.5 (0.8)	22.8 (2.5)
Completeness (%) ^c	98.9 (90.7)	100.0 (100.0)	99.3 (94.1)	99.7 (98.5)	99.8 (99.9)
No. of observations	776,896	676,933	91,230	135,558	108,324
No. of unique reflections ^{c,d}	30,229 (2,703)	52,358 (5,120)	7,200 (649)	10,614 (1,027)	8,524 (845)
Redundancy ^c	25.7 (25.2)	12.9 (13.5)	12.7 (11.1)	12.8 (12.4)	12.7 (13.4)
Refinement					
Resolution (Å)		50.0 – 2.1		40.0 – 4.0	
No. of reflections		52,342		7,867 ^e	
No. of reflections test set		2,618 (5.0%)		789 (10.0%)	
<i>R</i> _{work} / <i>R</i> _{free}		19.9 / 23.0		30.4 / 35.2	
No. atoms		5,998		5,895	
Protein		5,581		5,895	
Water		387		0	
Ligand/Ions		30		0	
<i>B</i> -factors		62		222	
Protein		63		222	
Water		57		-	
Ligand/Ions		79		-	
RMSD					
Bond lengths (Å)		0.002		0.003	
Bond angles (°)		0.5		0.5	
Ramachandran plot^f					
Favored (%)		97.6		96.8	
Additionally allowed (%)		2.4		3.2	
Outliers (%)		0.0		0.0	
MolProbity					
Clashscore ^f		0.18 (100 th percentile)		1.95 (100 th percentile)	
Molprobability score ^f		0.79 (100 th percentile)		1.46 (100 th percentile)	

^aAPS, Advanced Photon Source^bSSRL, Stanford Synchrotron Radiation Lightsource^cHighest-resolution shell is shown in parentheses^dFriedel pairs were merged^eRefinement was performed with ellipsoidally truncated data^fAs determined by MolProbity^gAs a reference, two different high-resolution cutoffs are shown

Table S6.X-ray crystallography analysis of *apo* Nup170^{CTD} and Nup170^{CTD}•Nup145N^{R3}

Data collection	Nup170 ^{CTD}	Nup170 ^{CTD}	Nup170 ^{CTD} •Nup145N ^{R3}
Protein	Nup170 ^{CTD} Y905M/L1007M/L1183M/V1292M	Nup170 ^{CTD}	Nup170 ^{CTD} •Nup145N ^{R3}
PDB ID	5HAY	5HAZ	5HB0
Synchrotron	SSRL ^a	APS ^b	APS
Beamline	BL12-2	23-ID-D	23-ID-D
Space group	P2 ₁ 2 ₁ 2 ₁	P2 ₁ 2 ₁ 2 ₁	P1
Cell dimensions			
<i>a</i> , <i>b</i> , <i>c</i> (Å)	61.8, 101.7, 193.8	69.2, 106.2, 120.1	74.6, 111.47, 111.75
α , β , γ (°)	90.0, 90.0, 90.0	90.0, 90.0, 90.0	91.8, 92.5, 91.4
	<i>Se Peak</i>		
Wavelength	0.9795	1.0332	1.0332
Resolution (Å)	50.0 – 2.8	50.0 – 2.1	50.0 – 3.5
<i>R</i> _{meas} (%) ^c	11.6 (99.9)	5.4 (89.5)	41.4 (179.9)
<i>R</i> _{pim} (%) ^c	2.8 (25.2)	2.1 (33.8)	15.6 (67.6)
<i>CC</i> _{1/2} ^c	99.9 (81.8)	99.9 (85.0)	98.4 (51.7)
$\langle I / \sigma I \rangle$ ^c	22.4 (2.9)	21.0 (2.0)	6.2 (1.3)
Completeness (%) ^c	98.2 (82.2)	97.8 (93.9)	98.8 (94.9)
No. of observations	500,568	325,202	317,882
No. of unique reflections ^c	30,966 (2,527)	47,908 (4,589)	45,493 (4,380)
Redundancy ^c	16.2 (14.2)	6.8 (6.8)	7.0 (6.9)
Refinement			
Resolution (Å)	50.0 – 2.8	50.0 – 2.1	50.0 – 3.5
No. of reflections	30,817	47,882	45,466
No. of reflections test set	1,544 (5.0%)	2,395 (5.0%)	2,011 (4.4%)
<i>R</i> _{work} / <i>R</i> _{free}	20.9 / 25.1	20.6 / 23.1	21.0 / 26.0
No. atoms (non-hydrogen)	8,613	4,919	16,998
Protein	8,564	4,517	16,998
Water	48	378	0
Ligand/Ions	1	24	0
B-factors	65	69	89
Protein	65	69	89
Water	57	64	-
Ligand/Ions	62	117	-
RMSD			
Bond lengths (Å)	0.003	0.004	0.005
Bond angles (°)	0.6	0.6	0.6
Ramachandran plot^e			
Favored (%)	97.2	97.5	95.1
Additionally allowed (%)	2.8	2.5	4.9
Outliers (%)	0.0	0.0	0.0
MolProbity			
Clashscore ^e	1.35 (100 th percentile)	1.44 (100 th percentile)	1.98 (100 th percentile)
Molprobability score ^e	1.29 (100 th percentile)	1.27 (100 th percentile)	1.55 (100 th percentile)

^aSSRL, Stanford Synchrotron Radiation Lightsource^eAs determined by MolProbity^bAPS, Advanced Photon Source^cHighest-resolution shell is shown in parentheses^dFriedel pairs were merged

Table S7.X-ray crystallography analysis of *apo* Nic96^{SOL}, Nup96^{SOL}•Nup53^{R2} and Nup192^{ΔHEAD}

Data collection				
Protein	Nic96 ^{SOL}	Nup96 ^{SOL} •Nup53 ^{R2}	Nup192 ^{ΔHEAD} ^f	Nup192 ^{ΔHEAD} ^f
PDB ID	5HB2	5HB3	5HB4	
Synchrotron	APS ^a	SSRL ^b	SSRL	SSRL
Beamline	23-ID-B	BL12-2	BL12-2	BL12-2
Space group	P2 ₁	P1	C2	C2
Cell dimensions				
a, b, c (Å)	53.0, 72.9, 122.7	59.5, 87.0, 98.1	190.7, 53.5, 171.8	190.7, 53.5, 171.8
α, β, γ (°)	90.0, 93.6, 90.0	100.7, 99.6, 95.7	90.0, 108.3, 90.0	90.0, 108.3, 90.0
	<i>Se Peak</i>		<i>Os Peak</i>	<i>Os Peak</i>
Wavelength	0.9792	1.0000	1.1250	1.1250
Resolution (Å)	50.0 – 3.3	50.0 – 2.65	50.0 – 3.2	50.0 – 3.5
R _{meas} (%) ^c	13.7 (104.2)	7.7 (83.7)	20.8 (325.0)	16.5 (151.7)
R _{pim} (%) ^c	5.0 (38.7)	3.9 (49.4)	5.7 (92.5)	4.5 (40.9)
CC _{1/2} ^c	99.8 (85.1)	99.9 (81.5)	99.9 (37.5)	99.9 (74.7)
< I / σI > ^c	12.0 (2.5)	15.1 (2.1)	12.1 (0.8)	15.5 (2.1)
Completeness (%) ^c	100.0 (99.8)	88.6 (82.4)	98.6 (92.0)	99.4 (99.1)
No. of observations	107,569	189,415	367,182	280,883
No. of unique reflections ^{c,d}	14,334 (1,400)	48,566 (4,513)	27,800 (2,557)	21,186 (2,077)
Redundancy ^c	7.5 (7.0)	3.9 (3.8)	13.2 (11.8)	13.3 (13.7)
Refinement				
Resolution (Å)	50.0 – 3.3	50.0 – 2.65	50.0 – 3.2	
No. of reflections	14,284	48,536	27,512	
No. of reflections test set	1,410 (9.9%)	2,368 (4.9%)	1,377 (5.0%)	
R _{work} / R _{free}	23.1 / 27.8	21.1 / 24.9	23.3 / 26.5	
No. atoms (non-hydrogen)				
Protein	5,674	11,569	11,035	
Water	-	71	0	
Ligand/Ions	-	3	5	
<i>B</i> -factors				
Protein	127	64	136	
Water	-	45	-	
Ligand/Ions	-	57	167	
RMSD				
Bond lengths (Å)	0.003	0.004	0.002	
Bond angles (°)	0.6	0.9	0.5	
Ramachandran plot^e				
Favored (%)	94.2	96.0	95.2	
Additionally allowed (%)	5.8	4.0	4.8	
Outliers (%)	0.0	0.0	0.0	
MolProbity				
Clashscore ^e	3.10 (100 th percentile)	3.71 (99 th percentile)	1.27 (100 th percentile)	
Molprobability score ^e	1.84 (100 th percentile)	1.43 (100 th percentile)	1.24 (100 th percentile)	

^aAPS, Advanced Photon Source^bSSRL, Stanford Synchrotron Radiation Lightsource^cHighest-resolution shell is shown in parentheses^dFriedel pairs were merged^eAs determined by MolProbity^fAs a reference, two different high-resolution cutoffs are shown

Table S8.X-ray crystallography analysis of Nup145N^{APD} and Nup145N^{APD}•Nup145C^N

Data collection		
Protein	Nup145N ^{APD}	Nup145N ^{APD} •Nup145C ^N
PDB ID	5HB5	5HB6
Synchrotron	SSRL ^a	ALS ^b
Beamline	BL12-2	8.2.2
Space group	P2 ₁	P1
Cell dimensions		
a, b, c (Å)	46.1, 34.9, 78.2	43.0, 44.1, 45.3
α, β, γ (°)	90.0, 99.4, 90.0	99.8, 111.0, 105.9
Wavelength	0.9795	1.0000
Resolution (Å)	30.0 – 1.5	30.0 – 1.3
R _{meas} (%) ^c	9.4 (100.4)	5.9 (110.5)
R _{rim} (%) ^c	3.6 (39.1)	2.2 (56.0)
CC _{1/2} ^c	99.9 (87.6)	99.9 (61.7)
< I / σ I > ^c	12.4 (2.3)	17.2 (1.4)
Completeness (%) ^c	97.2 (92.8)	94.7 (88.9)
No. of observations	257,064	461,854
No. of unique reflections ^{c,d}	38,743 (3,651)	66,722 (6,234)
Redundancy ^c	6.6 (6.3)	6.9 (3.8)
Refinement		
Resolution (Å)	30.0 – 1.5	30.0 – 1.3
No. of reflections	38,683	66,707
No. of reflections test set	2,012 (5.2%)	1,792 (2.7%)
R _{work} / R _{free}	16.1 / 18.9	15.1 / 17.4
No. atoms (non-hydrogen)		
Protein	2,331	2,351
Water	331	472
Ligand/Ions	91	25
B-factors		
Protein	21	25
Water	32	36
Ligand/Ions	61	37
RMSD		
Bond lengths (Å)	0.005	0.008
Bond angles (°)	0.8	1.0
Ramachandran plot^e		
Favored (%)	95.9	94.6
Additionally allowed (%)	4.1	5.1
Outliers (%)	0.0	0.3
MolProbity		
Clashscore ^e	0.42 (100 th percentile)	1.47 (99 th percentile)
Molprobability score ^e	0.99 (99 th percentile)	1.31 (91 st percentile)

^aSSRL, Stanford Synchrotron Radiation Lightsource^bALS, Advanced Light Source^cHighest-resolution shell is shown in parentheses^dFriedel pairs were merged^eAs determined by MolProbity

Table S9.X-ray crystallographic analysis of Nup53^{RRM}

Data collection					
Protein	Nup53 ^{RRM e}	Nup53 ^{RRM e}	Nup53 ^{RRM}	Nup53 ^{RRM}	Nup53 ^{RRM}
PDB ID	5HB7			5HB8	
Synchrotron	SSRL ^a	SSRL ^a	SSRL	SSRL	SSRL
Beamline	BL12-2	BL12-2	BL12-2	BL12-2	BL12-2
Space group	P2 ₁ 2 ₁ 2 ₁	P2 ₁ 2 ₁ 2 ₁	P2 ₁ 2 ₁ 2 ₁	P3 ₁ 2 ₁	P3 ₁ 2 ₁
Cell dimensions					
a, b, c (Å)	35.0, 50.4, 60.0	35.0, 50.4, 60.0	34.9, 50.4, 60.0	94.7, 94.7, 115.5	93.8, 97.8, 114.1
α, β, γ (°)	90.0, 90.0, 90.0	90.0, 90.0, 90.0	90.0, 90.0, 90.0	90.0, 90.0, 120.0	90.0, 90.0, 120.0
			<i>Se Peak</i>		<i>Os Peak</i>
Wavelength	0.7293	0.7293	0.9794	0.9794	1.1399
Resolution (Å)	40.0 – 0.80	40.0 – 1.0	40.0 – 1.1	50.0 – 1.7	20.0 – 3.1
<i>R</i> _{meas} (%) ^b	4.1 (94.5)	3.8 (12.1)	10.4 (111.0)	7.9 (155.6)	13.5 (154.4)
<i>R</i> _{pim} (%) ^b	1.3 (33.2)	1.2 (3.7)	2.1 (28.1)	1.3 (29.6)	3.7 (41.8)
CC _{1/2} ^b	99.9 (66.4)	99.9 (99.6)	99.9 (66.6)	100.0 (74.5)	99.8 (76.1)
< σ > ^b	29.3 (2.3)	43.5 (18.8)	19.8 (2.1)	37.3 (2.2)	20.2 (1.8)
Completeness (%) ^b	88.4 (50.3)	97.1 (94.8)	95.4 (66.8)	91.1 (93.1)	99.9 (99.3)
No. of observations	890,036	550,262	984,014	2,169,719	147,214
No. of unique reflections ^{b,c}	92,712 (5,211)	56,349 (5,425)	42,372 (2,914)	60,735 (6,155)	10,957 (1,073)
Redundancy ^b	9.6 (7.6)	9.8 (10.3)	23.2 (14.6)	35.7 (25.9)	13.4 (13.2)
Refinement					
Resolution (Å)	40.0 – 0.8			50.0 – 1.7	
No. of reflections	92,709			59,806	
No. of reflections test set	4,650 (5.0%)			1,812 (3.0%)	
<i>R</i> _{work} / <i>R</i> _{free}	11.8 / 13.2			16.3 / 21.0	
No. atoms (non-hydrogen)	1,448			4,176	
Protein	1,192			3,632	
Water	253			466	
Ligand/Ions	3			78	
<i>B</i> -factors	15			38	
Protein	11			37	
Water	31			43	
Ligand/Ions	16			73	
RMSD					
Bond lengths (Å)	0.008			0.010	
Bond angles (°)	1.1			1.0	
Ramachandran plot^d					
Favored (%)	98.6			99.3	
Additionally allowed (%)	1.4			0.7	
Outliers (%)	0.0			0.0	
MolProbity					
Clashscore ^d	0.43 (95 th percentile)			0.96 (99 th percentile)	
Molprobity score ^d	0.65 (98 th percentile)			0.88 (100 th percentile)	

^aSSRL, Stanford Synchrotron Radiation Lightsource^bHighest-resolution shell is shown in parentheses^cFriedel pairs were merged^dAs determined by MolProbity^eAs a reference, two different high-resolution cutoffs are shown

Table S10.

Molecular masses and nucleoporin stoichiometry in composite structure

<i>C. thermophilum</i> Protein	Stoichiometry	Molecular Mass (kDa)	Total Mass (kDa)
Symmetric Core (observed in composite structure)			
Nup120	32	141.8	4537.6
Nup37	32	80.3	2569.6
-	-	-	-
Nup85	32	128.1	4099.2
-	-	-	-
Sec13	32	33.8	1081.6
Nup145C	32	88.8	2841.6
Nup84	32	108.1	3459.2
Nup133	32	150.7	4822.4
Nup170	48	156.2	7497.6
Nup192	32	196.9	6300.8
Nic96	32	121.5	3888.0
Nup57	32	36.9	1180.8
Nup49	32	48.6	1555.2
Nsp1	32	67.1	2147.2
Nup53	48	47.0	2256.0
Nup145N	48	99.8	4790.4
Nup188	16	203.8	3260.8
TOTAL			56288.0
Cytoplasmic Filaments			
-	-	-	-
Nup159	-	156.2	
Nup82	-	98.1	
Gle1	-	58.0	
Gle2	-	39.4	
Nup42	-	58.0	
Nuclear Basket			
Mlp1	-	231.1	
Nup152	-	152.2	
Nup56	-	56.2	
ELYS	-	33.1	
POMs/Other			
Pom152	-	141.5	
-	-	-	
Ndc1	-	71.8	
Pom34	-	34.2	
-	-	-	

<i>H. Sapiens</i> Protein	Stoichiometry	Molecular Mass (kDa)	Total Mass (kDa)
Symmetric Core (observed in composite structure)			
Nup160	32	162.1	5187.2
Nup37	32	36.7	1174.4
Nup43	32	42.2	1350.4
Nup85	32	75.0	2400.0
Seh1	32	39.7	1270.4
Sec13	32	35.5	1136.0
Nup96	32	105.9	3388.8
Nup107	32	106.4	3404.8
Nup133	32	129.0	4128.0
Nup155	48	155.2	7449.6
Nup205	32	227.9	7292.8
Nup93	32	93.5	2992.0
Nup54	32	55.4	1772.8
Nup58	32	53.2	1702.4
Nup62	32	53.3	1705.6
Nup53	48	34.8	1670.4
Nup98	48	91.7	4401.6
Nup188	16	196.0	3136.0
TOTAL			55563.2
Cytoplasmic Filaments			
Nup358	-	358.2	
Nup214	-	213.6	
Nup88	-	83.5	
Gle1	-	79.8	
Rae1	-	41.0	
Nup12	-	44.9	
Nuclear Basket			
TPR	-	267.3	
Nup153	-	153.9	
Nup50	-	50.1	
ELYS	-	252.5	
POMs/Other			
Gp210	-	205.1	
POM121	-	127.7	
NDC1	-	76.3	
ALADIN	-	59.6	